


Fall 2008

Parameter Estimation of the Arterial System

James Charles Carter II
Old Dominion University

Follow this and additional works at: https://digitalcommons.odu.edu/mae_etds

 Part of the [Biomedical Engineering and Bioengineering Commons](#), and the [Mechanical Engineering Commons](#)

Recommended Citation

Carter, James C.. "Parameter Estimation of the Arterial System" (2008). Doctor of Philosophy (PhD), dissertation, Mechanical Engineering, Old Dominion University, DOI: 10.25777/hsyr-mw37
https://digitalcommons.odu.edu/mae_etds/108

This Dissertation is brought to you for free and open access by the Mechanical & Aerospace Engineering at ODU Digital Commons. It has been accepted for inclusion in Mechanical & Aerospace Engineering Theses & Dissertations by an authorized administrator of ODU Digital Commons. For more information, please contact digitalcommons@odu.edu.

PARAMETER ESTIMATION OF THE ARTERIAL SYSTEM

by

James Charles Carter II
BSME, 1996, Old Dominion University
ME, 1999, Old Dominion University

A Dissertation Submitted to the Faculty of
Old Dominion University in Partial Fulfillment of the
Requirement for the Degree of

DOCTOR OF PHILOSOPHY
MECHANICAL ENGINEERING
OLD DOMINION UNIVERSITY
2008

Approved by:

Avodeii O. Demuren (Director)

Sebastian Y. Bawab (Co-Director)

Gene J. Hou (Member)

Frederic D. McKenzie (Member)

ABSTRACT

PARAMETER ESTIMATION OF THE ARTERIAL SYSTEM

James Charles Carter II
Old Dominion University, 2008
Director: Dr. Ayodeji O. Demuren

There are a number of disorders that originate from or involve faulty operation of the cardiovascular system. Diseases such as atherosclerosis, diabetes and hypertension can have a debilitating effect on blood flow. This makes the tools for simulating the effects of such diseases on blood flow important. Measures, such as pulse wave velocity, that are generated by models of the cardiovascular system can be important indicators of cardiac health.

Although physically measurable, obtaining some parameters comes with a high cost and discomfort to the patient. Models can provide an assessment of many important parameters.

The purpose of this project was to create a robust computer generated model of the arterial system. This model is a one-dimensional/Womersley model that used transmission line hemodynamic theory to calculate the blood pressure waveforms and then the Womersley theory to calculate the flow velocity in various areas of the human body. The accuracy of the model was tested using data from eight subjects. The model provided realistic and individualized cardiovascular parameters without requiring any major adjustment to the internal algorithms.

ACKNOWLEDGMENTS

First I would like to express my love and appreciation to my wife, Dorcas, and the rest of my family who stood patiently by my side during this long journey. Secondly, I would like thank my advisor, Dr. Ayodeji O. Demuren, for his patience and support when I required it. Finally, I would like to thank my committee, Drs. Sebastian Y. Bawab, Gene J. Hou and Rick D. McKenzie, for their valuable suggestions.

TABLE OF CONTENTS

Chapter	Page
1. Introduction.....	1
1.1 Arterial System.....	4
1.2 Arterial Modeling	9
2. Theoretical Basis.....	13
2.1 Properties of Arteries.....	13
2.2 Vessel Stiffness	19
2.3 Aging, Gender and Body Surface Area	23
2.4 Parameter Estimation.....	28
3. Mathematical Model	35
3.1 Fourier Analysis	35
3.2 Wave Propagation	40
3.3 Fluid Flow.	47
3.4 Windkessel Model.....	53
3.5 The Arterial Tree Model.....	59
3.5.1 Physiological data.....	64
3.5.2 Boundary	71
3.5.3 Calculations	74
4. Results and Discussion.....	80
4.1 Test Cases.....	80
4.2 Error.....	80
4.3 Model Results.....	83

4.3.1 Increasing segment increments from 10 to 30.....	119
4.3.2 Sensitivity to parameter change.....	124
4.3.2.1 Increasing / decreasing age.....	124
4.3.2.2 Increasing / decreasing height	126
4.3.2.3 Increasing / decreasing weight	127
4.3.2.4 Increasing / decreasing heart rate	128
4.3.2.5 Changing Gender	130
4.4 Discussion.....	132
5. Conclusion	136
5.1 The benefits of the model	136
5.2 Concluding Remarks	136
5.3 Future work	137
REFERENCES.....	138
APPENDIXES A. COMPUTER PROGRAM FLOW CHART	146
VITA	148

LIST OF TABLES

Table	Page
1.1. Characteristics of Arterial and Pulmonary System	5
2.1. Various Vessel Taper Coefficients.....	16
2.2. Equations for various artery diameters.....	24
3.1. The arterial model nomenclature	66
3.2. Average percent flows trough major arteries	72
4.1. The normalized error between model and actual parameters.....	82
4.2. Cardiovascular parameters derived for subject 471	85
4.3. Physiological data for arterial model of Subject 471	86
4.4. Cardiovascular parameters derived for subject y11	89
4.5. Physiological data for arterial model of Subject y11	90
4.6. Cardiovascular parameters derived for subject 730	93
4.7. Physiological data for arterial model of Subject 730	94
4.8. Cardiovascular parameters derived for subject 281	97
4.9. Physiological data for arterial model of Subject 281	98
4.10. Cardiovascular parameters derived for subject 472	101
4.11. Physiological data for arterial model of Subject 472	102
4.12. Cardiovascular parameters derived for subject 671	105
4.13. Physiological data for arterial model of Subject 671	106
4.14. Cardiovascular parameters derived for subject Cr	110
4.15. Physiological data for arterial model of Subject Cr	111

4.16. Cardiovascular parameters derived for subject Lf	115
4.17. Physiological data for arterial model of Subject Lf	116
4.18. Cardiovascular parameters derived for subject 471 (30 segments)	119
4.19. Physiological data for arterial model of Subject 471 (30 segments)	120
5.1. Benefits of the project model	136

LIST OF FIGURES

Figure	Page
1.1. Diagram of Circulation Showing Multiple Parallel Routes from the Arterial to Venous Side	2
1.2. A representation of discrete sites of occurrences of atherosclerotic lesions and their associated complication from the United States Department of Health, Education and Welfare.....	3
1.3. The Primary Components of a Typical Pressure Pulse Wave.....	6
1.4. RLC representation on a vessel.....	7
1.5. Pressure and flow wave patterns in different locations of the body.....	8
1.6. Avolio's schematic of the arterial system	10
1.7. 28 Vessel Arterial Model	11
2.1. Human Arterial Tree	14
2.2. Dog Arterial Tree	15
2.3. Cross section of a typical arterial vessel	17
2.4. Diameter and wall thickness relative to percentage of vessel wall components.....	18
2.5. Fitted Eh/r_0 curve to data	22
2.6. Length of thoracic aorta versus age.....	23
2.7. Distensibility versus age for the femoral and carotid arteries	26
2.8. The dynamic elastic modulus versus frequency of applied pressure for the human carotid, thoracic, abdominal, iliac and femoral arteries	27
2.9. Large artery compliance and SVR versus age.....	28
2.10. Methods used to derive transfer functions between radial artery and aorta	30

2.11. Comparison of transfer functions for amplification of blood pressure pulse from aorta to radial artery.....	31
2.12. Parameters of a pulse wave used to calculate cardiovascular parameters.....	32
2.13. Second derivative of radial pressure wave.....	34
3.1. Fourier decomposition of hypothetic wave.....	36
3.2. Representation of a single harmonic in a Fourier analysis.....	38
3.3a. Fourier Approximation of the 1 st Order.....	39
3.3b. Fourier Approximation of the 2 nd Order.....	39
3.3c. Fourier Approximation of the 10 th Order.....	39
3.4 Composite pressure wave from incident and reflected waves.....	42
3.5. 3-element windkessel.....	54
3.6 Three windkessel models.....	55
3.7. Pressure Decay in the Diastolic Phase of a Radial Pulse.....	57
3.8. The Goldwyn and Watt 4 element windkessel.....	58
3.9. The arterial tree model.....	65
3.10. A detailed depiction of the Aortic portion of the arterial tree model.....	65
3.11. Modified 4-Element Windkessel.....	71
3.12. Flowchart of overall program inputs, gross calculations and outputs.....	75
4.1. Depiction of error determination.....	81
4.2. Flow and pressure results for subject 471.....	87
4.3. Flow and pressure results for subject y11.....	91
4.4. Flow and pressure results for subject 730.....	95
4.5. Flow and pressure results for subject 281.....	99

4.6. Flow and pressure results for subject 472	103
4.7. Flow and pressure results for subject 671	107
4.8. Flow and pressure results for subject Cf	112
4.9. Flow and pressure results for subject Lf	117
4.10. Flow and pressure results for subject 471 (30 segments).....	121
4.11. Sensitivity to age variation.....	124
4.12. Sensitivity to height variation	126
4.13. Sensitivity to weight variation	127
4.14. Sensitivity to heart rate variation	129
4.15. Sensitivity to gender variation	130

NOMENCLATURES

A	cross sectional area of artery
A_0	cross sectional area of artery at artery inlet
AI	augmentation index
A_n, B_n	Fourier coefficients
A^*	complex conjugate ($A_n - iB_n$)
BSA	body surface area
C	compliance
c_0	Moens-Korteweg equation for wave speed
CO	cardiac output
D	diameter
E	modulus of elasticity
E_c	magnitude of the complex modulus
E_{dyn}	dynamic modulus of elasticity
f	frequency
F_{10}	a Wormersely flow parameter
h	vessel thickness
i	$\sqrt{-1}$
HR	heart rate
$J_0(\cdot)$	bessel function of zero order
$J_1(\cdot)$	bessel function of the first order
k	vessel taper coefficient
k_1, k_2, k_3	coefficients for Eh/ r_0 equation

L	inertance (or inductance)
MAP	mean arterial pressure
m, n, pp	coefficients for Goldwyn and Watt's equation
M_0	component of Bessel function
M_{10}	$1 - \frac{\sqrt{2}}{\alpha} + \frac{1}{\alpha^2}$
p	pressure in vessel
P_{ave}	average pressure
P_d	diastolic pressure
P_I	pressure of incident wave
P_n	pressure of harmonic n
P_R	pressure of reflected wave
P_T	transmitted pressure
P_1	pressure at first shoulder of pressure wave
P_2	pressure at second shoulder of pressure wave
Q	volumetric flow rate
Q_{ave}	Average flow
r, r_0	vessel radius
R	resistance
SVR	systemic vascular resistance
T	tension in vessel wall
t	time
time _A	time of the maximum value of the second derivative of pressure wave
time _B	time of the minimum value of the second derivative of pressure wave

T_1	time of first shoulder in pressure wave
T_2	time of second shoulder in pressure wave
T_{ej}	time of blood ejection into arterial system (T_I)
T_{eff}	transmission coefficient
T_I	time of incisura in pressure wave (T_{ej})
T_f	time of start of pressure wave
T_T	total time of pressure wave
ν	blood dynamic viscosity
x	distance
x_1, x_2, x_3	coefficients for Goldwyn and Watt's equation
x_4, x_5, x_6	coefficients for Goldwyn and Watt's equation
z	vessel length
Z	input impedance
Z_0	characteristic impedance
Z_T	terminal impedance
α	alpha, a Womersley parameter
ΔD	change in diameter
ΔP	change in pressure
ε_0	component of Bessel function
ε_{10}	$\frac{\sqrt{2}}{\alpha} + \frac{1}{\alpha^2} + \frac{19}{24} \frac{1}{\alpha^3 \sqrt{2}}$
Γ	reflection coefficient
ϕ	phase angle between applied pressure and vessel wall motion

ϕ_0	initial phase angle between applied pressure and vessel wall motion
ρ	density of blood
η	wall viscosity (viscoelastic coefficient for motion of vessel wall)
γ	propagation constant
κ	coefficient in phase angle equation
μ	blood viscosity
θ	pressure phase angle
φ	flow phase angle
ω	Angular frequency
σ	circumferential stress in vessel wall
ν	Poisson's ratio of the vessel wall

CHAPTER 1

1. Introduction:

The cardiovascular system can be considered a complex fluid flow transport network, designed to distribute various substances and help maintain homeostasis among the other systems of the body. Oscillating pulsations of blood flow carry blood cells and other substances throughout the body to exchange oxygen for carbon dioxide, distribute hormones to appropriate locations, remove metabolic waste, and absorb and distribute heat. The vessels, through which the blood flows, expand and contract to provide a more continuous stream of blood. The arterial vessels also dilate and constrict to accommodate for blood flow demands placed on the cardiovascular system. Blood flow through the smallest vessels (capillaries) is regulated by the difference between the inner vessel hydrostatic pressure and the external pressure from the fluid and tissue surrounding the vessels. This pressure difference basically dictates the hydrostatic-osmotic relation that allows transport of fluid into and out of the capillaries. The regulation of these pressure relationships at different locations is essential for transport via blood flow. The vessels divide into smaller branches that are sized to maintain proper pressure and flow throughout the cardiovascular system, which ensures proper organ and metabolic function. Figure 1.1 shows a coloring book view where dispersed branches of the human arterial system are lumped into single elements to represent major distribution points for blood flow.

1

¹ The format / citation style followed by this report comes from the Journal of Biomechanics

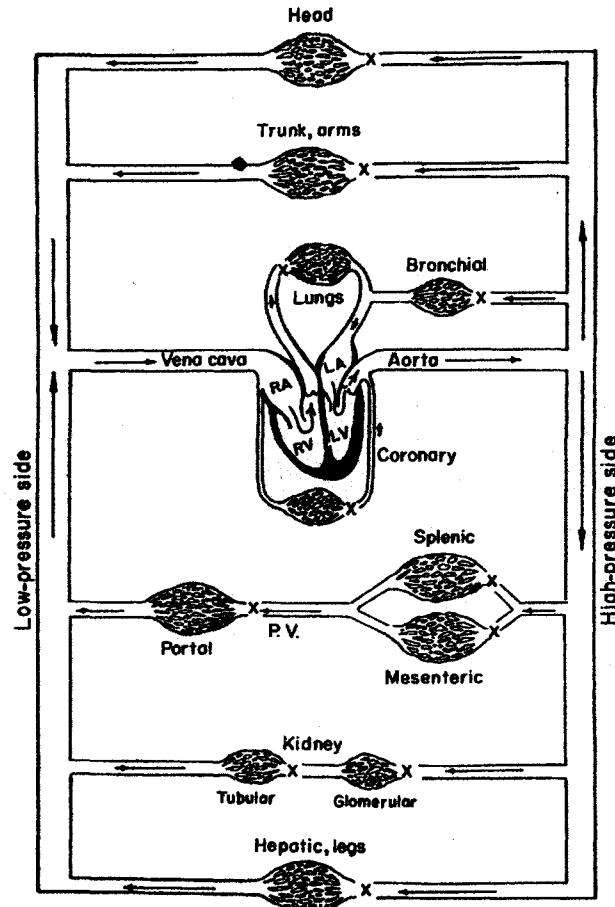


Fig. 1.1 Diagram of Circulation Showing Multiple Parallel Routes from the Arterial to Venous Side (Fraser, 1981)

Although this is a simplified view of oxygen and transport through the body, it can be seen that drugs or diseases that affect the cardiovascular system can impact the maintenance of tissue throughout the body. This is but one of many aspects of cardiovascular health that makes knowledge of the workings of this system important. (Marieb, 1995)

Clichés are often ill received - probably due to their perceived lack of authenticity. Still, clichés remain clichés because of their inherent value. Therefore, with regard to the importance of understanding the workings of the human arterial system (as depicted in figure 1.2), a picture speaks a thousand words.

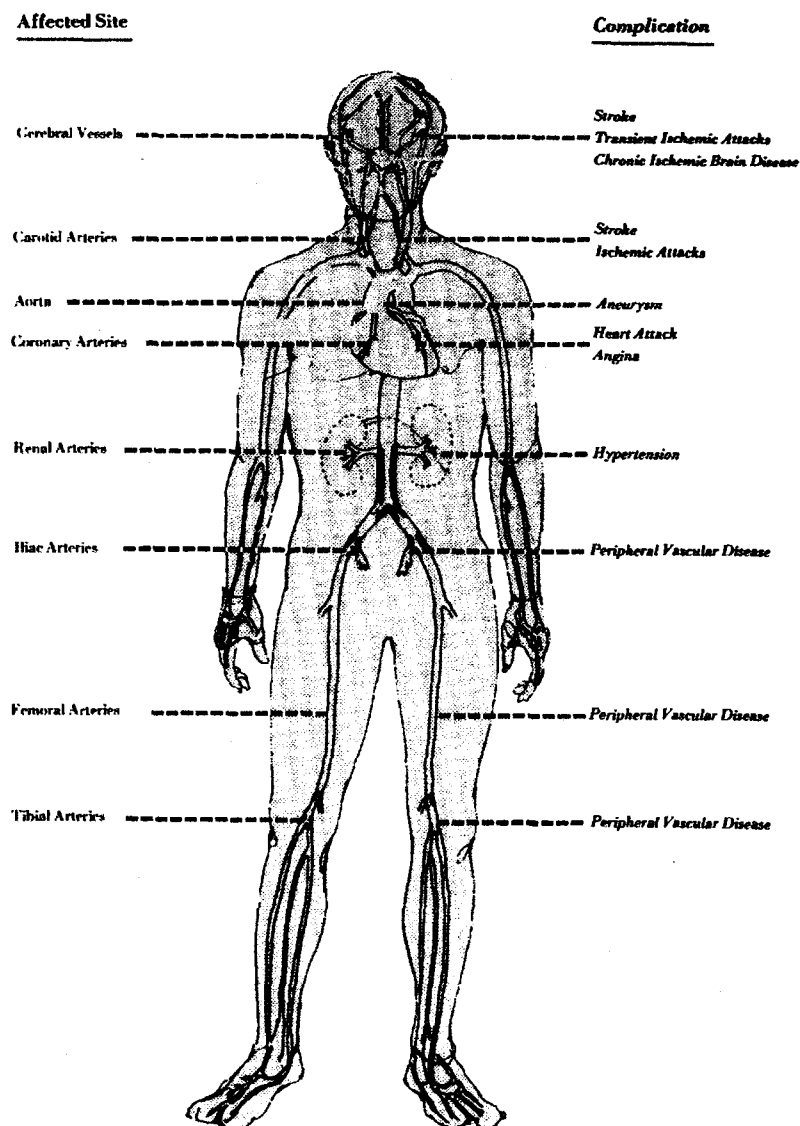


Fig. 1.2 A representation of discrete sites of occurrences of atherosclerotic lesions and their associated complication from the United States Department of Health, Education and Welfare (1977)

Arteriosclerosis is a broad term used to define any condition that causes an arterial vessel wall to thicken and become less flexible. Atherosclerosis is a type of Arteriosclerosis that creates this detrimental condition through the buildup of fatty or connective tissue of smooth muscle (Patel and Vaishnav, 1980). The hardening of arterial walls and reduction of vessel diameter are properties that profoundly affect blood flow.

This project focuses on creating a computer generated model of the arterial system that will incorporate robust methodology for parameter predictions, such as blood pressure and flow in various regions of the body. Its accuracy will be compared against results given in similar endeavors. The model will use age, gender, height, weight and a digitized wave of blood pressure measured at the radial artery to make the predictions.

1.1 Arterial System

As a subset of the cardiovascular system - arteries are a network of vessels responsible for distributing blood throughout the body. As these vessels branch out from the Aorta - a central artery directly connected to the heart - they gradually decrease in diameter and vary in wall thickness (Mates, 1995). Like Yin and Yang or positive and negative, the arterial system is mirrored by the pulmonary system. This system is composed of veins that are responsible for collecting the oxygen-spent blood from tissue and delivering it to the right side of the heart and then the lungs. Some of the general differences between the systems are given in table 1.1 (Nichols et al., 1998; Li, 1987).

Table 1.1 Characteristics of Arterial and Pulmonary System

Arterial System	Pulmonary System
Greater musculature through out system High pressure blood flow (up to 6 times greater than pulmonary) Generally circular vessel cross section	Smaller degree of musculature Low pressure blood flow Generally elliptical vessel cross section
Wall thickness (1 μ to 2mm)	Wall thickness (2 μ to 1.5mm)
High distensibility	Lower distensibility than arteries
Longer vessel length along a vascular section	Shorter vessel lengths

Generally, each component of one system has an opposite in the other system, and, as can be seen above, they are distinct entities. Both are important to cardiovascular health, but historically, modeling of the arterial system has generated the most interest. This may be due to the host of arterial disorders with compounding effects that can be explained or even mapped given a proper understanding of the system properties.

Before embarking on a numerical simulation, it is always best to frame a qualitative picture of the system dynamics and the associated properties. We start off with the ejection of blood from the heart into the primary branch, which is the aorta. Arteries are not rigid tubes. They possess a degree of elasticity that is termed *compliance*. Often compared to the electrical property of capacitance, compliance allows the vessel to expand and functionally store fluid. Once the elastic limit is reached, the vessel contracts to push the fluid down stream. This property ensures a fairly constant mean pressure

throughout the system despite the intermittent pumping action of the heart. Figure 1.3 shows a typical blood pressure waveform, which is the byproduct of one beat of the heart. The systolic portion of the wave represents the period of time the heart actively expels blood through the artery. A rapid increase in pressure often denotes the onset of the systolic phase. The diastolic period occurs once the outlet valve for the left ventricle, the aortic semilunar valve, shuts and is usually characterized by an exponential decrease in pressure.

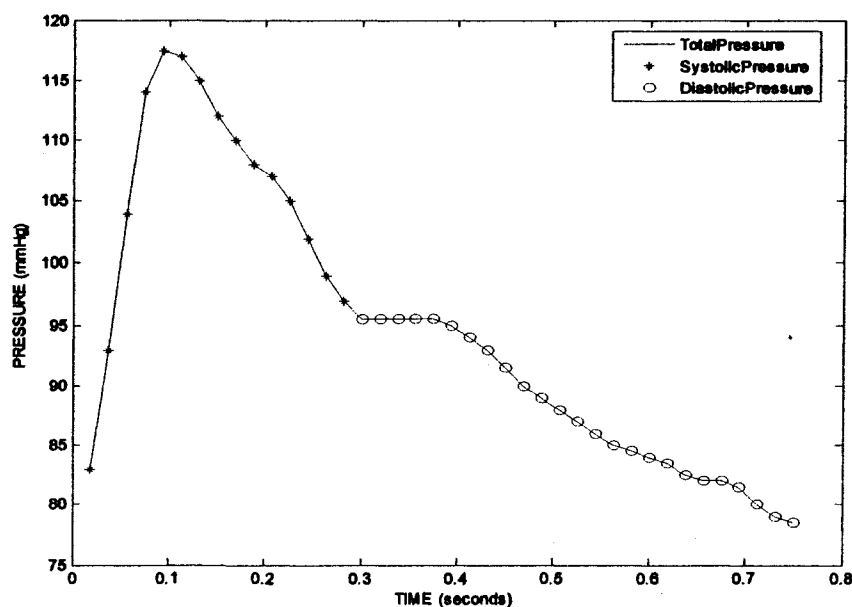


Fig. 1.3 The Primary Components of a Typical Pressure Pulse Wave

Since blood has mass, the motion imparted on it tends to keep it in motion. This is known as fluid momentum, but it has also been called inductance. Unimpeded, the fluid would remain in motion; however, the blood's viscosity opposes this constant motion. As the blood moves through the vessels, viscous drag occurring at the vessel wall impose

an opposing force on the fluid; this is called resistance. To create a visual of the aforementioned properties, a single section of blood vessel could be abstracted into a composition of the three elements in parallel. These three elements can be called resistance, capacitance and inductance as shown in figure 1.4:

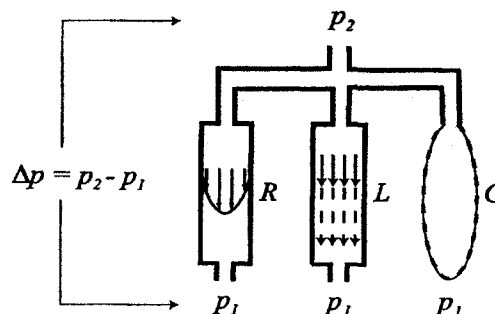


Fig. 1.4 RLC representation on a vessel (Zamir, 2005)

Due to a differential pressure across the vessel, flow is enhanced by inductance, L , and restricted by resistance, R . It should also be noted that capacitance, C , often referred to as compliance (the balloon), initially diverts some flow through the composite, however, at some critical point the balloon contracts to enhance flow through. This is but one of many ways the gross properties can be conceptualized. Abstraction is a wonderful thing. The parallel element model can be rearranged to place the elements in series. Still, although there is great flexibility in the arrangement of the elements, under realistic conditions, the expansion of a vessel occurs simultaneously with a resistance of flow and is enhanced with fluid inertia. Therefore, figure 1.4 is presented as a basic abstraction of those conditions. Additionally, the properties can be represented by electrical components, such as a capacitor, inductor coil and resistor. A vessel can be conceptualized as a discrete element possessing volume with inlet and outlet fluid flow.

Another important property of the arterial system is the blood pulse pattern (or pulse wave), which originates from the heart and gradually changes as it moves through the peripheries. This is due to the aforementioned properties, as well as variations in diameter, dampening and wall thickness. The diameter plays the dominant role in pulse patterns due to vessels that gradually taper to smaller diameters the farther the arteries are from the heart. Figure 1.5, reproduced from *McDonald's Blood Flow in Arteries* (Nichols et al., 1998), demonstrates the variation of blood pulse patterns with respect to location. The two things that should be noted are:

- 1) The shape of the pressure wave changes considerably as it travels away from the heart and on to the leg;
- 2) Although the diastolic and, ultimately, the mean pressure drop as blood gets farther from the heart, systolic pressure rises.

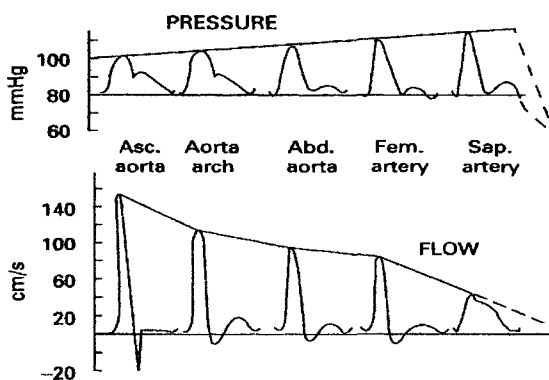


Fig. 1.5 Pressure and flow wave patterns in different locations of the body (Nichols et al., 1998)

1.2 Arterial Modeling

Researchers have developed many models to describe the operation of the cardiovascular system. These models include:

- Direct models in fluid-mechanical form;
- Electrical network analogs;
- Models using analog, digital or hybrid equipment;
- Computer generated models.

The subsequent improvement of these models has led to a greater understanding of some of the factors effecting cardiovascular behavior.

Avolio (1980) created a model of the arterial system, which was an improvement of previous ones (Jager et al., 1965; Snyder et al., 1968; Westerhof, 1969; Westerhof, 1970 and Raines et al., 1974). It gave an analysis of arterial system pressure based on flow resistance and physical properties of the arteries themselves. However, the model did not account for variability in aging or anthropometric parameters. Figure 1.6, reproduced from Avolio (1980) shows the schematic used in the analysis.

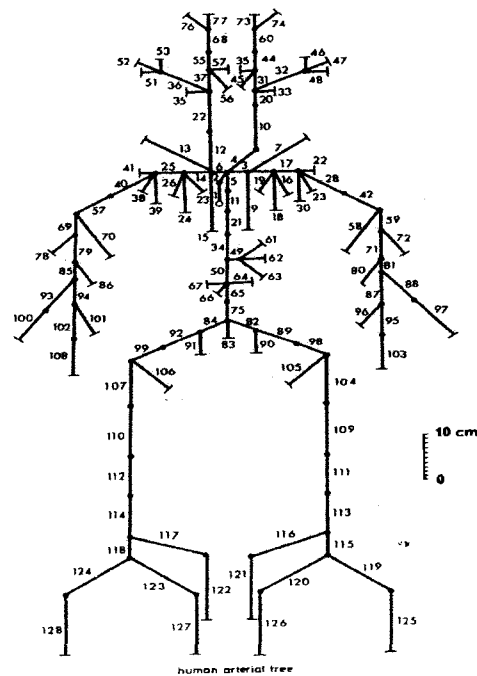


Fig. 1.6 Avolio's schematic of the arterial system (Avolio, 1980)

It should be noted that other workers have had success with computer generated models since Avolio; notably--Stergiopoulos, Young and Rogge (1992); Olufsen (1998); Formaggia, Lamponi and Quarteroni (2003); and Sherwin, Formaggia, Piero and Franke (2003). These workers created time-based models of arterial flow using linearized versions of the Navier - Stokes equation. Although insight can be gained through observing the propagation along a given path during a given period of time, the time-based models do not lend themselves easily to parameter identification. Among the drawbacks of using time-based approaches encountered during this investigation were the need of

knowledge of pressure and flow at all boundaries and prohibitive model runtimes due to the small time steps required for finite element methods (10^{-5} seconds).

Ozawa (1996) developed a one-dimensional, finite difference model that used versions of momentum and continuity equations. The model consisted of 28 vessels and paid closer attention to the boundary points. Like many other models before, the terminating ends were simulated as lumped parameters, but there was also included a leakage function to account for the smaller vessels and vascular beds that were too small and numerous to model independently. Properties such as pulse wave reflection, arterial branch angles and ventricular action were incorporated into the model. Figure 1.7 is a depiction of the model:

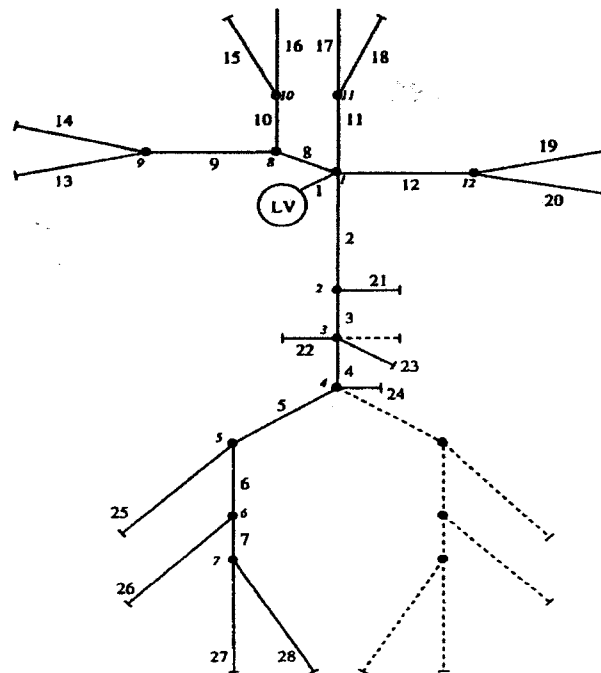


Fig. 1.7 28 Vessel Arterial Model (Ozawa, 1996)

The baseline model parameters were varied in each of the multiple computations of this model. For each iteration of the model the resulting blood pressure parameters were stored in a computer-based library. Radial, as well as other pulse wave measurements were then obtained from 6 test subjects. The radial readings were used to match the best fit iteration of the model to each subject, using the Shepard and Nelder-Mead routines. The other calculated parameters of the model were then compared to those obtained from the subject. The work focused on prediction of the subject's systemic vascular resistance (SVR), as well as prediction of pressure and flow wave forms in their brachial, femoral and carotid arteries.

CHAPTER 2

This chapter addresses physiological parameters of the arterial system that play a significant role in how blood is distributed. Also in this discussion is a treatment of clinical measures that are used to determine the state of the arterial system.

2.1 Properties of Arteries

The arterial network of an individual is composed of a multitude of blood vessels with varied size and physical properties. Remarkably, these properties, and even sizes, exist proportionately across many species. This facilitates the use of information from other animals as input on work involving the human arterial system. In fact, due to the invasive nature of determining many of these properties, data from anatomically similar animals such as dogs, cats and pigs is frequently substituted or extrapolated into human models. Figure 2.1 illustrates the overall shape of the network, which is often called a human arterial tree. Figure 2.2 is a well-published reproduction of the arterial tree of a dog to provide some perspective on the similarities between dog and man.

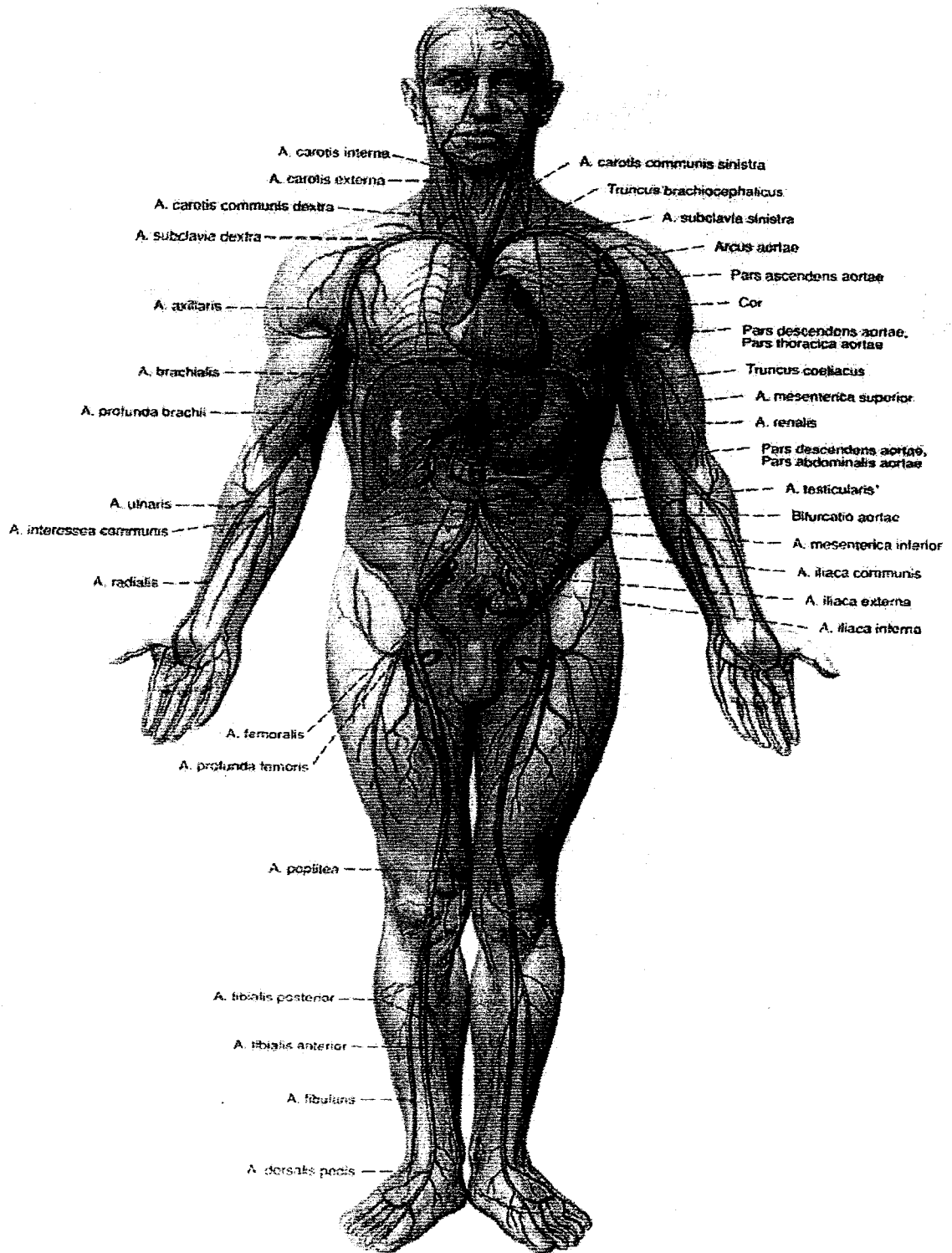


Fig. 2.1 Human Arterial Tree (Putz and Pabst, 1994)

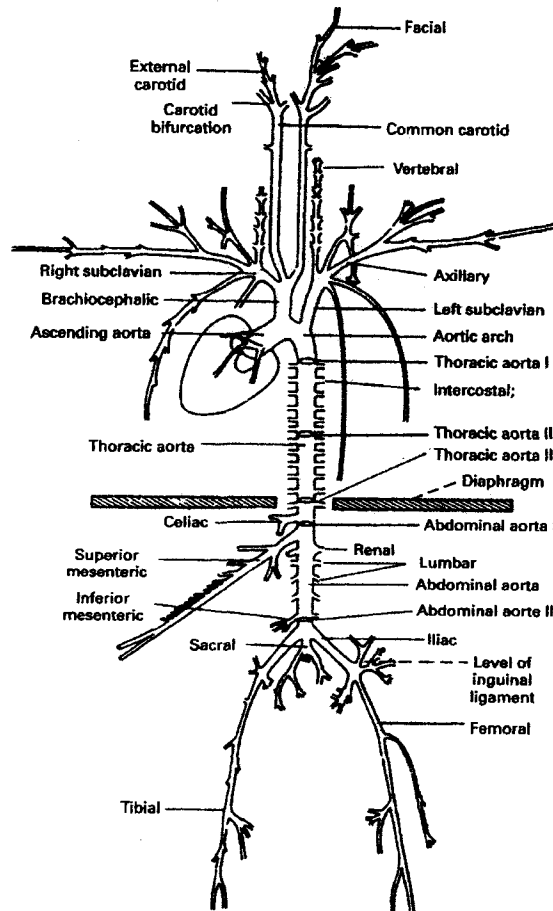


Fig. 2.2 Dog Arterial Tree (Nichols et al., 1998)

Starting with the typical shape of an artery, each vessel gradually tapers to a smaller diameter as the vessel location moves away from the heart. This tapering may not always be symmetrical and varies between vessels. Li (1987) developed a formula to define this taper based on the vessel lumen (cross sectional) area of a vessel, A_0 , and a taper factor k and z distances away from some initial point.

$$A = A_0 e^{-kz} \quad (2.1)$$

Table 2.1 contains some of the taper factors for various vessels when the cross section includes the external diameter.

Table 2.1: Various Vessel Taper Coefficients

Applicable Vessel	k (cm ⁻¹)
Abdominal aorta	0.027±0.007
Iliac artery	0.021±0.005
Femoral artery	0.018±0.007
Carotid artery	0.008±0.004

The arterial walls are anisotropic material composed primarily of elastic elastin fiber, fibrous collagen fiber, muscle cells and an endothelium liner. Smooth muscle provides a degree of stiffness and dilation control through activation by the nervous system.

Collagen fibers laced throughout the vessel wall provide the stiffness, while elastin fibers add elasticity to the vessel. To varying extents, the fibers, along with muscle tissue, exist in most arteries and work together to give the composite wall a membrane like quality.

The endothelium is the inner most lining of the composite artery and aids in vascular transport through the vessel. Though not regarded as a structural component of the arterial vessel, a number of vessel properties have been attributed to its function. For example, the permeability of the lining has been linked to the amount of shear (fluid speed) occurring at a given point. It was discovered that excessive flow, to the point of

excessively high turbulence, could induce a state of excessive permeability that may damage the lining and ultimately produce atherosclerotic regions due to the deposition of material at that point. (Patel and Vaishnav, 1980)

Figure 2.3 depicts a cross section of a typical vessel to show the various layers of an arterial wall, where the three major groups of layers are adventitia, media and intima. The intima is composed primarily of endothelium. The media is composed of elastin, collagen, nonstructural tissue and muscle cells. Finally, the adventitia is mostly composed of collagen and fatty connective tissue.

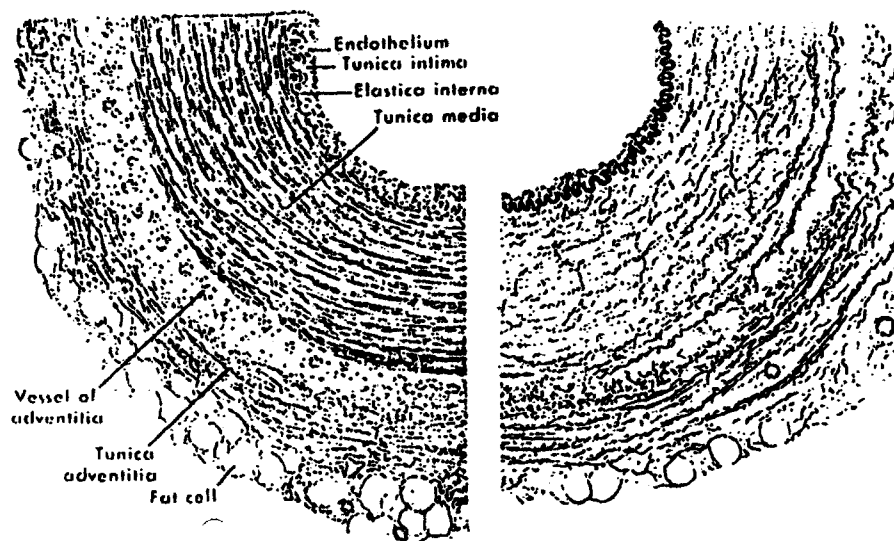


Fig. 2.3 Cross section of a typical arterial vessel (Li, 1987)

Figure 2.4 illustrates the four major constituents, in their relative proportions, according to vessel type. It should be noted that arterial muscle content increases as vessel location

moves away from the heart. Consequently, the radial artery, located in the forearm, contains a much higher percent of muscle than the aorta, which is the first vessel off the heart.

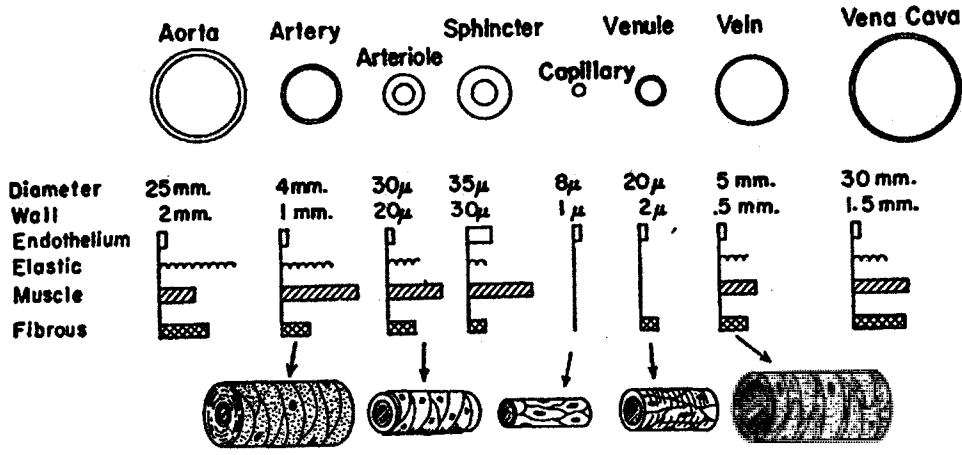


Fig. 2.4 Diameter and wall thickness relative to percentage of vessel wall components (Li, 1987)

The membrane quality means that the walls behave nonlinearly under applied pressure and are considered elastic boundaries for model making purposes. Additionally, the vessel wall thickness to diameter ratio is large enough to consider the larger vessels as thin walled elements. Therefore, Laplace's law for tension, T , relative to applied pressure, p , in a vessel with radius, r , is

$$T = p \cdot r \tag{2.2}$$

and circumferential stress in wall (σ) is

$$\sigma = \frac{p \cdot r}{h} \quad (2.3)$$

where internal pressure - external pressure is p , intramural pressure - extramural pressure results in *transmural pressure*, internal radius is r and vessel thickness is h . Furthermore, it was found that the wall material approaches incompressibility with a poisson's ratio of 0.4998 (or approximately 0.5).

2.2 Vessel Stiffness

The viscoelastic property causes blood vessels exposed to an incremental increase in pressure to gradually move toward a different radius or length. Conversely, an incremental increase in the vessel dimension will initially cause an increase in stress followed by a subsequent decay to a lower stress. This dynamic nature adds a level of complexity to determining vessel stiffness. Arterial compliance, C , is a common parameter assessed to gain knowledge of arterial stiffness and is defined as the change in volume divided by change in diameter with an increase in pressure (Woodman and Watts, 2003). It has the same meaning as arterial capacitance and is commonly determined from changes in vessel diameter with changes in pressure and can be written as:

$$C = \frac{\Delta D}{\Delta P} \quad (2.4)$$

Snyder et al. (1968) give an approximation for volume compliance, C , that can be derived as

$$C \approx \frac{3A z r}{2Eh} \quad (2.5)$$

where z is the vessel length, E is the modulus of elasticity, r is the internal radius, A is the internal cross sectional area and h is the vessel thickness. This approximation (where A and r are average values for the vessel) can be useful for populating a model with parameters. Furthermore, for the purpose of this report, compliance and capacitance shall be used interchangeably.

Distensibility expresses compliance relative to some initial diameter, D , and can be determined by

$$\text{Distensibility} = \frac{\Delta D}{(\Delta P \cdot D)} \quad (2.6)$$

Generally, the modulus of elasticity is the inverse of distensibility, or

$$\text{ElasticModulus} = \frac{\Delta P \cdot D}{\Delta D} \quad (2.7)$$

Young's elastic modulus E is the elastic modulus per unit of vessel thickness h and can be written as

$$E = \frac{\Delta P \cdot D}{\Delta D \cdot h} \quad (2.8)$$

Since the diameter and thickness change nonlinearly with a change in pressure, there have been efforts to track the modulus throughout these changes (Li, 1987; Woodman and Watts, 2003; Taylor, 1966 and Peterson et al., 1960).

The incremental Young's modulus, E , is the result, which is a complex quantity E_c that varies with the frequency of a pressure or flow wave (Li, 1987).

$$E = E_{\text{dyn}} + \eta\omega \quad (2.9)$$

Where:

$$E_{\text{dyn}} = |E_c| \cos\phi \quad (2.10)$$

$$\eta\omega = |E_c| \sin\phi \quad (2.11)$$

The wall viscosity, η , varies with angular frequency, ω ; however, their product is small compared to E_{dyn} (~10% of elastic modulus) and is nearly constant above 2 Hz.

There is a lag between applied pressure and the subsequent motion of the vessel wall.

This attribute is tracked as the phase angle, ϕ between pressure and wall motion. Taylor (1966) derived values for the quantity using:

$$\phi = \tan^{-1}\left(\frac{\omega\eta}{E}\right) \quad (2.12a)$$

which converted to

$$\phi = \phi_o (1 - e^{-\kappa\omega}) \quad (2.12b)$$

where κ can be 1 or 2.

Avolio (1980) and Karamanoglu (1995) later limited k to 2 and determined values for ϕ_o and ϕ .

Olufsen (1998) extrapolated a relation between elastic modulus E , vessel thickness h and vessel radius r_o from data given by Stergiopoulos (1992). The graphical representation of the fitted curve is given in figure 2.5.

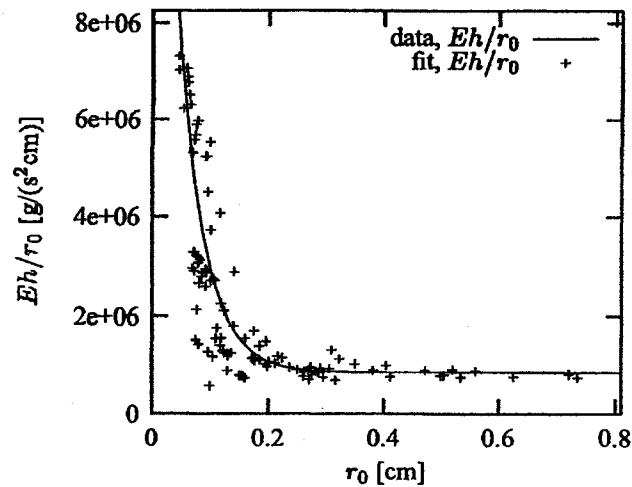


Fig. 2.5 Fitted Eh/r_o versus r_o curve (Olufsen, 1998))

The equation of the fitted curve is given as

$$\frac{Eh}{r_o} = k_1 e^{k_2 r_o} + k_3 \quad (2.13)$$

where $k_1 = 2.00 \times 10^7$ ($g/(s^2 cm)$), $k_2 = -22.53$ (cm^{-1}) and $k_3 = 8.65 \times 10^5$ ($g/(s^2 cm)$).

At this point, it should be noted that there are a number of models from which data can be gathered to construct an arterial model (Westerhof, 1969; Raines et al., 1974; Stergiopoulos, 1992; Olufsen, 1998; Karamanoglu et al., 1995 and Schaaf et al., 1972). Yet, care should be exercised because certain vessels exhibit variations in elasticity with age and health and all

exhibit variations in radius, length and elasticity with variations in a subject's weight and height (Nichols, 1998; Karamanoglu et al., 1995; Steinberg et al., 1992; Sonesson et al., 1993; Ahlgren et al., 2002; Dotter et al., 1950). Equation 2.13 was used for select vessels in earlier versions of the program but was later replaced with additional statistical data.

2.3 Aging, Gender and Body Surface Area

When trying to account for changes due to aging the picture quickly becomes more complex. For instance, it is fairly instinctual to consider a lengthening of vessels as individuals grow from child to adulthood. However, it has been reported that the aorta, which is the main branch of the arterial tree, continues to grow in length long into adulthood (Dotter et al., 1950). Figure 2.6 plots the length of the thoracic portion of the aorta versus age.

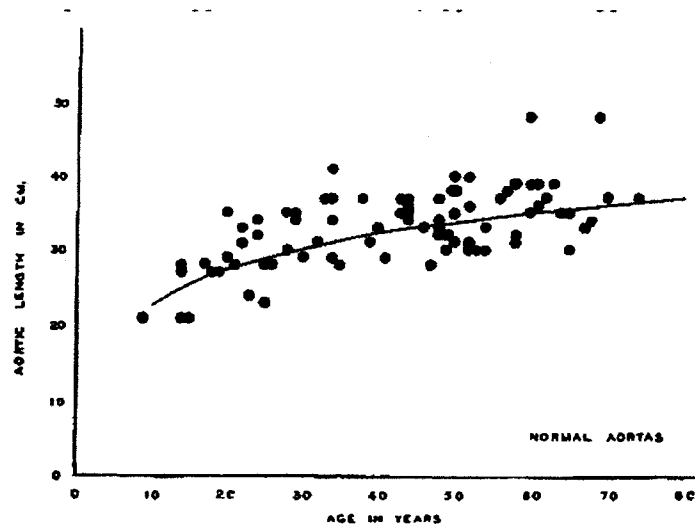


Fig. 2.6 Length of thoracic aorta versus age reproduced from Dotter, et al. (1950)

The curve fitted to the data depicted in figure 2.6 is given in equation 2.14.

$$\text{length} = 6.76 + 15.86(\text{Log (age)}) \quad (2.14)$$

Pennington and Soames (2005) have attributed this extended growth period to a gradual shrinkage of the intervertebral discs and a corresponding shortening of the spinal column with advancing years. As a direct result, the variation in aorta length leads to variations in distance between its branches (celiac, renal, etc.), which can be important when investigating the aorta in detail. (Pennington et al., 2005; Yahel et al., 1998)

The diameter of the aorta, as well as more muscular vessels such as the brachial artery, has been known to steadily increase with advancing age (Sonesson et al., 1994; Kiechl and Willeit, 1999; van der Heijden-Spek et al., 2000). Additionally, a rise in mean arterial pressure (MAP), which has been found to increase with age (Nichols et al., 1985), has been correlated to an increase in radial and carotid artery diameters (Laurent et al., 1994 and Boutouyrie et al., 1999). Furthermore, there have even been correlations drawn between gender and body surface area (BSA). Table 2.2 shows some of the relationships:

Table 2.2 Equations for various artery diameters

Equation for artery diameter	Source
$\text{Aortic diameter} = 0.495 + 8.6907(\text{BSA})$ <p>where: diameter is in mm and BSA is in sq. meters (2-15)</p>	Steinberg et al. (1992)
$\text{Carotid artery diameter} = 0.336(\text{BSA}) + 0.307$ <p>where: diameter is in cm and BSA is in sq. meters (2-16)</p>	Steinberg et al. (1992)
$\text{Femoral diameter} = 0.350(\text{BSA}) + 0.256$ <p>where: diameter is in cm and BSA is in sq. meters (2-17)</p>	Steinberg et al. (1992)

Generally, above the age of 20 years, gender and age have varying degrees of influence on vessel diameter (Benetos et al., 1993; Sonesson et al., 1994; Sass et al., 1998; Kiechl and Willeit, 1999 and van der Heijden-Spek et al., 2000). For example, aortic and carotid diameters correlate well with age, while the femoral artery does not. Yet, with regard to gender, males exhibited larger diameters than females for all vessel types examined.

Due to its viscoelastic properties, the vessel wall thickness decreases in response to a pressure induced increase in diameter. Therefore, one could conclude that the increase in mean arterial pressure with age would cause a decrease in wall thickness. This, however, is not the case. O'Rourke and Hashimoto (2007) reported thickening of arterial walls due to an increase of material in the intima and media layers. It should be noted that the increase of non-load bearing material at the media progressively separates the elastin fibers and is accompanied by a thinning of the fibers. Now combine this with an increase in the percentage of collagen content, as reported by Nichols and O'Rourke (1998), and it becomes clear that the stiffness of the vessel increases with age. An increase in vessel stiffness with age is a fairly broad statement, but it can be assessed as an increase of vessel elastic modulus with age. Since the inverse of the elastic modulus is distensibility, an increasing elastic modulus with advancing age means a decreasing distensibility. Again this property is not uniform across the arterial tree with increasing age. Benetos et al., (1993) showed that while distensibility did decrease with age, the distensibility of the femoral artery increased slightly; then it decreased with age (see figure 2.7). Centrally located arteries like the aorta tend to exhibit increased stiffness. The behavior of other peripheral vessels is still questionable.

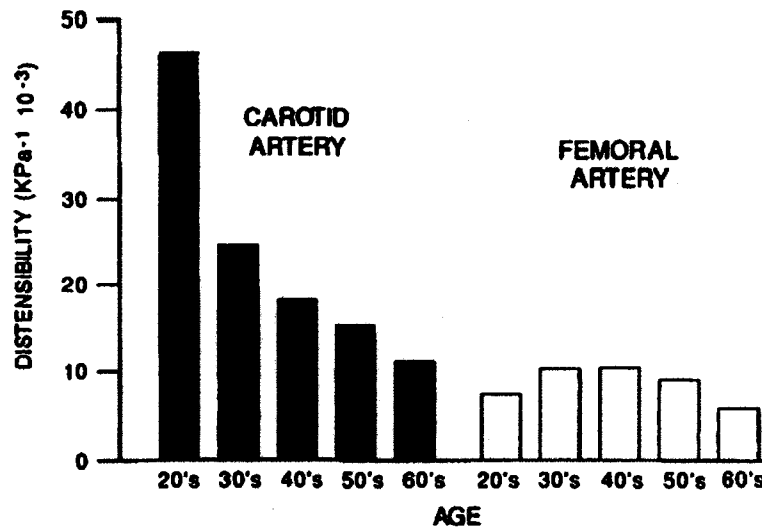


Fig. 2.7 Distensibility versus age for the femoral and carotid arteries (Benetos et al., 1993)

Following the work of Bergel (1961a and b), who charted the reaction of a dog's arterial tree to static and dynamic pressure loads, Learoyd and Taylor (1966) observed the reaction of various vessels in the human arterial tree. The age from which the samples were drawn ranged from 11 - 52 years of age and was ultimately segregated into 2 groups - those above 35 and those below 35. It is rare to find dynamic wall properties extracted from the human carotid, thoracic, abdominal, iliac and femoral arteries of one group of subjects. The sample size was small, but the results provided valuable insight into the dynamic characteristics of the arterial tree across age, frequency of pulsatile pressure and location on the arterial tree. Figure 2.8 depicts trends in dynamic elastic modulus for various arteries across two age groups.

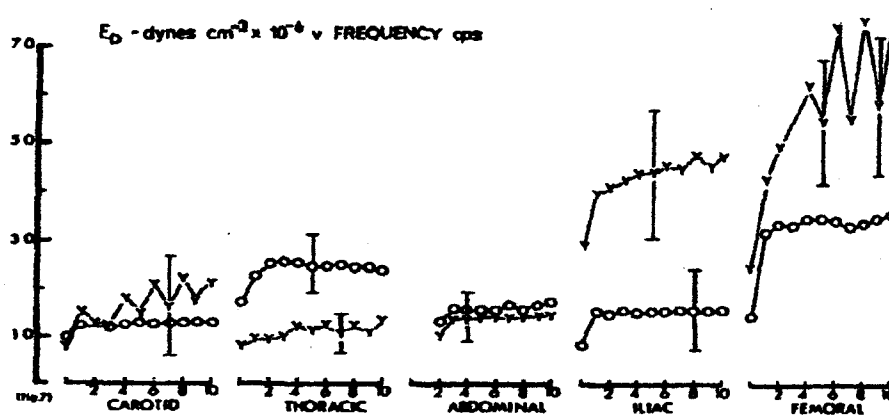


Fig. 2.8 The dynamic elastic modulus versus frequency of applied pressure for the human carotid, thoracic, abdominal, iliac and femoral arteries, where subjects above 35 years of age are represented by 'O' and those below 35 years of age are represented by 'Y' (Learoyd and Taylor, 1966)

Still, the results of the study conducted by Learoyd and Taylor (1966) illustrate that the trends in wall properties with age are not consistent across the arterial tree. Furthermore, it should be emphasized that the data gathered by Learoyd and Taylor required the harvesting of the arteries from the subjects. Obtaining this information from a live subject in a clinical environment is impractical if not impossible. The medical community has, however, reached a compromise by using more dispersed parameters to get an overall picture of the health of the arterial system. The reduction of properties such as large artery and oscillatory compliance has been linked to impaired pulsatile function of the cardiovascular system (McVeigh et al., 1999). Similar in concept to the arterial compliance of a vessel, large artery compliance (or capacitive compliance) is basically the ratio of the fall of blood volume to the fall of pressure during the diastolic period of a pressure pulse. This measure

This measure lumps the total compliance of the arterial system into one parameter. The oscillatory compliance is a similar ratio, however, only the oscillating portion of both volume and pressure are considered (O'Rourke and Mancia, 1999). McVeigh, et al. (1999), showed how the large artery and oscillatory compliances declined with age, which was in sharp contrast to the systemic vascular resistance (SVR). Figure 2.9 depicts large artery compliance and SVR versus age.

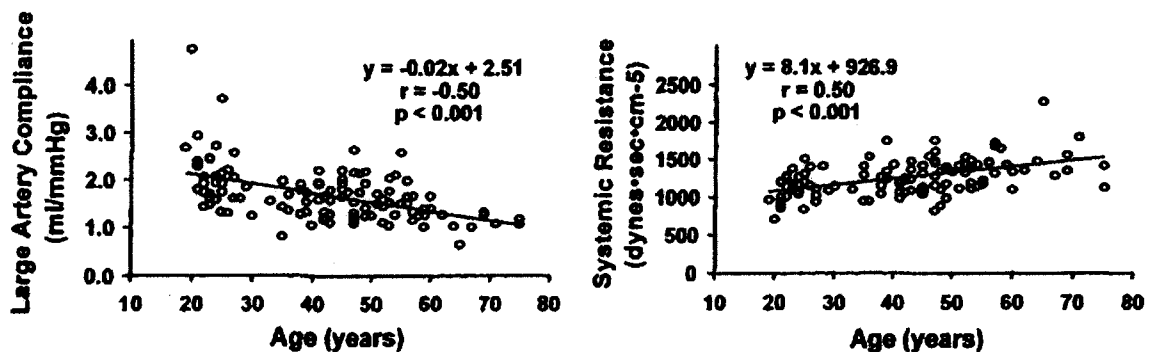


Fig. 2.9 Large artery compliance and SVR versus age. Data obtained through invasive measurements. (McVeigh et al., 1999)

Large artery and oscillatory compliances are further addressed in the discussion of Windkessel models. As for SVR, most of the resistance that opposes blood flow from the heart comes from small arteries and arterioles and capillaries. In hypertensive individuals, these vessels increase resistance above normal levels. SVR is a measure that can be used to monitor medical treatment of those suffering from hypertension (Patel and Vaishnav, 1980).

2.4 Parameter Estimation

As previously discussed, determination of cardiovascular parameters is important to the identification and/or treatment of many ailments. Some of these parameters must be

obtained through invasive means. For instance, systemic vascular resistance (SVR), a parameter important for determining the dosage of vasodilatory medication, is derived from two invasively measured parameters. SVR is usually calculated by dividing the difference between mean arterial pressure and central venous pressure by the cardiac output (CO) (invasively obtained) (Xiao et al., 2002). Once CO is known, one way of calculating SVR (Nichols et al., 1998), in (dyne-secs)/cm⁵, is

$$SVR = \left(\frac{MAP}{CO} \right) \cdot 80 \quad (2.18)$$

An example of the use of calculations to replace the need for invasive measures is the noninvasive derivation of pressure in the aorta (Karamanoglu, 1997). A once exclusively invasive measurement, noninvasive measures of peripheral pulse pressure can be fed through a transfer function to derive aortic pressure (Li, 1987; Mates, 1995 and Nichols and O'Rourke, 1998). These transfer functions can be described as a lumping of various arterial properties between the point of noninvasive measure and the area of interest in the arterial system. This function shows the percent amplification of each frequency of the aortic pressure wave as it moves from the heart to the radial artery (A-R amplification). Multiplying the aortic pressure value by the amplification value at the corresponding frequency will produce a theoretical representation of a blood pressure wave in the radial artery. Conversely, the inverse of the aorta-radial transfer function will provide a radial-aorta transfer function for multiplication with a radial wave for determination of aortic pressure (R-A amplification). Doppler devices are normally used to provide data for use with these transfer functions. In a reply to O'Rourke et al.,

(2003), Hope et al., (2003a) gives an outline of the various methods used to obtain a transfer function between the radial artery and the aorta.

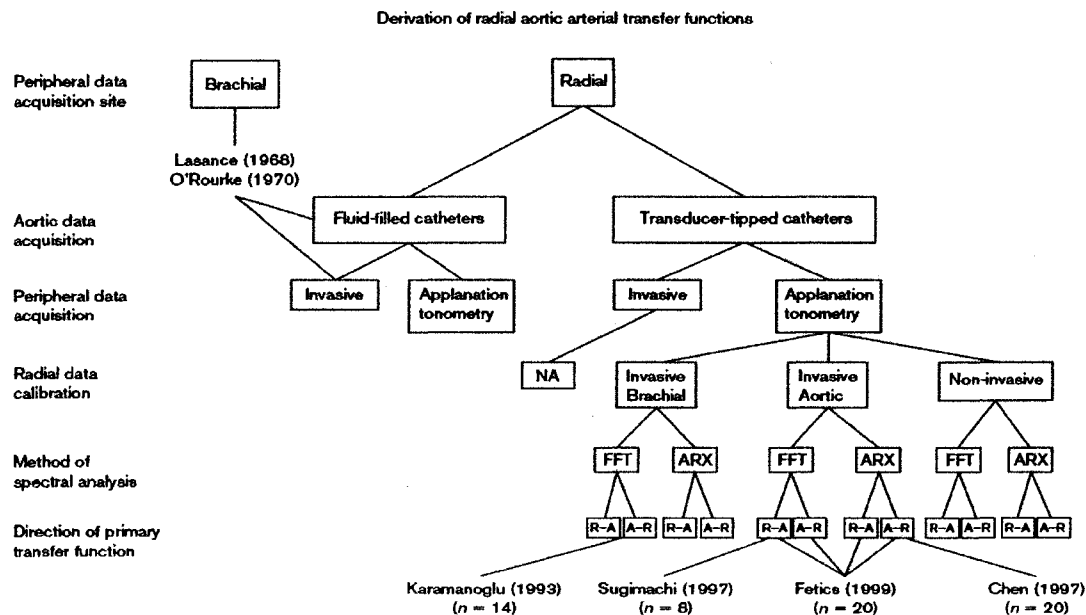


Fig. 2.10 Methods used to derive transfer functions between radial artery and aorta

Basically, figure 2.10 outlines the steps used by various workers to create generalized transfer functions. Starting with simultaneous pressure waves measured at the aorta and some peripheral site – two pressure waves are measured either invasively (via a catheter) or noninvasively (via Applanation tonometry). After indexing and cleaning them up, the signals are then decomposed via Fast Fourier Transformation or some parametric identification method (such as an Autoregressive exogenous model, ARX). Based on changes from the decomposed outputs, transfer functions are created. The data is usually averaged across a sampled population to create a generalized transfer function.

There have been transfer functions developed for carotid-aorta and brachial-aorta as well (Karamanoglu and Feneley, 1996 and Stergiopoulos et al., 1998). O'Rourke et al., (2004) provided a compilation of aorta-radial transfer functions from Hope (2003b), Chen (1997) and Karamanoglu et al., (1993), which is reproduced in figure 2.11.

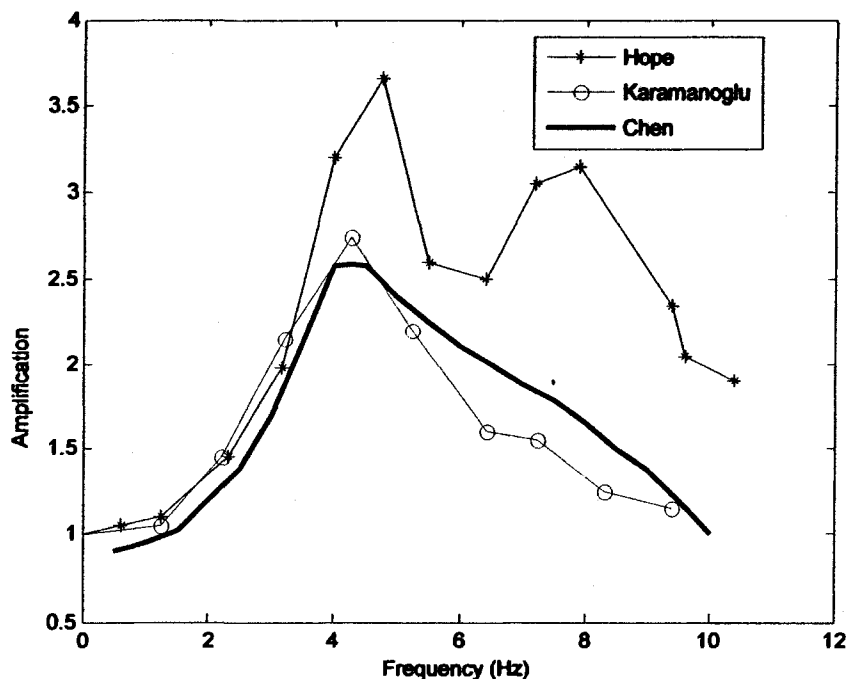


Fig. 2.11 A comparison of transfer functions for amplification of blood pressure pulse from aorta to radial artery (as interpreted from O'Rourke et al., 2004)

Considering other useful measures, Karamanoglu (1997) illustrated some methods for the estimation of cardiovascular parameters from the features of a blood pulse wave. The figure below is a reproduction of his example of 5 key features of a blood pulse wave that are often used to calculate other cardiovascular based parameters.

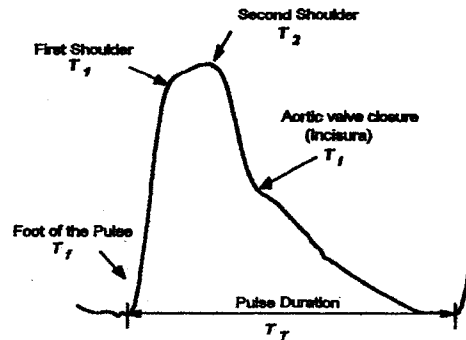


Fig. 2.12 Parameters of a pulse wave used to calculate cardiovascular parameters
(Karamanoglu, 1997)

Referring to figure 2.12, one of the useful features that can be determined is the time of aortic valve closure (T_i), which will subsequently provide the duration of blood ejection from the heart, as well as mark the cessation of the systolic phase and the onset of the diastolic phase. The extent of wave reflection (a subject addressed in section 3.2), sometimes referred to as Augmentation Index, AI , is a ratio of the difference between the initial pulse pressure at T_1 and the resulting reflected pressure at T_2 to the pulse pressure (Woodman and Watts, 2003). Pulse pressure should be considered any part of the pressure wave above the foot of the pulse (at T_f), while the maximum pressure due to injection occurs at T_1 and the wave reflected from downstream (or distal) superimposes itself on the forward travelling wave to produce a composite wave with pressure augmentation at point T_2 . This parameter provides some insight into the stiffness of the system and can be determined by

$$AI = 100 \cdot \left(\frac{P_2 - P_d}{P_1 - P_d} \right) \quad (2.19)$$

Where, P_1 and P_2 are pressures corresponding to points T_1 and T_2 respectively, and P_d is the diastolic pressure corresponding to point T_f . The actual indexing of the points, via some algorithm, is not entirely straightforward and requires deriving several derivatives of the given pressure wave. Kelly et al., (1989), provide a detailed methodology for locating these points.

The cardiac output (CO), which is an average of the total amount of blood expelled from the heart, is another useful parameter. Measured in liters (or milliliters) per minute, this value varies with age, ejection duration (T_{ej}), heart rate (HR) and body surface area (BSA). Segers et al., (2001), used the following equation to derive CO:

$$CO = \frac{HR}{1000} [-6.6 + 0.25(T_{ej} - 35) - 0.62(HR) + 40.4(BSA) - 0.51(\text{age})] \quad (2.20)$$

This was an empirically derived equation and it should be noted that, in each instance mentioned, the ejection duration is represented by a different notation to show that there may exist some difference in how each author defined this value.

Takazawa et al. (1998) were able to predict a subject's age by interpreting various points on the second derivative of the photoplethysmogram pressure wave taken at her/his fingertip. Applying these principles to the second derivative of a pressure wave recorded from the

radial artery, figure 2.13 is one interpretation. The ratio of $\frac{time_B}{time_A}$ can be determined from a given age range.

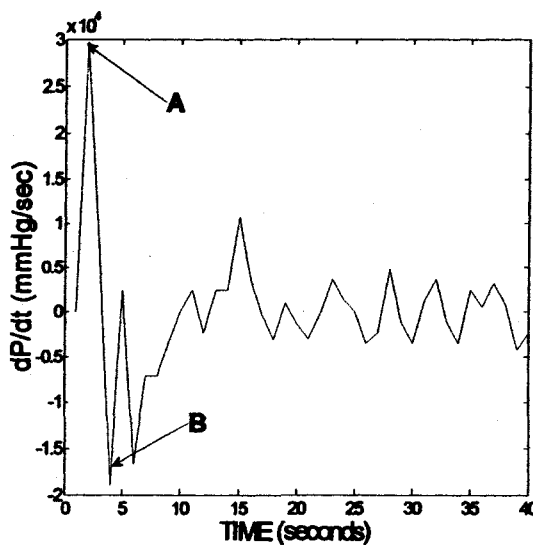


Fig. 2.13 Second derivative of radial pressure wave

For calculating body surface area (BSA) Livingston and Lee (2001) give, among a selection,

$$BSA = 0.1037(\text{weight}^{0.6724}) \quad (2.21)$$

for a subject's weight less than 10 kg, and for those above

$$BSA = 0.102(\text{weight}^{0.6854}) \quad (2.22)$$

and

$$BSA = 0.0495(\text{weight}^{0.6046})(\text{height}^{0.2061}) \quad (2.23)$$

for all weights.

CHAPTER 3

3. Mathematical Model

The prerequisite theory for developing the transmission line model used in this report is provided in this chapter. This treatment includes the derivation of pressure and flow equations, the use of Fourier theory in model calculations and an introduction to windkessel models.

3.1 Fourier Analysis

Although a pulse wave is usually considered one beat, this one wave can be broken down into a combination of many waves. Each individual wave will have its own frequency of occurrence that is a harmonic of the overall pulse frequency. The relative strengths of each harmonic are what give a pulse pattern its shape. Figure 3.1, reproduced from *McDonald's Blood Flow in Arteries* (Nichols and O'Rourke, 1998), shows some of the harmonic content of a hypothetical pulse wave.

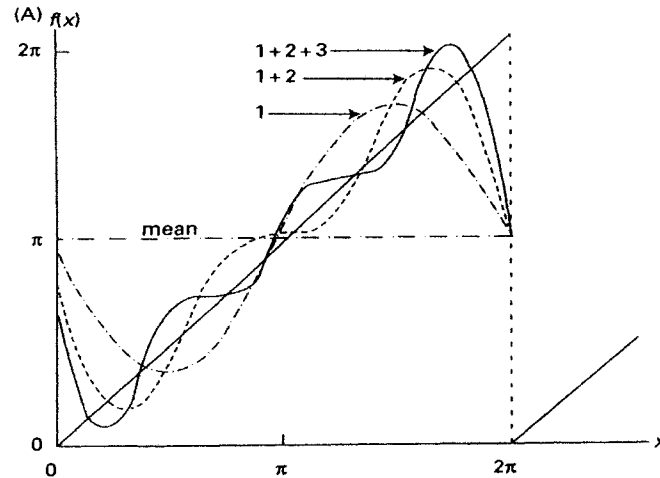


Fig. 3.1 Fourier decomposition of hypothetical wave. The original wave (solid) and constituent harmonics (dashed and dotted lines) (Nichols and O'Rourke, 1998)

Note the arbitrary function depicted with a solid line, in figure 3.1, and its harmonic components for the first three harmonics. The three harmonics, respectively, represent 1, 2 and 3 times the frequency of the original wave. The dotted wave represents the subtraction of the third harmonic component from the original wave. The dashed line represents the subtraction of both the second and third harmonics.

The above decomposition is arrived at by first considering the original function, which is in the time domain, as a finite but repeating function $F(t)$ in the frequency domain. The function may be pressure, flow or any quantity versus some period of time. Frequency, f , of the function would be given by the inverse of its total time period, T_T , or;

$$f = \frac{1}{T_T} \quad (3.1)$$

Then angular frequency ω is given by

$$\omega = 2\pi f \quad (3.2)$$

Fourier theorem states (Nichols and O'Rourke, 1998) that if $F(t)$ is a continuous function of time t and repeats every time period T_T , then

$$F(t) = [0.5A_0 + A_1 \cos(\omega t) + A_2 \cos(\omega t) + \dots + A_n \cos(\omega t) + B_1 \sin(\omega t) + B_2 \sin(\omega t) + \dots + B_n \sin(\omega t)] \quad (3.3)$$

Which can then be multiplied by the change in time dt and integrated between 0.0 and 2π and reduced further to

$$F(t) = 0.5A_0 + \sum (A_n \cos(n\omega t) + B_n \sin(n\omega t)) \quad (3.4)$$

where,

$$A_n = (1/\pi) \int_0^{2\pi} F(t) \cos(n\omega t) dt \quad (3.4a)$$

and

$$B_n = (1/\pi) \int_0^{2\pi} F(t) \sin(n\omega t) dt \quad (3.4b)$$

$A_0/2$ is considered the mean value, and each harmonic n is composed of a phase angle ϕ , a sin and cosine component that can be expressed with trigonometry as

$$M = (A^2 + B^2)^{0.5} \quad (3.5)$$

$$\text{Tan } \phi = B/A \quad (3.6)$$

and graphically, as depicted in figure 3.2.

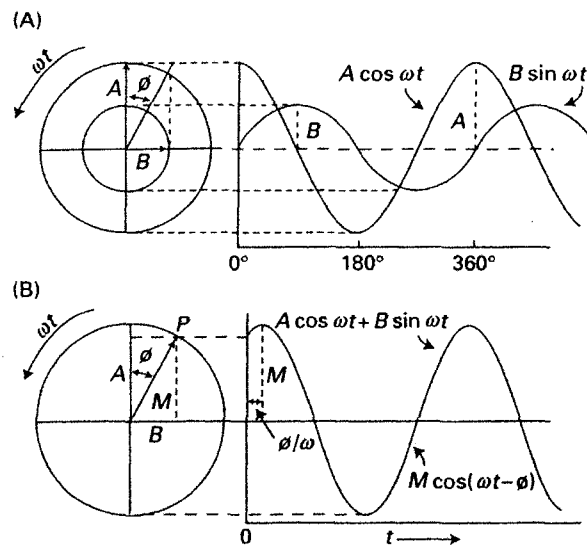
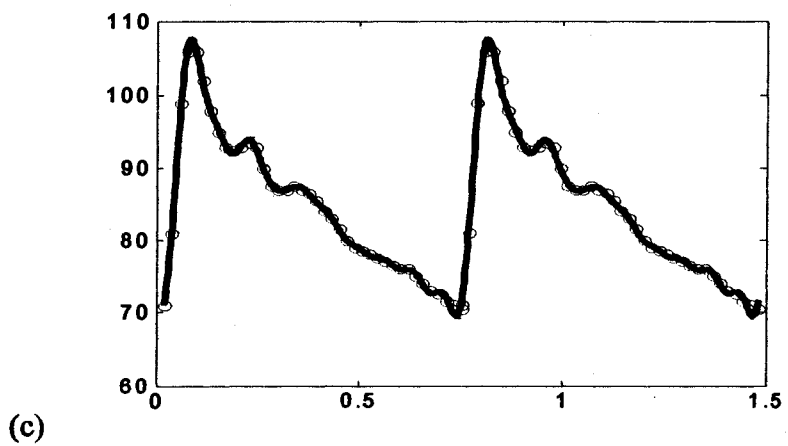
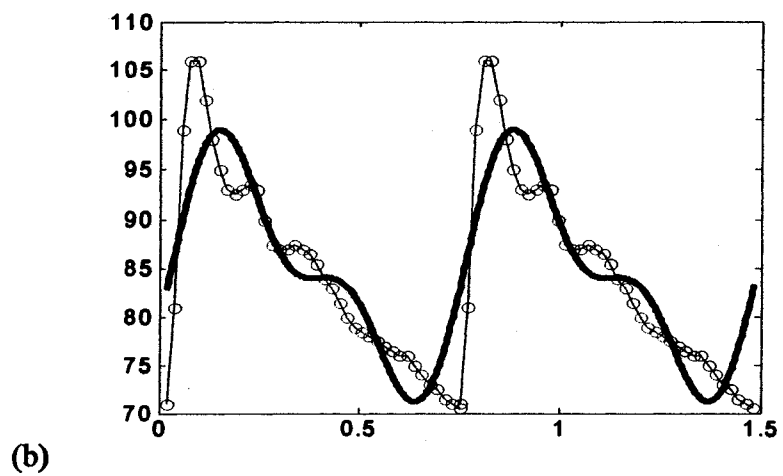
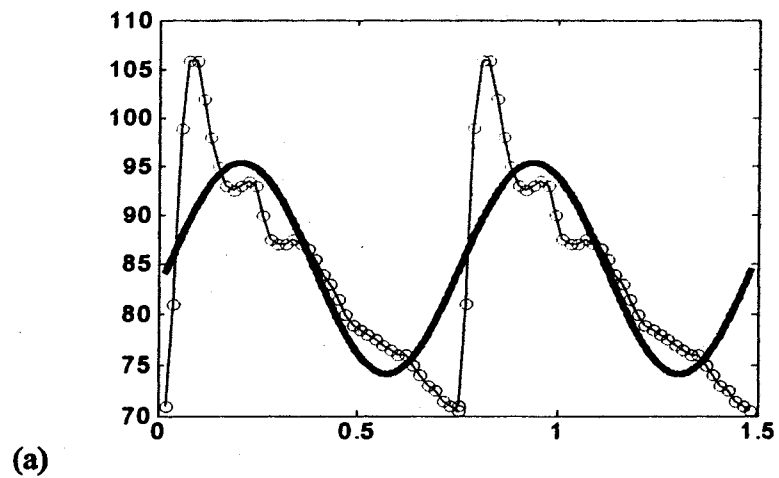


Fig. 3.2 Representation of a single harmonic in a Fourier analysis (Nichols and O'Rourke, 1998)

M is named modulus, which is the amplitude, and the phase angle ϕ is an additional value used for the argument

$$M \cos(\omega t - \phi) = A \cos(\omega t) + B \cos(\omega t) \quad (3.7)$$

Figures 3.3 (a) - (c) show the gradual approximation of two pressure waves (highlighted with 'o') using Fourier curves (solid lines) of 1, 1+2 and then the summation of the first 10 harmonics. Usually, 10 harmonics are sufficient for approximating pressure waves.



Figs. 3.3 a,b & c Fourier Approximation of the 1st, 2nd & 10th Order, respectively.

3.2 Wave Propagation

Wave propagation can scarcely be discussed without addressing the speed of the wave.

In a blood vessel, wave velocity can be determined from the Moens-Korteweg equation:

$$c_0^2 = \frac{E h}{2 r \rho} \quad (3.8)$$

This equation is used with the assumption that the vessel is a thin wall tube, where E is the modulus of elasticity, h is the wall thickness, r is the radius and ρ is blood density.

Additionally, it has been shown (Chandran, 1992) that this equation varies with frequency components of the composite wave and, with the help of angular frequency ω , can be expressed as

$$c_0^2 = \frac{E h}{2 r \rho} [1 - (\omega^2 \rho (\pi r^2)^2) (E^{-1})] \quad (3.9)$$

Flow through the arteries is basically a series of pulsed waves of blood with each wave comprised of a forward moving component and a backward component. Analogous, in principle, to waves that radiate from the center of a bathtub and reflect off the tub wall and back to the point of origin, the backward component is a wave reflected from some location distal (downstream) of the point where readings are being gathered. The reflection normally reaches the advancing wave near the onset of the forward wave's

diastolic period and often amplifies diastolic and part of the systolic pressure. A forward traveling wave, in a vessel, can be represented by the equation:

$$P_{\text{forward}} = P_I (e^{i\omega(t - (x/c_o))}) \quad (3.10)$$

where P_I is the magnitude of the forward or incident wave, t is the time it takes to traverse the vessel (z/c_o) in seconds, ω is the angular frequency, x is the distance from the vessel inlet and c_o is the wave speed. Upon reaching the end of the vessel, the reflected wave can be

$$P_{\text{reverse}} = P_R (e^{i\omega(t - (z/c_o) - (z-x)/c_o)}) \quad (3.11)$$

where z is the vessel length and P_R is the magnitude of the reverse wave. Using P_{forward} and P_{reverse} , and assuming that after the initial reflection no others occur, the percentage of wave reflection, or reflection coefficient Γ , can be defined by ($P_{\text{reverse}} / P_{\text{forward}}$). By adding the forward and backward waves to determine a composite pressure P_A at $x=0$, the following equation can represent a pressure wave:

$$P_A = P_I (e^{i\omega t}) + P_R (e^{i\omega(t - (2z/c_o))}) = P_I e^{i\omega t} (1 + \Gamma e^{-2i\omega z/c_o}) \quad (3.12)$$

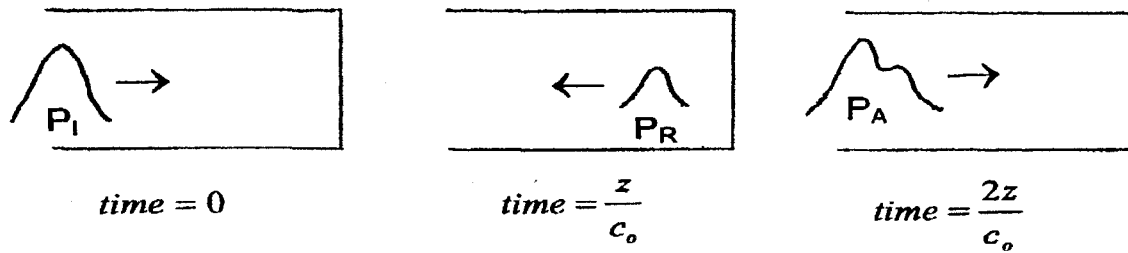


Fig. 3.4 Composite pressure wave from incident and reflected waves

In the case of figure 3.4, $\Gamma = 1$ since 100% of the incident is reflected back. Now if a slight opening existed at the end of the length, a percentage of the wave would be reflected while the remaining percentage would be transmitted through. The ratio of transmitted pressure, P_T , to incident pressure, P_I , can be written as

$$T_{eff} = \frac{P_T}{P_I} = 1 + \Gamma \quad (3.13)$$

This is good for calculations in the time domain and is intuitive to grasp; however, a more abstract form will be required to perform calculations in the frequency domain. The concept of *impedance* makes it convenient to derive pulse pressure values in the frequency domain. Impedance is a term that describes the resistance to flow and is determined by the ratio of pressure to flow. The three types of impedance referenced by this include *Input Impedance*, *Characteristic Impedance* and *Terminal Impedance*.

Terminal Impedance (Z_T) is the ratio of average pressure to average flow across a vascular bed. It is often used to lump together the parameters of a vascular bed to reduce

the complexity of models. Although it is similar to resistance, it is usually much smaller, due to the relatively small pressure drop across vascular beds. If Q_{ave} and P_{ave} represented average flow and average pressure, respectively, terminal impedance could be determined from the following equation:

$$Z_T = \frac{P_{ave}}{Q_{ave}} \quad (3.14)$$

Characteristic Impedance (Z_o) is a conceptual form of impedance. It can be derived from the ratio of pressure and flow, or from the water-hammer as shown below

$$Z_o = \frac{(\rho c_o)}{(\pi r^2)} \quad (3.15)$$

but, it is frequently derived from vessel properties and Womersley factors (Taylor, 1966; Avolio, 1980; Li, 1987 and Nichols and O'Rourke, 1998). This parameter determines the amount of impedance present if the vessel, or system of vessels, was infinitely long and no reflection occurred. Despite this abstraction, characteristic impedance simplifies the calculation of input impedance. Womersley (1957) derived a formula for Z_o , which is

$$Z_o = \frac{(\rho c_o)}{((1 - v^2)^{0.5})} (1 - F_{10})^{-1/2} \quad (3.16)$$

To account for lag between pressure increase and subsequent motion of the vessel wall, Taylor (1966) later modified the equation to:

$$Z_o = \frac{(\rho c_o)}{((1 - v^2)^{0.5})} \cdot ((1 - F_{10})^{-1/2}) [\cos(\phi/2) + j\sin(\phi/2)] \quad (3.17)$$

In this instance v is the Poisson's ratio of the vessel wall and, as discussed in section 2, ϕ is the phase angle (in radians) between pressure and vessel wall. F_{10} is a parameter that uses the zero order Bessel function J_0 and first order Bessel function J_1 of the Womersely number α to quantify the stability of the propagating fluid as shown below

$$F_{10} = \frac{(2J_1(\alpha j^{3/2}))}{(\alpha j^{3/2} J_0(\alpha j^{3/2}))} \quad (3.18)$$

Similar in concept to the Reynolds number, the Womersely number, α , is the ratio between inertial forces and viscous forces (fluid viscosity, μ) as shown below:

$$\alpha^2 = \frac{r^2(\omega \rho)}{\mu}, \quad \text{where } \alpha \text{ is dimensionless.} \quad (3.19)$$

Input Impedance (Z) is derived from a measure of the flow and pressure at the inlet of a vessel. It is affected by wave reflection and is frequency dependent. The ratio of pressure to flow of each individual harmonic is calculated and then the harmonics for the calculated values are combined to give input impedance versus frequency. If $|Q|$, $|P|$, θ and ϕ represented the magnitude of flow, the magnitude of pressure, the phase angle of flow and the phase angle of pressure respectively, then Z for a given frequency in the time domain would look like:

$$Z = \frac{|P| \exp^{j(\omega t + \theta)}}{|Q| \exp^{j(\omega t + \phi)}} \quad (3.20)$$

In the frequency domain, input impedance can be calculated by the following equation

$$Z = Z_0 \frac{(1 + \Gamma e^{-2\gamma z})}{(1 - \Gamma e^{-2\gamma z})} \quad (3.21)$$

Γ is the reflection coefficient, which represents the percentage (from 0.0 to 1.0) of a wave that is reflected back toward the origin of the wave and can be calculated using terminal and characteristic impedances as follows:

$$\Gamma = \frac{(Z_T - Z_o)}{(Z_T + Z_o)} \quad (3.22)$$

The propagation constant, γ , can be determined using

$$\gamma = \frac{\omega}{c_o} \cdot (1 - F_{10})^{-1/2} [\cos(\phi/2) - j\sin(\phi/2)] \quad (3.23)$$

Since P_A can be a sinusoidal function that is equal to $P_o(e^{-z\gamma})$, Avolio (1980),

Karamanoglu (1995) and Van den Wijngaard et al. (2007) were able to use a transfer equation to determine the pressure wave at the vessel outlet (or pressure transmitted, P_T), given the pressure wave at the inlet. Using equations 3.12,13 & 23, the transfer equation is:

$$\frac{P(l)}{P(0)} = \frac{P_1(1 + \Gamma)}{P_1 e^{i\omega t}(1 + \Gamma^{-2} i\omega z/c_0)} = \frac{1 + \Gamma}{e^{\gamma z} + \Gamma e^{-\gamma z}} \quad (3.24)$$

Fourier decomposition of a pressure wave that is a function of time is required to use this equation. The resulting components represent harmonic wave forms of $P(l)$ s or $P(0)$ s. The constituents of the transfer function are derived for an equal number of harmonics. Then the corresponding pressure and transfer function are used to determine a pressure harmonic wave. The subsequent harmonics are summed to produce a pressure wave that is a function of time. The resulting pressure can be considered instantaneous pressure.

Given the pressure at opposing ends of a vessel, the pressure gradient across the vessel, at a given time, can be determined. And just like instantaneous pressure, this pressure can be decomposed into harmonic components. This pressure gradient can be characterized as

$$\frac{\partial p}{\partial z} = A^* e^{i\omega t} = P_{avg} + \sum_{n=1}^N P_n e^{i\omega t}, \quad (3.25)$$

where A^* is the complex conjugate ($A_n - iB_n$), i is $\sqrt{-1}$, ω is angular frequency $2\pi f$ and t is the time. The second equality is a more intuitive form for Fourier manipulation, where P_{avg} is the mean pressure and P_n are the individual pressure harmonics of a set of N components.

Now that pressure can be calculated at the outlet of a vessel there still remains a need to calculate flow rate.

3.3 Fluid Flow

Blood flow through the arteries is generally classified as steady or oscillatory flow.

Though the oscillatory pulsations from the heart are known to remain persistent into the capillary level (Li, 1987), the application of steady flow theory does have some merit.

Steady laminar flow methodology allows the application of non-slip assumptions to hemodynamic models, determination of flow shear stresses or hydraulic resistance. It also simplifies the analysis of phenomenon such as arterial stenosis (an abnormal constriction of an artery) (Ku, 1997). Therefore, for completeness, the equation for the flow rate of a steady stream of fluid through an elastic tube can be determined from Poiseuille's equation as given below

$$Q = \Delta P \frac{\rho r^4}{8 z \nu} \quad (3.26)$$

where Q is the volumetric flow rate through a rigid tube, ν is the blood dynamic viscosity, ΔP is the pressure gradient across a vessel and z is the vessel length.

Poiseuille's equation assumes:

1. Rigid axial symmetric cylinder where elasticity and variations in vessel shape across the axis of fluid flow are neglected.
2. Newtonian flow, which assumes a constant coefficient of viscosity and neglects non-linear shear stresses versus shear rates that are more indicative of flow through the smaller vessels. This can be considered realistic for the major arteries.

3. Laminar flow where fluid is considered to travel through the vessels in layered, cylindrical, sections.
4. No slip at walls, which approximates the adhesive forces between the blood and the endothelial cells that line the vessel wall.
5. Symmetrically uniform velocity profile, which ignores variations due to asymmetric vessel cross section or entrance and bifurcation effects.
6. Steady flow where the pulsatile component of blood flow is ignored.
7. Incompressibility, which is an acceptable assumption for blood.

To arrive at periodic flow, the conservation of mass and Navier - Stokes (N.S.) equations must be examined to make additional assumptions. The equations for continuity and fluid momentum can be written in cylindrical format as

Mass-conservation

$$\frac{\partial u}{\partial r} + \frac{u}{r} + \frac{\partial w}{\partial z} = 0 \quad (3.27)$$

Navier-Stokes in the z (axial) direction

$$\frac{\partial w}{\partial t} + u \frac{\partial w}{\partial r} + w \frac{\partial w}{\partial z} = -\frac{1}{\rho} \frac{\partial p}{\partial z} + \nu \left(\frac{\partial^2 w}{\partial r^2} + \frac{1}{r} \frac{\partial w}{\partial r} + \frac{\partial^2 w}{\partial z^2} \right) \quad (3.28)$$

Navier-Stokes in the r (radial) direction

$$\frac{\partial u}{\partial t} + u \frac{\partial u}{\partial r} + w \frac{\partial u}{\partial z} = -\frac{1}{\rho} \frac{\partial p}{\partial r} + \nu \left(\frac{\partial^2 u}{\partial r^2} + \frac{1}{r} \frac{\partial u}{\partial r} + \frac{\partial^2 u}{\partial z^2} - \frac{u}{r^2} \right) \quad (3.29)$$

which are generally regarded as the fundamental equations for hemodynamic calculations and are subject to the boundary conditions:

$$w(r, z, t) \Big|_{r=R} = 0, \text{ axial velocity is zero at the vessel wall}$$

$$\frac{\partial w}{\partial r}(r, z, t) \Big|_{r=0} = 0, \text{ due to symmetry the slope of the axial velocity is 0}$$

$$u(r, z, t) \Big|_{r=0} = 0, \text{ due to symmetry the radial velocity is 0 at axial centerline}$$

These equations consider velocities w and u as functions of radius r , axial distance z and time t and neglect angular velocity in the ϕ direction, as well as gravitational forces.

Again, the conditions of Newtonian, isotropic flow that is axially symmetric apply.

Womersley (1957) neglected the contribution of the vessel wall motion to fluid flow.

However, within the physiological range this assumption is considered insignificant.

Assuming the vessel walls are rigid eliminates velocities in the radial direction.

Furthermore, since there is no radial motion, the N.S. equation in the radial direction reduces to

$$\frac{\partial p}{\partial r} = 0$$

This implies that pressure only varies in the z direction or $p(z, t)$. Therefore, the continuity equation reduces to

$$\frac{\partial w}{\partial z} = 0$$

This implies $w(r, t)$.

With the lack of radial motion, changes due to convective acceleration

$(u \partial w / \partial r + w \partial w / \partial z)$ and viscous acceleration $(\partial^2 w / \partial z^2)$ are expected to be insignificant when compared to flow due to local accelerations $(\partial w / \partial t)$. Therefore, a relation between pressure and radius are linearized and N.S. in the z direction reduces to

$$\frac{\partial w}{\partial t} = -\frac{1}{\rho} \frac{\partial p}{\partial z} + \nu \left(\frac{\partial^2 w}{\partial r^2} + \frac{1}{r} \frac{\partial w}{\partial r} \right) \quad (3.30)$$

where kinematic viscosity, ν , is viscosity, μ , divided by density, ρ . Furthermore, it has already been shown that the pressure gradient $\partial p / \partial z$, equation 3.24, can have the periodic form of $A^* e^{i\omega t}$. It can, therefore, be assumed that $w(r,t)$ can have the same form.

With these substitutions, the N.S. equation for the z direction can take the form

$$i\omega w e^{i\omega t} = -\frac{A^* e^{i\omega t}}{\rho} + \frac{\mu}{\rho} \left[\frac{d^2 w}{dr^2} + \frac{1}{r} \frac{dw}{dr} \right] e^{i\omega t} \quad (3.31)$$

or

$$\frac{d^2 w}{dr^2} + \frac{1}{r} \frac{dw}{dr} - \frac{i\omega\rho}{\mu} w = \frac{A^*}{\mu} \quad (3.32)$$

Remembering that w varies across laminar layers, from the central axis to the vessel wall at R , the equation can be put into non-dimensional form using

$$y = \frac{r}{R} \quad (3.33)$$

where r is some radial distance from the axis and R is the radius at the vessel wall. The result is

$$\frac{d^2 w}{dy^2} + \frac{1}{y} \frac{dw}{dy} - i\alpha^2 w = \frac{A^* R^2}{\mu} \quad (3.34)$$

Equation 3.34 has the form of Bessel's equation of zero order

$$\frac{d^2 y}{dx^2} + \frac{1}{x} \frac{dy}{dx} + k^2 y = 0 \quad (3.35)$$

which has the general solution

$$y = AJ_0(kx) + BY_0(kx) \quad (3.36)$$

where A and B are arbitrary constants, J_0 is a zero order function of the first kind, Y_0 is a zero order function of the second kind (Bowman, 1958). Since, for positive values of k and x , $Y_0 \rightarrow \infty$ as $x \rightarrow 0$, B must equal 0 to comply with a finite velocity at the axis.

$$w = \frac{A^* R^2}{i\mu\alpha^2} \left[1 - \frac{J_0\left(\alpha y \left(i^{3/2}\right)\right)}{J_0\left(\alpha \left(i^{3/2}\right)\right)} \right] \quad (3.37)$$

and, subsequently,

$$w = \frac{A^* R^2}{i\mu\alpha^2} \left[1 - \frac{J_0\left(\alpha y \left(i^{3/2}\right)\right)}{J_0\left(\alpha \left(i^{3/2}\right)\right)} \right] e^{i\omega t} \quad (3.38)$$

Then, to get instantaneous volumetric flow rate, Q , through a cross section

$$Q = 2\pi R^2 \int_0^1 w y \, dy \quad (3.39)$$

or

$$Q = \frac{\pi R^2 A^* e^{i\omega t}}{i\omega\rho} \left[1 - \frac{2J_1\left(\alpha \left(i^{3/2}\right)\right)}{\alpha \left(i^{3/2}\right) J_0\left(\alpha \left(i^{3/2}\right)\right)} \right] \quad (3.40)$$

For the real component of a complex pressure gradient (which can be written

as: $M \cos(\omega t - \phi)$), w and Q can be given in trigonometric form as

$$w = -\frac{|A|R^2}{\mu} \frac{M'_o}{\alpha^2} \sin(\omega t - \phi + \varepsilon'_o) = \frac{2P_{avg}}{\pi R^2} \left(1 - \frac{r^2}{R^2}\right) + \sum_{n=1}^N \frac{P_n R^2 M'_o}{\mu \cdot \alpha^2 \cdot L} \cos\left(\omega t - \phi - \varepsilon'_o + \frac{\pi}{2}\right) \quad (3.41)$$

where

$$M'_o = \left[1 - \frac{2 \cdot M_o\left(\alpha \frac{r}{R}\right)}{M_o(\alpha)} \cos\left[\theta_o\left(\alpha \frac{r}{R}\right) - \theta_o(\alpha)\right] + \left[\frac{M_o\left(\alpha \frac{r}{R}\right)}{M_o(\alpha)}\right]^2 \right]^{0.5} \quad (3.41a)$$

and

$$\varepsilon'_o = \frac{\frac{M_o\left(\alpha \frac{r}{R}\right)}{M_o(\alpha)} \sin\left[\theta_o\left(\alpha \frac{r}{R}\right) - \theta_o(\alpha)\right]}{1 - \frac{M_o\left(\alpha \frac{r}{R}\right)}{M_o(\alpha)} \cos\left[\theta_o\left(\alpha \frac{r}{R}\right) - \theta_o(\alpha)\right]} \quad (3.41b)$$

where the functions M_o and ε_o as functions of alpha (α), radial distance to vessel wall (R) and some radial distance (r) between the axial centerline and vessel wall, are tabulated by McLachlan (1961)

$$Q = \frac{|A|\pi R^4}{\mu} \frac{M'_{10}}{\alpha^2} \cos\left(\omega t - \phi - \varepsilon'_{10} + \frac{\pi}{2}\right) = \frac{\pi R^4 P_{avg}}{8\mu} + \sum_{n=1}^N \frac{\pi R^4 P_n}{\mu \alpha^2} \cos\left(\omega t - \phi - \varepsilon'_{10} + \frac{\pi}{2}\right) \quad (3.42)$$

where M_{10} and ε_{10} can be calculated using methods identified by Nichols et al. (1998) or interpolated from values given by Womersley (1957).

3.4 Windkessel Model

Windkessels are lumped parameter models, generally used to derive global cardiovascular parameters, such as flow and pressure from the heart, as well as total compliance of the arterial system. The individual components of these models can be used to mimic the effect of the arterial system on the heart, or, act as boundaries to simulate arterial properties downstream of a vessel.

First presented by Otto (1899), the windkessel is a representation that consists of an air filled chamber in which fluid is pumped and then subsequently released through a metered outlet. The term dates back to the operation of fire engines of the 1800's, which used an air filled chamber (which is termed windkessel in German) to get a more continuous stream of water, and it has stuck in the present. This concept also resembles the phenomenon of blood flow through arteries, where the air filled chamber represents the expandable volume for capacitance (or compliance) and the metered outflow would represent vessel resistance. This concept is known as a 2-element windkessel. Since Frank Otto's time, the windkessel model has seen many modifications. Figure 3.5 is one such modified windkessel used by Elzinga and Westerhof (1973).

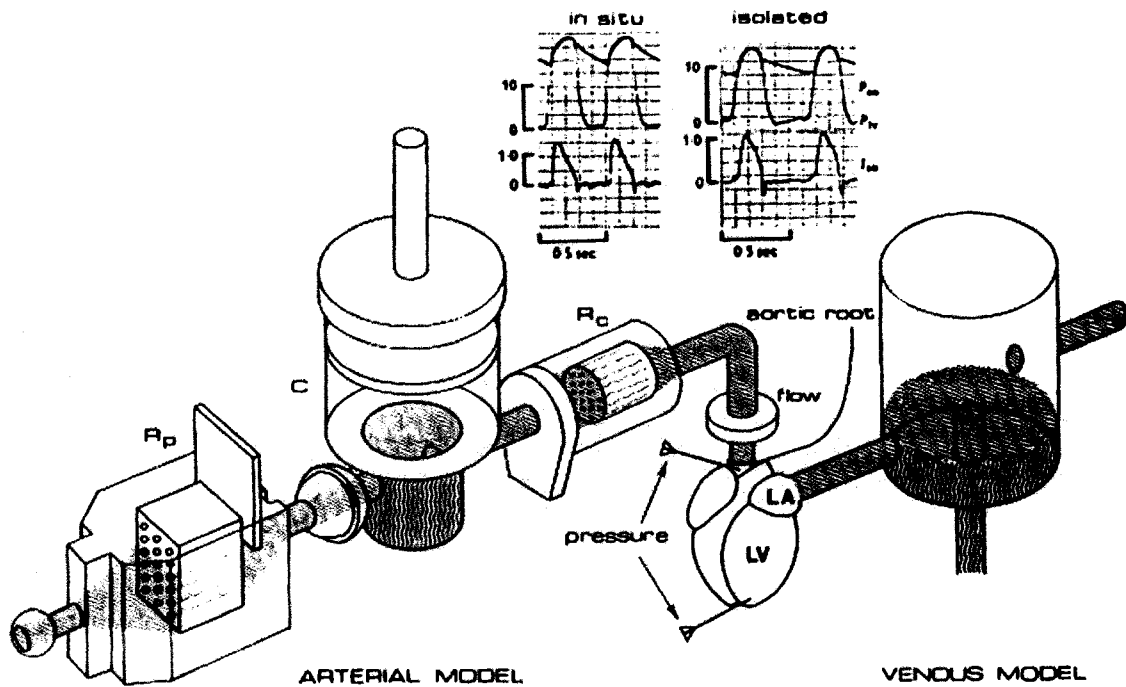


Fig. 3.5 3-element windkessel used by Elzinga and Westerhof (1973)

In this modified windkessel the restrictions of the filters R_c and R_p are a characteristic resistance (or characteristic impedance) and a vascular resistance, respectively. The expandable cylinder is the capacitance for arterial flow. Note the inclusion of the heart as the pressure source and the venous portion as a fluid supply for the pump. The relative simplicity of this system alludes to the primary use of windkessel models. When determining an operational such as arterial load (the load experienced by the left ventricle of the heart) or vascular compliance it is more practical to lump the cardiovascular network into a few manageable quantities. This concept has proved useful in approximating or mimicking gross response of the arterial system to normal pressure and flow, as well as abnormal conditions such as vasoconstrictions (reduction in vessel diameter) or vasodilations (increases in vessel diameter) due to drugs (Segers and

Verdonck, (undated); Hlavac, (undated); Stergiopoulos et al., 1999 and Lambermont et al., 2003). These models are both depicted in figure 3.6 and are solved as electric circuits.

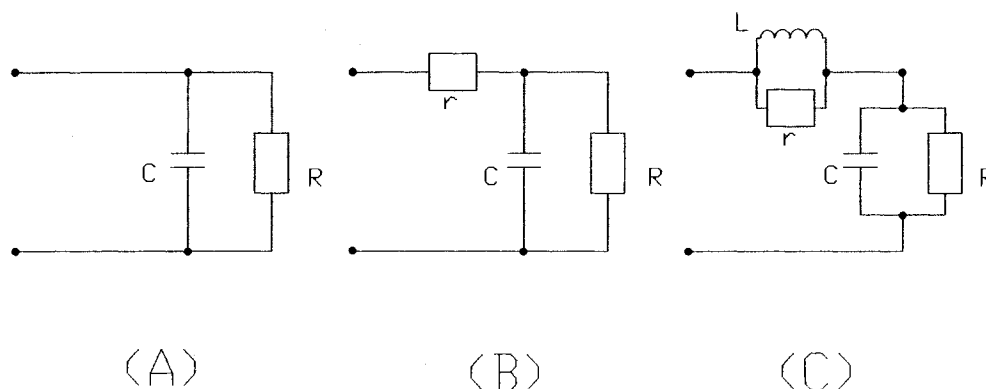


Fig. 3.6 Three windkessel models. Where (a) is the original 2-element windkessel, (b) is a 3-element model popularized by Westerhof and (c) is a 4-element model first conceptualized by Buratti and Gnudi (1982)

Capacitance, C , in figure 3.6 retains its definition from Chapter 2, while $i(t)$, $u(t)$ and R are considered to be flow, pressure and resistance, respectively. L , in the 4-element model, represents inductance (inertance), which can be considered fluid momentum. Resistance, R , conceptualized as the vascular resistance, is a ratio between the product of blood viscosity, μ , and change in distance, Δz , divided by vessel radius to the power of 4 (Snyder et al., 1968), or

$$R = \frac{81 \mu \Delta z}{8 \pi r^4} \quad (3.43)$$

and

$$L = \frac{4 \rho \Delta z}{3 \pi r^2} \quad (3.44)$$

Inertance (L), is given by the above equation, where r is the fluid density, Δz is the vessel length and r is the vessel radius. Referring back to figures 3.6b and 3.6c, the lower case r , in series with R and C , has been conceptualized as characteristic impedance. The input impedance, Z , of figure 3.6c can then be represented as (Segers et al., 2003)

$$Z = \frac{i\omega L r}{r + i\omega L} + \frac{R}{1 + i\omega RC} \quad (3.45)$$

Determining the *physical* components, like systemic inertance, can be tedious if not impossible using the above equation. Normally, a parameter such as pressure or flow versus time is measured. Then the above components, used to describe this flow or pressure, are varied until the equation can approximate the measured value. Figure 3.7 is an example of the Goldwyn and Watt's method (1967) for deriving systemic parameters by using a windkessel for approximating the diastolic decay of an arterial pressure wave.

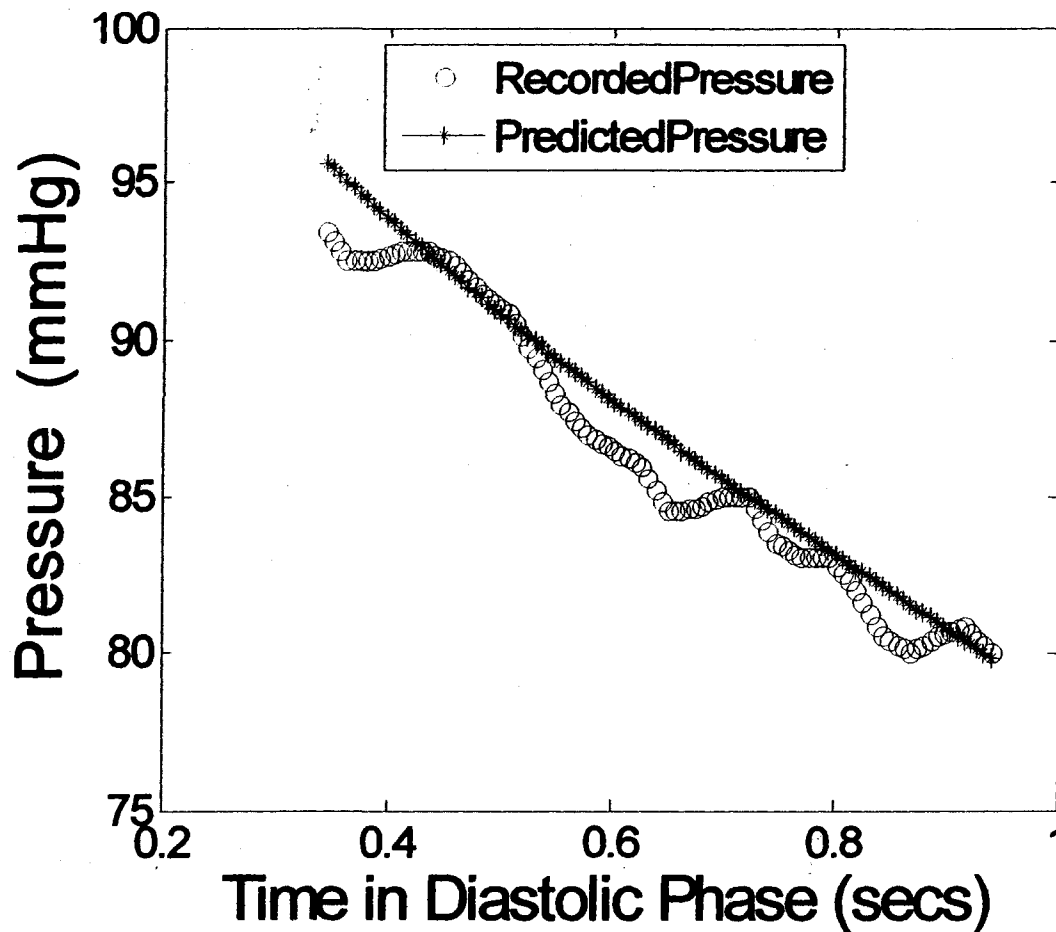


Fig. 3.7 Pressure Decay in the Diastolic Phase of a Radial Pulse

First, using the methods for identifying the ejection duration (Karamanoglu, 1997 and Takazawa et al., 1995), the time of aortic valve closure (or the beginning of the diastolic phase of the pressure is identified. This is accomplished by determining the time (time of the second shoulder in figure 2.12) for which the fourth derivative of the pressure wave crosses the x-axis from the negative y direction to the positive y direction as given by Takazawa. After this, using Karamanoglu's methodology, the time of valve closure occurs at the first positive to negative x-axis crossing of the third derivative of pressure

after the time of the second shoulder. Then, using the Davidon-Fletcher-Powell method, by a variation of the Goldwyn and Watt's equation (Watt and Burrus, 1976) for pressure, $P(t)$:

$$P(t) = x_1 e^{-x_2 t} + x_3 e^{-x_4 t} \cos(x_5 t + x_6) \quad (3.46)$$

the coefficients x_1 through x_6 are adjusted until $P(t)$ approximates the measured diastolic pressure. These coefficients can then be used to solve the components of the 4 element windkessel depicted in figure 3.8.

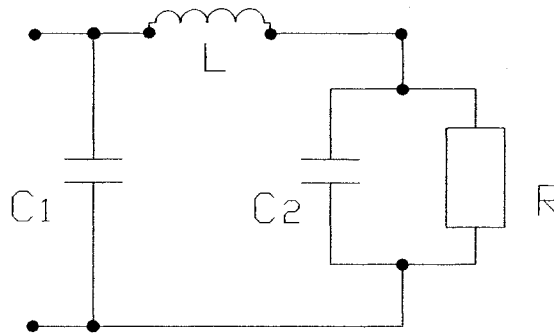


Fig. 3.8 The Goldwyn and Watt 4 element windkessel (Watt and Burrus, 1976)

Referring to figure 3.8, if

$$m = x_2 + 2x_4, \quad (3.47)$$

$$pp = x_2[(x_4)^2 + (x_5)^2], \quad (3.48)$$

$$n = 2x_2 x_4 + (x_4)^2 + (x_5)^2, \text{ and} \quad (3.49)$$

then inertance, L , can be calculated with:

$$L = \frac{m^2 \cdot R}{m \cdot n - pp} \quad (3.50)$$

Large artery compliance, C_1 , can be calculated with:

$$C_1 = \frac{m \cdot n - pp}{m \cdot pp \cdot SVR} \quad (3.51)$$

Oscillatory compliance, C_2 , can be determined with:

$$C_2 = \frac{1}{m \cdot SVR} \quad (3.52)$$

3.5 The Arterial Tree Model

Using the theory described in sections 3.1, 3.2 and 3.3, the mathematical model used in this report can now be assembled.

Basically, the model can be described as a one-dimensional network of 45 vessels that are arranged to mimic the approximate location of the major arterial vessels of a human. The vessels are linked at common points, called nodes. Each vessel is in turn divided into N segments. The vessels were divided into 10 segments for the primary portion of the pressure and flow analysis.

Due to its flexibility, relatively small computational cost and ease of use, transmission line theory is used to determine pressure $P(t)$ throughout the model and flow $w(t)$ from selected sections.

To consider the mathematics involved, we can discuss the equations required to determine $P(t)$ and $w(t)$ in one segment. First, we determine key parameters such as the wave velocity, which can be determined from the Moens-Korteweg equation;

$$c_0^2 = \frac{E h}{2 r \rho} \quad (3.8)$$

Then, in keeping with the modified version of the Womersely derivation of fluid flow in elastic arteries, we determine the ratio between inertial forces and viscous forces (fluid viscosity μ) as the Womersely number α , which is defined as:

$$\alpha^2 = \frac{r^2(\omega \rho)}{\mu}, \quad \text{where } \alpha \text{ is dimensionless.} \quad (3.19)$$

From there, we determine another one of Womersely's parameters - F_{10} . This is a parameter that uses the zero order Bessel function J_0 and first order Bessel function J_1 of the Womersely number to quantify the stability of the of the propagating fluid as shown below

$$F_{10} = \frac{(2J_1(\alpha j^{3/2}))}{(\alpha j^{3/2} J_0(\alpha j^{3/2}))} \quad (3.18)$$

There is a lag between applied pressure and the subsequent motion of the vessel wall.

This attribute is tracked as the phase angle, ϕ , between pressure and wall motion, which can be calculated as

$$\phi = \tan^{-1}\left(\frac{\omega\eta}{E}\right) \quad (2.12a)$$

Then the characteristic impedance can be calculated using

$$Z_o = \frac{(\rho c_o)}{((1 - \nu^2)^{0.5})} \cdot ((1 - F_{10})^{-1/2}) [\cos(\phi/2) + j\sin(\phi/2)] \quad (3.17)$$

where ν is the Poisson's ratio of the vessel wall (0.045 $g/(cm \cdot sec)$) and ρ is the density of blood (1.056 g/cm^3)

The propagation constant, γ , can be determined using

$$\gamma = \frac{\omega}{c_o} \cdot (1 - F_{10})^{-1/2} [\cos(\phi/2) - j\sin(\phi/2)] \quad (3.23)$$

Next, if we assume that this segment is terminated with a terminal impedance, Z_T , and the Γ is the reflection coefficient, which represents the percentage (from 0.0 to 1.0) of an incident pressure wave, P_1 , that is reflected back toward the origin and can be calculated using terminal and characteristic impedances as follows

$$\Gamma = \frac{(Z_T - Z_o)}{(Z_T + Z_o)} \quad (3.22)$$

Some wave reflection is expected at any discontinuity along the flow path of a segment (this includes reductions in diameter and bifurcation points); however, in this model only reflection at the terminal node of each segment is considered.

Since inlet pressure can be a sinusoidal function that is equal to $P_I(e^{-z'})$, a transfer equation can be used to determine the pressure wave at the vessel outlet (or pressure transmitted, $P(l)$), given the pressure wave at the inlet, $P(0)$. The transfer equation can be in the forms:

$$\frac{P(l)}{P(0)} = \frac{P_I(1 + \Gamma)}{P_I e^{i\omega t}(1 + \Gamma^{-2} i\omega z/c_o)} = \frac{1 + \Gamma}{e^{\gamma z} + \Gamma e^{-\gamma z}} \quad (3.24)$$

With the pressure gradient across the segments identified, instantaneous velocity at the segment outlet can be determined using

$$w = -\frac{|A|R^2}{\mu} \frac{M_o'}{\alpha^2} \sin(\omega t - \phi + \varepsilon_o') = \frac{2P_{avg}}{\pi R^2} \left(1 - \frac{r^2}{R^2}\right) + \sum_{n=1}^N \frac{P_n R^2 M_o'}{\mu \cdot \alpha^2 \cdot L} \cos\left(\omega t - \phi - \varepsilon_o' + \frac{\pi}{2}\right) \quad (3.41)$$

Upon examination of how the velocity data was obtained from the eight subjects, it was determined that Doppler ultrasound was used to make the measurements. This method

relies on radiating a sound wave of a given frequency from a source toward the desired point of measure. Then the shift in frequency experienced by the sound wave is measured to determine velocity of the blood cells. Artifacts due to motion of the pulsating vessel wall and noise due to very low flow or rapid changes in flow necessitate the use of filtering software and manual manipulation of data. Adding to this was the fact that blood flow velocity varies from the vessel's central axis to the inner wall. With this in mind, a certain amount of variability was expected between subjects and even between results from the same subject. After a few trials, it was decided that the diameter should be divided into 50 cylindrical flow regions. The radial measure, r , from equation 3.41 was varied from 1-49 at the vessel outlet until the value that best approximated the recorded value was obtained.

3.5.1 Physiological data

The overall topology of the arterial tree, used by this model, is based on the example given by Marieb (1995). The models of Olufsen (1998) and Stergiopulos (1992) were then used to reduce the number of arteries. Small vessels, like the coronary arteries, were ignored because they represented a small fraction of flow from the heart. Other small arterial branches were lumped into Windkessel models to reduce model complexity. Uflacker (1997) was consulted to address the possible variations of arterial branching. It was determined that there are other possible branching variations (such as the number of renal arteries or the flow path for the left carotid artery). However, the model configuration was found to be representative of the most likely branching arrangement. The abbreviated model contains 45 vessels and has content comparable to previous models of the arterial tree; as depicted in figures 3.9 and 3.10.

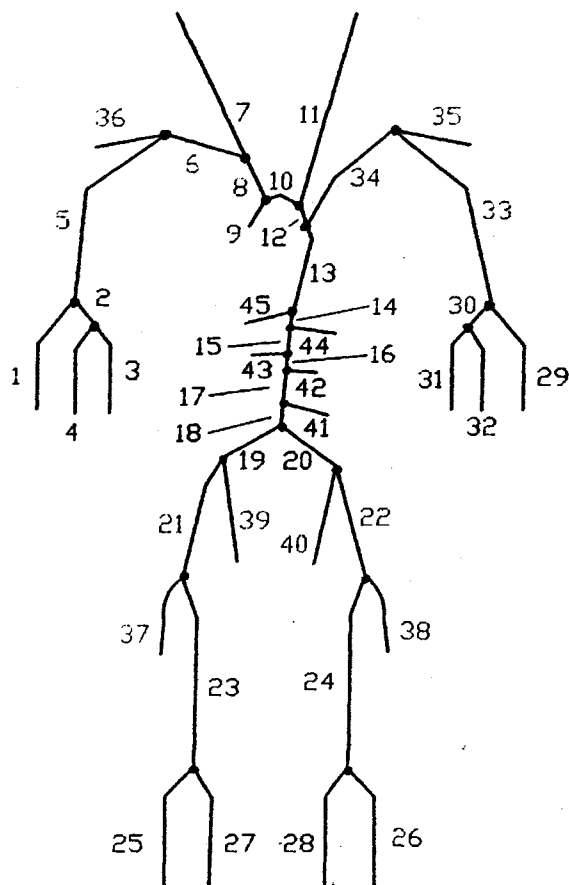


Fig. 3.9 The arterial tree model

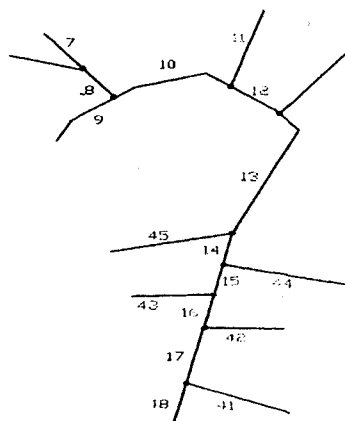


Fig. 3.10 A detailed depiction of the Aortic portion of the arterial tree model

Table 3.1 The arterial model nomenclature

Vessel	Artery name	Vessel	Artery name	Vessel	Artery name
1	R. Radial	16	Abdominal aorta	31	L. Ulnar
2	R. Ulnar	17	Abdominal aorta	32	L. Interosseous
3	R. Ulnar	18	Abdominal aorta	33	L. Brachial
4	R. Interosseous	19	R. Iliac	34	L. Subclavia + Axillaris
5	R. Brachial	20	L. Iliac	35	L. Vertebral
6	R. Subclavia + Axillaris	21	R. Femoral	36	R. Vertebral
7	R. Common Carotid	22	L. Femoral	37	Deep Femoral
8	Brachiocephalic	23	R. Femoral	38	Deep Femoral
9	Ascending aorta	24	L. Femoral	39	Internal Iliac
10	Aortic arch	25	R. Anterior tibial	40	Internal Iliac
11	L. Common Carotid	26	L. Anterior tibial	41	Inferior Mesenteric
12	Aortic arch	27	R. Posterior tibial	42	Renal
13	Thoracic aorta	28	L. Posterior tibial	43	Renal
14	Abdominal aorta	29	L. Radial	44	Superior Mesenteric
15	Abdominal aorta	30	L. Ulnar	45	Celiac

**L = Left and R = Right

It should be noted that physiological parameters are not included in table 3.1 because they vary between subjects. This is where the robustness of this model is demonstrated. By inputting one digitized pressure wave from a subject's radial artery, her/his weight, height, gender, heart rate and age, the model adjusts the physical parameters of the arterial tree to statistically approximate that of the subject. The required parameters for pressure and flow calculations included vessel length, diameter, thickness, vessel wall viscosity and modulus of elasticity, as well as cardiac output (CO), systemic vascular resistance (SVR), systemic inertance (SI), large artery compliance, oscillatory compliance and mean flow rate to various branches of the arterial network.

Predicting the vessel lengths and their topographical relation to each other was tedious. It required combining the works of Dotter et al. (1950), Romanes (1981), Stergiopoulos et al. (1992), Marieb (1995), Olufsen (1998), Yahel et al. (1998) and Pennington et al. (2005) into the anthropometric framework for a man or woman in the 50th percentile range which is given by Henry Dreyfuss Associates (1993). Then using data provided by Learoyd and Taylor (1966), Imura et al. (1990), Steinberg et al. (1992), Sonesson et al. (1993 and 1994), Benetos et al. (1993), Laurent et al. (1994), Olufsen (1998), Kiechl et al. (1999), Van der Heijden-Spek et al. (2000), Livingston et al. (2001), Riekkinen et al. (2003), Li et al. (2004), the diameter and vessel thickness were determined, based on the subject's age, weight and gender. This data was determined for a small number of locations (the key locations being the radial artery, brachial artery, carotid artery, femoral artery, iliac artery, ascending aorta, thoracic aorta and abdominal aorta) and then extrapolated or interpolated in the form of the ratio $h/2r$ to provide radius and thickness for each segment of the model. The method for linear interpolation / extrapolation of the ratio $h/2r$ is similar to that performed for the ratio Eh/r . Furthermore, the $h/2r$ ratio is interpolated primarily for the derivation of vessel thickness h because it was noted that vessel thickness is related the radius.

Estimating the vessel wall viscosity, modulus of elasticity and mean flow rate through various branches proved equally as challenging. It relied on determining the global parameters of SVR, CO, large artery compliance and oscillatory compliance, SI as felt by

the heart as it pumps blood into the arterial system. This is accomplished first by determining CO with the empirical formula given as

$$CO = \frac{HR}{1000} [-6.6 + 0.25(T_{ej} - 35) - 0.62(HR) + 40.4(BSA) - 0.51(\text{age})] \quad (2.20)$$

The CO, which is an average of the total amount of blood expelled from the heart, is measured in liters per minute, and this value varies with age, eject duration (T_{ej}) in milliseconds, heart rate (HR) in beats/min. and body surface area (BSA) in m^2 . The ejection duration, which is the total time of blood flow out of the heart during a single pressure pulse, was determined using the methods identified by Takazawa et al. (1995) and Karamanoglu (1997) where the time of aortic valve closure (or the beginning of the diastolic phase of the pressure was identified as the first positive to negative x-axis crossing of the third derivative of pressure after the time of the second shoulder (or reflected wave).

SVR is calculated, in (dyne-secs)/ cm^5 as

$$SVR = \left(\frac{MAP}{CO} \right) \cdot 80 \quad (2-18)$$

Next, SI, large artery compliance and oscillatory compliance are derived with the use of the Goldwyn and Watt's equation for pressure, $P(t)$;

$$P(t) = x_1 e^{-x_2 t} + x_3 e^{-x_4 t} \cos(x_5 t + x_6) \quad (3.45)$$

where the coefficients x_1 through x_6 are adjusted until $P(t)$ approximates the measured diastolic pressure. These coefficients can then be used to solve the components of the 4 element windkessel given below.

$$m = x_2 + 2x_4, \quad (3.46)$$

$$pp = x_2[(x_4)^2 + (x_5)^2], \quad (3.47)$$

$$n = 2x_2x_4 + (x_4)^2 + (x_5)^2, \text{ and} \quad (3.48)$$

$$SI = \frac{m^2 \cdot SVR}{m \cdot n - pp} \quad (3.49)$$

Large artery compliance, C_1 , can be calculated with:

$$C_1 = \frac{m \cdot n - pp}{m \cdot p \cdot SVR} \quad (3.50)$$

Oscillatory compliance, C_2 , can be determined with:

$$C_2 = \frac{1}{m \cdot SVR} \quad (3.51)$$

Once the global parameters of large artery compliance, SVR and SI are determined, the individual contribution of each vessel to these values can be approximated as

$$C \approx \frac{3AZr}{2Eh} \quad (2.5)$$

$$R = \frac{81 \mu \Delta z}{8 \pi r^4} \quad (3.43)$$

Where C is vessel compliance, and R is vessel resistance. The C s were simply summed together to create model compliance. Then the compliance not accounted for by the

model (residual compliance) can be determined by large artery compliance - model compliance. While model resistance was treated more like an electrical circuit where the R_s were first summed for each vessel and then the resistance of two parallel vessels was summed as

$$\frac{1}{R_T} = \frac{1}{R_1} + \frac{1}{R_2} \quad (3.52)$$

to create a model resistance. This model resistance is calculated for the three different radii sizes. SVR, at this point, was considered a median value. To create the range of high, medium and low, the high and low model resistances were divided by the medium and the resulting values multiplied by the SVR to obtain a high and low SVR, respectively. It was then possible to obtain high and low values for CO and SI, using equations 2.18 and 3.49, respectively.

With the determination of radii (r), thickness (h) and modulus of elasticity (E) at the aforementioned key locations, the extrapolation / interpolation of the ratio $\frac{Eh}{r}$ can be done. Unlike the calculations determining the $\frac{h}{2r}$ values, the $\frac{Eh}{r}$ ratios for the key locations are first multiplied by a weighting factor or rule, then extrapolated and interpolated. This rule compares the subject's large artery compliance to the statistical average. Based on this, the $\frac{Eh}{r}$ ratios for the carotid artery, ascending aorta, thoracic aorta, abdominal aorta and iliac arteries are corrected. Oscillatory (small artery) compliance is used to correct the radial, brachial and femoral arteries. It should be noted

that this was done because it was noted that this ratio is, in part, the inverse of compliance. It was deduced that the state of large artery compliance provided some indication of the state of this ratio. Similarly, oscillatory compliance is thought to provide insight into the compliance of the peripheral arteries and was therefore used for determining ratios at the radial, brachial and femoral arteries.

3.5.2 Boundary

With regard to the terminal segments of the model, the properties of the vasculature beyond these points can be lumped into four-element windkessels. The 4-element version was selected over, say, a 3-element windkessel because it can track the inertial aspects of blood flow. Referring to figure 3.11, the 4-element windkessel was modified by changing one of the resistance elements to a characteristic impedance, Z_o , element. We consider the properties of the vascular immediately downstream of the terminal segment to be close enough to assume that this windkessel characteristic impedance equals that of the terminal segment.

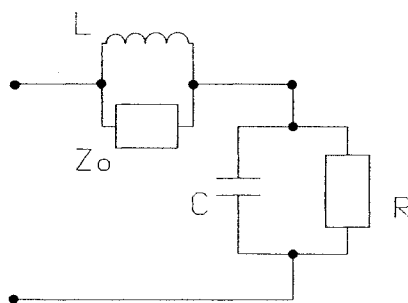


Fig. 3.11 Modified 4-Element Windkessel

The components of the resulting 23 windkessels are given values based on the average percent blood flow expected at that portion of the arterial tree. The cardiac output represents 100% blood flow. Then, as modified from Steele et al. (2007) and Nichols et al. (1998), each of the 23 windkessels receives a percentage of the total blood flow. The percentage of blood flow specified for various areas of the arterial tree are shown in table 3.2.

Table 3.2 Average percent flows trough major arteries

Arterial Branch	Percent Blood Flow
thoracic	66
renal	11.5
superior mesenteric	12
inner iliac (x2)	13.5

Table 3.2 Average percent flows trough major arteries (continued)

Arterial Branch	Percent Blood Flow
deep femoral (x2)	1
Femoral (x2)	4
inferior mesenteric	4
celiac	14
Carotid (x2)	13
Arm (x2)	4

Additional modifications were implemented by considering the amount of available flow to terminal points in the legs and arms, the cross sectional area at these terminal points and the combined area of the terminal points of a given branch. Basically, flow at these terminal points were based on a ratio of cross sectional area of a terminal point to the combined area at that branch.

Then a terminal compliance, C , (windkessel compliance) for terminal point, i , can be written as (Stergiopoulos et al., 1992)

$$\text{terminal compliance}_i = (\text{residual compliance}) \frac{\text{flow at terminal point}(i)}{\text{CO}} \quad (3.53)$$

and terminal resistance, R , is then

$$\text{terminal resistance}_i = (\text{SVR}) \frac{\text{residual compliance}}{\text{terminal compliance}_i} \quad (3.54)$$

Realizing that inertance (flow inertia) at the boundaries is dependant on flow rate, as well as the total amount of inertance recorded for the system, it was deduced that

$$\text{terminal inertance}_i = \frac{(\text{SI})(\text{CO})}{\text{flow at terminal point}(i)} \quad (3.55)$$

3.5.3 Calculation

Calculations were performed using computer programs created with MATLAB, release 14. Upon entry of a subject's height, weight, gender, age and a digitized measure of one radial pressure wave, the program calculates the length, modulus of elasticity and thickness of each of the 10 segments for each of the 45 vessels of the model. It should be noted that the radii, thickness and modulus of elasticity are calculated for three different cases to cover the range of statistical possibilities. Additionally, the number of segments desired for subdividing the vessels can also be specified. The global parameters are then determined and used for parameterization of the windkessel elements at the 23 terminal points of the model. The ascending aorta (vessel 9) is not regarded as a terminal point since it is the source of the pressure wave for the arterial system. The wave speed, propagation coefficient and characteristic impedance are then determined. With this completed, the input impedance can then be derived to assemble pressure equations. The pressure equations are calculated for ten harmonics to track the most pressure data with high efficiency. Figure 3.12 provides an outline of program inputs, gross calculations and program outputs. Refer to appendix A for more specifics.

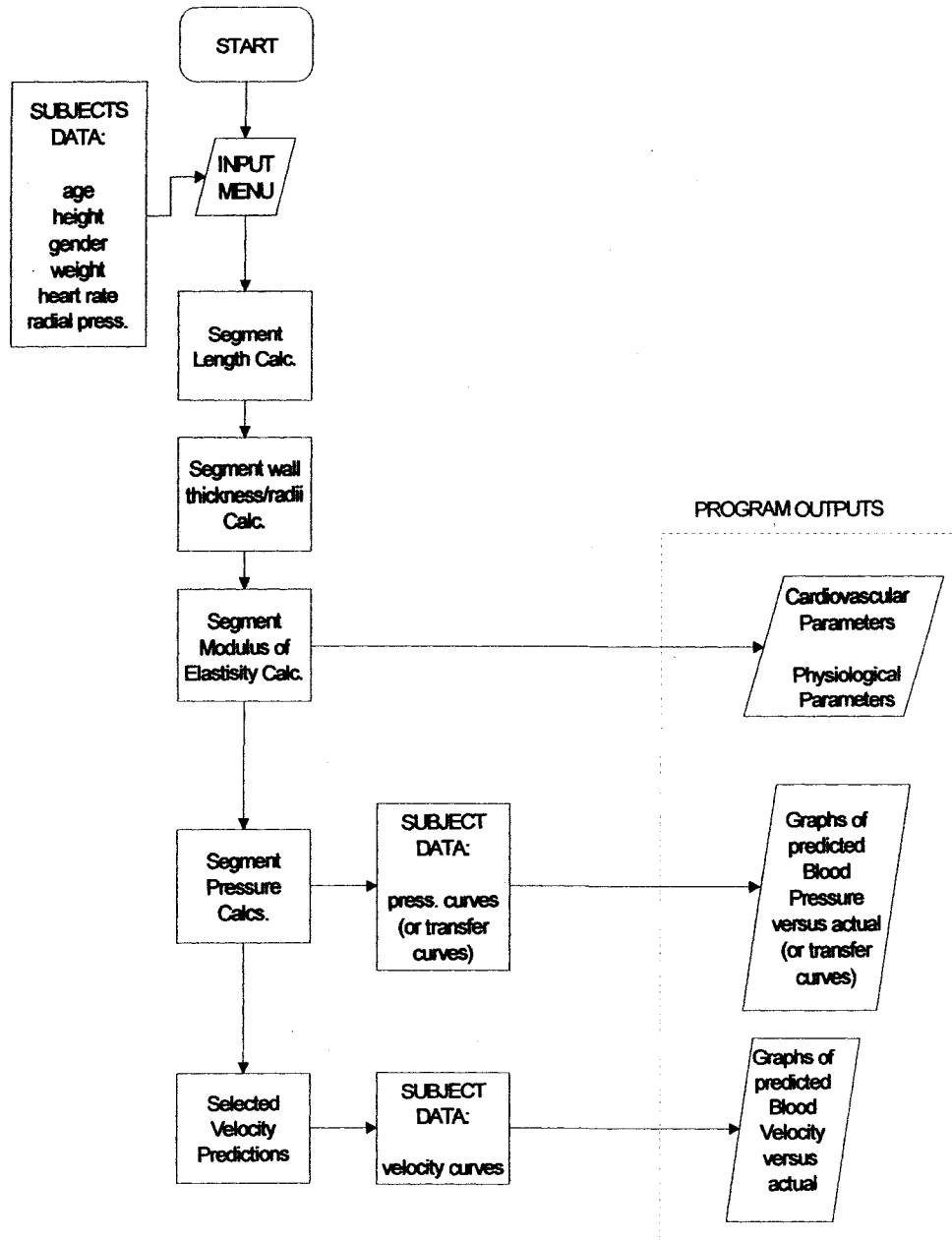


Fig. 3.12 Flowchart of overall program inputs, gross calculations and outputs

Returning to assembly of the pressure equations, first, the windkessel input impedance is calculated using

$$Z = \frac{i\omega LZ_o}{Z_o + i\omega L} + \frac{R}{1 + i\omega RC} \quad (3.45a)$$

Then, in systematic fashion, the corresponding reflection coefficient, Γ , is determined from equation 3.22, which is used to determine the input impedance of the preceding segment using

$$Z = Z_o \frac{(1 + \Gamma e^{-2\gamma z})}{(1 - \Gamma e^{-2\gamma z})} \quad (3.21)$$

This procedure is carried out from the terminal node to the node where parallel segments meet. At the intersecting node, the parallel input impedances are summed to create an equivalent input impedance for use in calculating a corresponding reflection coefficient for the next segment. This is analogous to calculating resistance in an electrical circuit.

After the input impedance is calculated back to the inlet of the ascending aorta, the pressure transfer equations, for pressure transmitted through a given segment, can then be assembled. Unlike other arterial tree models, which supplied an input pressure wave at the aorta, this model uses the digitized radial pulse as $P(l)$ to determine $P(0)$. The pulse is input at the terminal point of either the right or left radial vessel, and the upstream pressure wave and subsequent waves are iteratively determined from the derived transfer function.

With the pressure waves calculated for every segment, pressure gradients and, subsequently, flow through predetermined segments can then be calculated. The model then outputs the subject's physiological parameters, cardiovascular parameters and selected pressure and flow velocity plots for three possible ranges. The observer can choose the best possible case based on the proximity of calculated SVR, oscillatory compliance and large artery compliance to statistical data, as well as the realistic behavior of pressure curves throughout the model. Transfer curves are also plotted with corresponding model curves to act as a qualitative barometer of the adequacy of the output. The implications of using these transfer curves are addressed in section 4.4.

Time is indexed throughout the model using the time of the radial wave input as a starting point. Since the speed of the pressure wave is dependent on the wave speed, c_0 , for the segment through which it travels and wave speed, varies with its harmonic; c_0 was averaged across all 10 harmonics to derive an average travel time through a given segment. Going upstream, back toward the terminal point of the aorta, travel time was subtracted from the preceding time period. At junctions where time is required in the downstream direction, travel time is added to the preceding time period. However, time was not established globally when subject data was recorded. This meant that, for example, no determination could be made as to how early a pressure wave at the ascending aorta occurred before the pressure wave in the radial artery. Therefore, when comparisons were made between curves created by the model and those recorded from previous studies, initial time for both curves was specified using initial time of the model curve while the recorded data retained its durational period for succeeding time.

In cases where age was unknown, this program employed a modified version of the method employed by Takazawa et al. (1998) where the ratio of the time of the minimum value of the second derivative ($time_B$) and its corresponding time of maximum value ($time_A$) of a pressure wave at the finger is used to predict age.

$$age = \left[\frac{\left(\frac{time_B}{time_A} \right) + 2.35864}{0.01976} \right] - 49 \quad (3.55)$$

Equation 3.55 was developed to obtain age from the radial artery pressure pulse. The rationale is that blood pressure at both the finger and the radial artery are similar enough to track MAP, and their proximity equates to similar vasculature. To limit possible bias, this equation was created using data from subjects not included in this report.

Gender can be estimated by comparing the subject's heart rate and calculated ejection time with values determined by Weissler et al. (1963). Weight can be determined from statistical data in the works of Sonesson et al. (1993 & 1994). Height can be calculated by rearranging the following:

$$BSA = 0.1037(\text{weight}^{0.6724}) \quad (2.21)$$

for a subject's weight less than 10 kg, and for those above

$$BSA = 0.102(\text{weight}^{0.6854}) \quad (2.22)$$

and

$$BSA = 0.0495(\text{weight}^{0.6046})(\text{height}^{0.2061}) \quad (2.23)$$

for all weights.

Refer to appendix A for an additional description of the calculation procedure.

CHAPTER 4

4. Results and Discussion

This chapter provides the results obtained from the model after data from eight subjects were input. The origin of subject data, tabulated results of model output and a discussion of the results are provided. Furthermore, the details of how this theory applies to the model used in this report are also discussed.

4.1 Test Cases

This model was tested using data from six subjects detailed by Xiao (1998) and two subjects detailed by Ozawa (1996). Of the six subjects from Xiao, four were healthy males, one was a healthy female and one was a male heart failure patient. Ozawa's subject consisted of two heart failure patients of unknown gender.

4.2 Error

Some consideration was given to the method of error analysis. The absolute difference between the recorded curve and the calculated model curve was first determined for each time (i), as shown in figure 4.1.

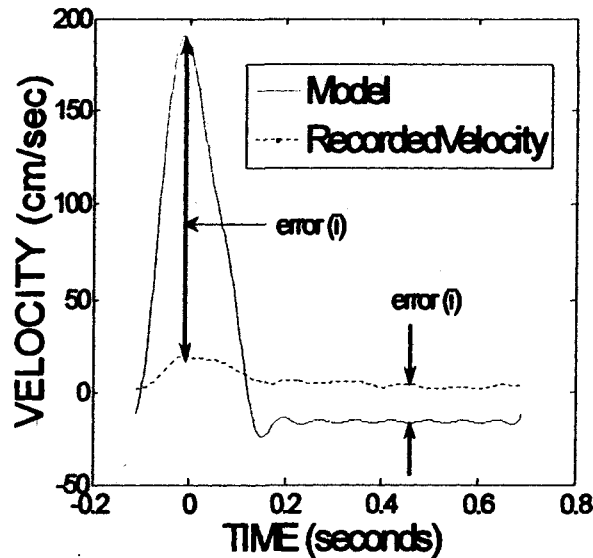


Fig. 4.1 Depiction of error determination

To obtain a normalized average of the overall deviation, each error (i) is divided by its corresponding recorded value (i) and averaged over the number of time periods of the pulse. This can be written as

$$\text{normalized error} = \frac{\sum_{i=1}^N \left| \frac{\text{error}(i)}{\text{recorded value}(i) + 1} \right|}{N} \quad (4.1)$$

Where, for the purposes of this model, N is 300.

Only a limited amount of recorded data was available, and the location from which it was recorded and the data type were not standard from subject to subject. Ozawa (1992) created a computer program to predict the cardiovascular parameters of two of the subjects used in this report. Later, Xiao (2000) used a modified version of Ozawa's program to make similar predictions for 6 of the subjects used in this report. Their results

are used in this report for comparison. For convenience, the normalized error calculated and the corresponding parameter for which they rated are given in tables 4.1(a)-(c).

Table 4.1(a) The normalized error between model and actual parameters

	Brachial Pressure	Brachial Velocity	Radial Velocity	Carotid Pressure
Subject 471	0.08 (0.08)	5.53 (7.73)	0.81 (0.50)	0.10 (0.14)
Subject y11	0.01 (0.07)	0.65 (0.34)	0.23 (0.33)	0.08 (0.09)
Subject 472	0.08 (0.06)	1.57 (8.83)	6.80 (16.71)	0.09 (0.06)
Subject 281	0.04 (0.05)	1.55 (8.43)	N/A	0.08 (0.04)
Subject 671	0.03 (0.04)	3.11 (5.48)	N/A	N/A
Subject 730	0.05 (0.04)	6.33 (11.38)	N/A	N/A

* The normalized error of Xiao's study (2000) are included in parenthesis.

Table 4.1(b) The normalized error between model and actual parameters

	Brachial Velocity	Femoral Velocity	Carotid Velocity
Subject Cr	3.72 (at left arm) (6.19)	9.00 (at left leg) (3.03)	N/A
	2.82 (at right arm) (4.94)	7.26 (at right leg) (2.20)	
Subject Lf	22.04 (at left arm) (5.08)	49.44 (3.38)	1.60 (0.87)
	21.82 (at right arm) (7.42)		

* The normalized error of Ozawa's study (1992) are included in parenthesis.

Table 4.1(c) The normalized error between model and actual parameters

	Age	Height	Weight	Gender
Subject 471	0	0.17	0.30	0
Subject y11	0	0.04	0.07	0
Subject 472	0.12	0.05	0.26	0
Subject 281	0.06	0.01	0.09	0
Subject 671	3.03	0.19	0.58	0
Subject 730	0.43	0.20	0.03	incorrect

4.3 Model Results

Overall, the results of the model were in agreement with observed characteristics of the arterial system (Nichols et al., 1998). Systolic pressure gradually increased as the distance increased from the ascending aorta. Peak flow velocity occurred prior to peak pressure, which is another common relation between flow and pressure. Flow and pressure results were compared to recorded measurements to examine the accuracy of the model. To quantify the closeness of the resulting curves to recorded data, the normalized error was calculated. The smaller the value the closer the calculated and recorded curves. These values ranged from 0.03 - 6.80 for values obtained from Xiao's subjects to 2.82 - 49.44 for Ozawa's subjects. To provide some perspective of how these values speak to the adequacy of the calculated values to the recorded values, the *error* was provided in the description of plots where those comparisons were made. The predicted cardiovascular parameters and physiological parameters are given in tables 4.2 - 4.17.

The pressure versus time and flow versus time are provided in figures 4.2 - 4.9. These results are based on dividing the individual vessels of the model into 10 segments. The vessels of the model were discretization to 30 segments, instead of 10, to examine the effects of this model attribute to evaluate a subject. The results of this change in discretization are provided in tables 4.18 and 4.19 (cardiovascular parameters and physiological parameters), and the pressure and flow plots are provided in figures 4.10 (a)-(g). Additionally, a sensitivity analysis was performed to detect areas of instability in the model calculations. The results of this sensitivity analysis are provided in figures 4.11 - 4.15.

Subject: 471

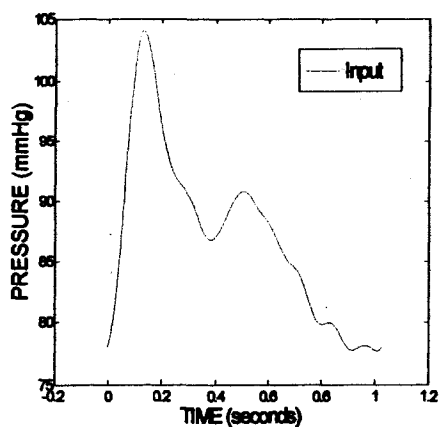
Age: 36 (years) [Predicted Age: 36]
 Height: 1830 (mm) [Predicted Height: 2133]
 Weight: 113.398 (kg) [Predicted Weight: 79.11]
 Gender: male [Predicted Gender: male]
 Heart Rate: 62 (beats/min)

Table 4.2 Cardiovascular parameters derived for subject 471

SVR	CO	Large Artery Compliance	Oscillatory Compliance
(dyne-sec/cm ⁵)	(L/min)	(ml/mmHg)	(ml/mmHg)
960.87	4.95	4.37	0.12

Table 4.3 Physiological data for arterial model of Subject 471

Vessel	length (mm)	radius (mm)		Elastic modulus (dyne/cm ²)x10 ⁶	Eh/r ratio (dyne/cm ²)x10 ⁶
		in	out		
1	244.58	2.60	1.14	37.27	2.01
2	122.29	3.33	3.33	35.93	1.93
3	122.29	1.74	0.89	38.52	2.01
4	122.29	0.44	0.44	38.52	2.01
5	426.38	3.49	1.96	30.69	1.84
6	29.87	3.67	3.67	9.15	0.70
7	110.53	3.78	3.01	6.59	0.45
8	35.39	10.04	7.77	4.54	0.28
9	51.89	14.63	13.84	3.39	0.16
10	2.59	13.84	13.03	6.16	0.25
11	129.89	3.77	3.01	6.59	0.45
12	5.19	13.04	12.24	7.93	0.46
13	194.60	12.24	11.44	8.27	0.71
14	15.72	11.44	10.64	6.46	0.49
15	9.43	10.64	9.84	6.19	0.45
16	9.43	9.84	9.04	5.96	0.41
17	44.01	9.04	8.24	5.17	0.24
18	40.87	8.24	7.45	3.08	0.06
19	65.84	3.72	3.50	4.31	0.25
20	65.84	3.72	3.50	4.31	0.25
21	166.05	3.50	3.01	12.75	0.77
22	166.05	3.50	3.01	12.75	0.77
23	442.27	4.33	2.38	18.84	0.83
24	442.27	4.33	2.38	18.84	0.83
25	367.06	1.19	1.19	26.20	1.19
26	367.06	1.19	1.19	26.20	1.19
27	342.95	1.19	0.57	26.2	1.19
28	342.96	1.19	0.57	26.2	1.19
29	244.59	2.44	1.07	33.96	2.01
30	122.29	0.83	0.83	30.71	1.75
31	122.29	0.85	0.44	36.82	2.01
32	122.29	0.38	0.38	36.82	2.01
33	426.38	3.49	1.98	18.93	1.48
34	37.34	3.67	3.67	8.79	0.57
35	148.86	1.63	1.28	18.98	1.13
36	148.86	1.63	1.28	30.61	1.62
37	124.94	2.57	2.57	18.84	0.83
38	124.94	2.57	2.57	18.84	0.83
39	57.26	2.02	2.02	8.93	0.43
40	57.26	2.02	2.02	8.93	0.43
41	42.68	1.81	1.81	4.21	0.22
42	27.74	1.31	1.31	5.82	0.40
43	27.74	2.37	2.37	6.07	0.44
44	51.21	10.64	10.64	6.29	0.48
45	8.54	2.64	2.64	6.61	0.55



(a) Input pressure at radial artery

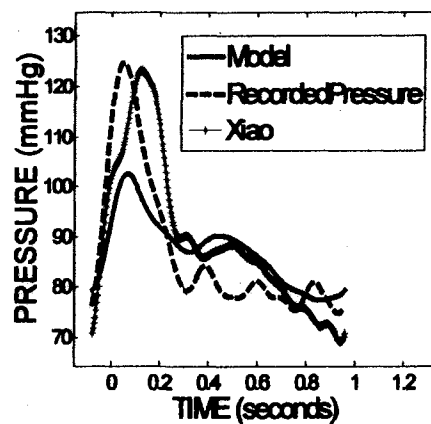
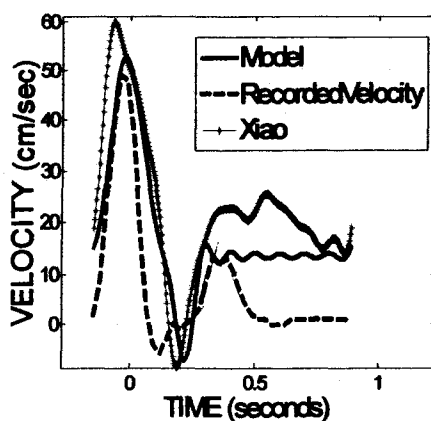
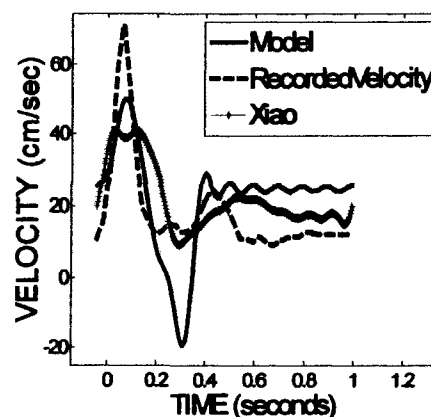
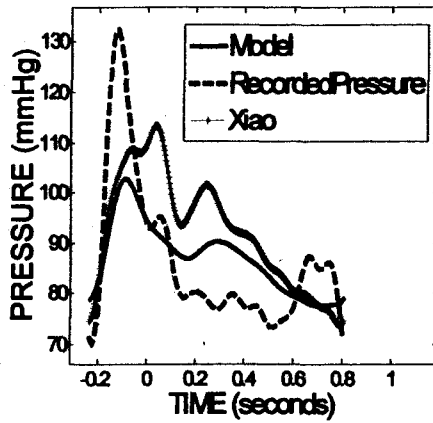
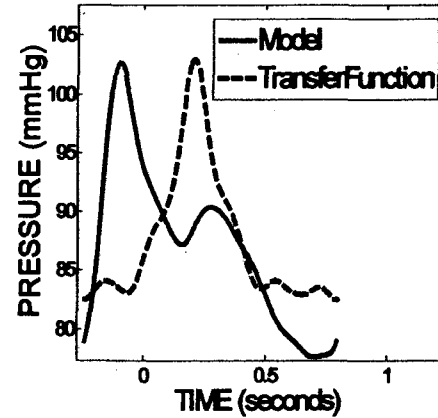
(b) Pressure at left brachial artery
(model error = 0.08)
(Xiao's error = 0.08)(c) Flow velocity at right brachial artery
(model error = 5.53)
(Xiao's error = 7.73)(d) Flow velocity at radial artery
(model error = 0.81)
(Xiao's error = 0.50)

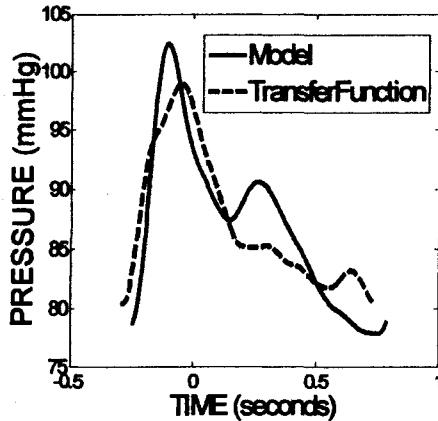
Fig. 4.2 (a)-(d) Flow and pressure results for subject 471



(e) Pressure at left carotid artery
(model error = 0.10)
(Xiao's error = 0.14)



(f) Pressure at aortic arch



(g) Pressure at ascending aorta

Fig. 4.2 (e)-(g) Flow and pressure results for subject 471

Referring to figures 4.2 (b), (c), (d) and (e), model error was low; however, maximum pressure was over 20 mmHg lower than recorded pressure. This may have been a contributing factor in the lower velocity at the radial artery (figure 4.2 (d)). The pressure magnitude predictions and overall form of the pressure waves at the aorta (figures 4.2 (f) and (g)) were close to those derived using a transfer function. Overall, the model error, which had an average error of 1.81, was lower than Xiao's model, which had an average error of 2.11.

Subject: y11

Age: 29 (years) [Predicted Age: 29]

Height: 1680 (mm) [Predicted Height: 1617]

Weight: 56 (kg) [Predicted Weight: 60]

Gender: female [Predicted Gender: female]

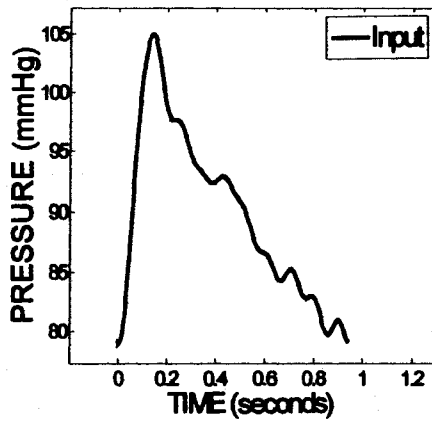
Heart Rate: 63.8 (beats/min)

Table 4.4 Cardiovascular parameters derived for subject y11

SVR	CO	Large Artery Compliance	Oscillatory Compliance
(dyne-sec/cm⁵)	(L/min)	(ml/mmHg)	(ml/mmHg)
1378.47	5.20	2.24	0.07

Table 4.5 Physiological data for arterial model of Subject y11

Vessel	length (mm)	radius (mm)		Elastic modulus (dyne/cm ²)x10 ⁶	Eh/r ratio (dyne/cm ²)x10 ⁶
		in	out		
1	165.62	1.95	1.11	27.00	1.70
2	82.81	2.49	2.49	28.16	1.77
3	82.81	1.37	0.87	25.77	1.70
4	82.81	0.43	0.43	25.77	1.70
5	385.88	3.29	1.92	36.08	1.88
6	26.25	3.46	3.46	11.09	0.84
7	74.84	3.26	2.74	4.89	0.34
8	23.96	7.22	5.67	3.77	0.23
9	47.77	10.70	9.96	3.02	0.14
10	2.39	9.96	9.22	5.97	0.22
11	87.96	3.25	2.74	4.89	0.34
12	4.78	9.22	8.49	8.07	0.44
13	179.15	8.49	7.75	10.77	0.86
14	14.47	7.75	7.02	9.36	0.59
15	8.68	7.02	6.28	8.87	0.53
16	8.68	6.28	5.55	8.47	0.48
17	40.52	5.55	4.81	7.12	0.26
18	37.63	4.81	4.08	3.56	0.04
19	65.26	2.04	1.82	3.85	0.20
20	65.26	2.04	1.82	3.85	0.20
21	164.59	1.82	1.33	14.11	0.67
22	164.59	1.82	1.33	14.11	0.67
23	404.25	3.73	2.05	19.67	0.77
24	404.25	3.73	2.05	19.67	0.77
25	337.84	1.03	1.03	24.89	1.12
26	337.84	1.03	1.03	24.89	1.12
27	315.64	1.03	0.46	24.89	1.12
28	315.64	1.03	0.46	24.89	1.12
29	165.62	1.82	1.04	21.37	1.69
30	82.81	0.81	0.81	20.48	1.52
31	82.81	0.83	0.53	22.10	1.69
32	82.81	0.37	0.37	22.10	1.69
33	385.88	3.29	1.92	15.42	1.35
34	32.81	3.46	3.46	9.25	0.56
35	134.71	1.54	1.23	14.64	1.04
36	134.71	1.54	1.23	31.40	1.70
37	114.19	1.14	1.14	19.67	0.77
38	114.19	1.14	1.14	19.67	0.77
39	56.75	1.05	1.05	9.19	0.37
40	56.75	1.05	1.05	9.19	0.37
41	37.50	1.06	1.06	5.47	0.24
42	24.38	1.29	1.29	8.24	0.48
43	24.38	1.23	1.23	8.66	0.53
44	45.00	7.02	7.02	9.04	0.58
45	7.50	2.18	2.18	9.60	0.66



(a) Input pressure at radial artery

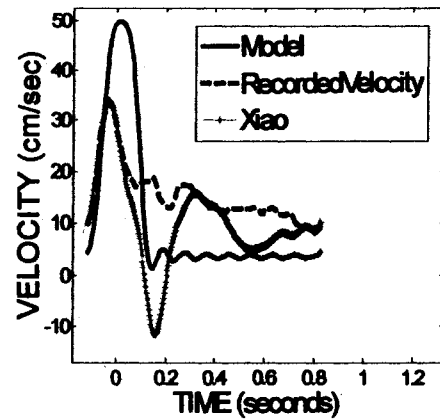
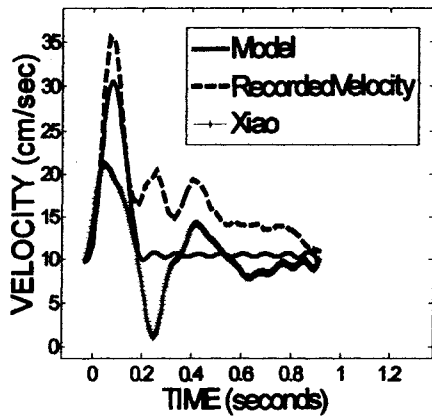
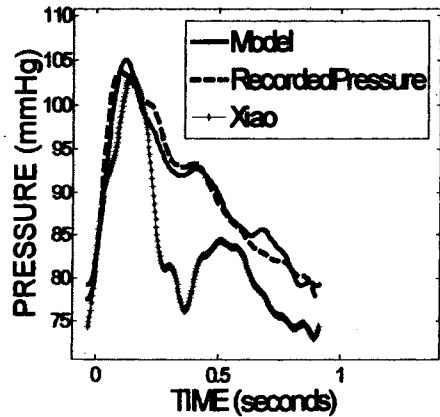
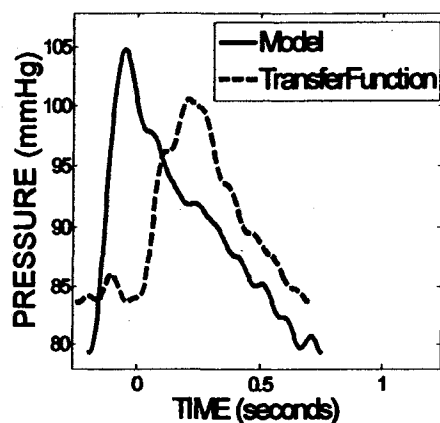
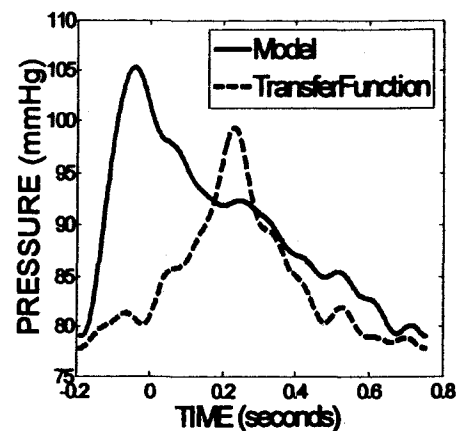
(b) Flow velocity at brachial artery
(model error = 0.65)
(Xiao's error = 0.34)(c) Flow velocity at radial artery
(model error = 0.23)
(Xiao's error = 0.33)(d) Pressure at brachial artery
(model error = 0.01)
(Xiao's error = 0.07)

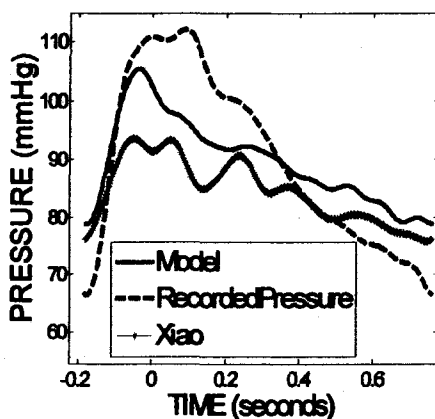
Fig. 4.3 (a)-(d) Flow and pressure results for subject y11



(e) Pressure at ascending aorta



(f) Pressure at aortic arch



(g) Pressure at carotid artery
(model error = 0.08)
(Xiao's error = 0.09)

Fig. 4.3 (e)-(g) Flow and pressure results for subject y11

Referring to figures 4.3 (b), (c), (d) and (g), model error was low. The pressure magnitude predictions at the aorta (figures 4.3 (e) and (f)) were slightly higher than those derived using a transfer function. However, the overall form of the aortic pressure waves were consistent with those derived using a transfer function. Overall, the model error, which had an average error of 0.06, was lower than Xiao's model, which had an average error of 0.21.

Subject: 730

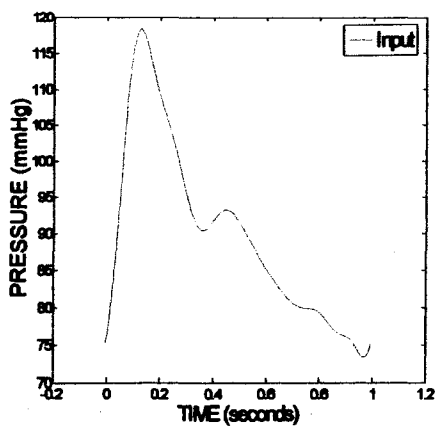
Age: 42 (years) [Predicted Age: 24]
 Height: 1560 (mm) [Predicted Height: 1875]
 Weight: 81.65 (kg) [Predicted Weight: 79.46]
 Gender: male [Predicted Gender: female]
 Heart Rate: 60 (beats/min)

Table 4.6 Cardiovascular parameters derived for subject 730

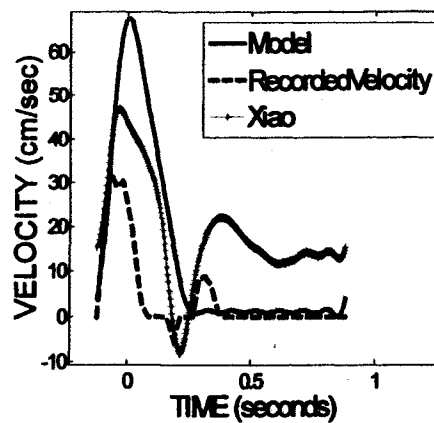
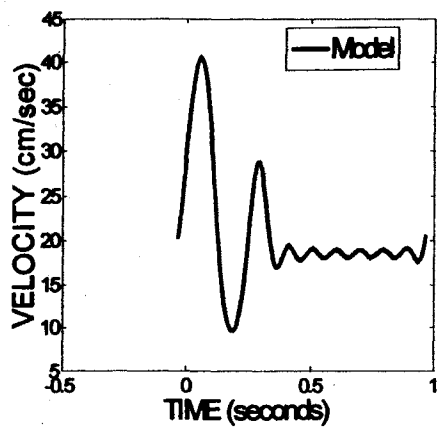
SVR	CO	Large Artery Compliance	Oscillatory Compliance
(dyne-sec/cm ⁵)	(L/min)	(ml/mmHg)	(ml/mmHg)
1006.71	4.72	2.31	0.09

Table 4.7 Physiological data for arterial model of Subject 730

Vessel	length (mm)	radius (mm)		Elastic modulus (dyne/cm ²)x10 ⁶	Eh/r ratio (dyne/cm ²)x10 ⁶
		in	out		
1	208.50	2.25	1.11	25.81	2.12
2	104.25	2.88	2.88	26.18	2.08
3	104.25	1.54	0.87	25.36	2.11
4	104.25	0.43	0.43	25.36	2.11
5	363.47	4.01	2.72	28.13	2.05
6	25.47	4.21	4.21	10.27	0.93
7	94.22	3.74	3.09	7.42	0.72
8	30.17	8.78	6.84	5.41	0.47
9	54.83	12.89	12.05	4.15	0.26
10	2.74	12.05	11.20	7.01	0.41
11	110.73	3.74	3.09	7.42	0.72
12	5.48	11.20	10.36	8.81	0.62
13	205.62	10.36	9.52	12.42	0.87
14	16.61	9.52	8.67	12.53	0.66
15	9.96	8.67	7.83	11.76	0.60
16	9.97	7.83	6.98	11.13	0.54
17	46.50	6.98	6.14	9.17	0.31
18	43.18	6.14	5.29	4.67	0.08
19	56.12	2.65	2.46	4.79	0.28
20	56.12	2.65	2.46	4.79	0.28
21	141.55	2.46	2.04	14.37	0.85
22	141.55	2.46	2.04	14.37	0.85
23	377.02	4.74	2.60	19.00	0.89
24	377.02	4.74	2.60	19.00	0.89
25	312.90	1.30	1.30	23.09	1.28
26	312.90	1.30	1.30	23.09	1.28
27	292.35	1.30	0.78	23.09	1.28
28	292.35	1.30	0.78	23.09	1.28
29	208.50	2.11	1.04	23.09	1.28
30	104.25	0.81	0.81	20.41	1.86
31	104.25	0.83	0.47	22.87	2.11
32	104.25	0.37	0.37	22.87	2.11
33	363.47	4.01	2.72	15.08	1.61
34	31.83	4.21	4.21	9.81	0.73
35	126.89	1.87	1.52	14.23	1.27
36	126.89	1.87	1.52	25.31	1.86
37	106.50	1.74	1.74	19.00	0.89
38	106.50	1.74	1.74	19.00	0.89
39	48.81	1.42	1.42	9.98	0.48
40	48.81	1.42	1.42	9.98	0.48
41	36.38	1.35	1.35	6.93	0.29
42	23.65	1.62	1.62	10.77	0.54
43	23.65	1.57	1.57	11.42	0.59
44	43.66	8.67	8.67	12.02	0.65
45	7.28	2.69	2.69	12.93	0.74

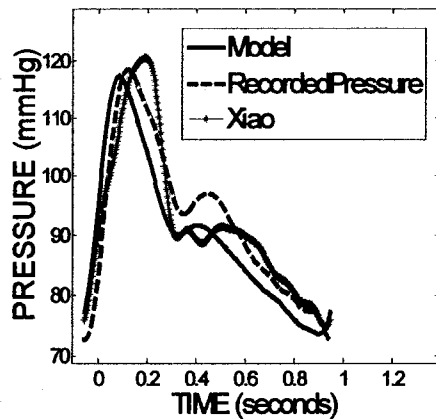


(a) Input pressure at radial artery

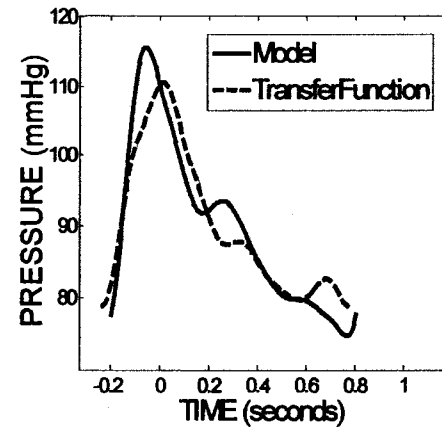
(b) Flow velocity at brachial artery
(model error = 6.33)
(Xiao's error = 11.38)

(c) Flow velocity at radial artery

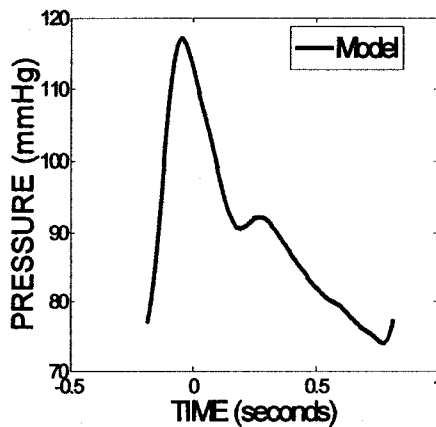
Fig. 4.4 (a)-(c) Flow and pressure results for subject 730



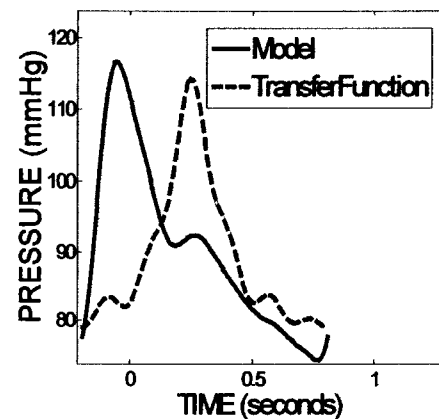
(d) Pressure at brachial artery
(model error = 0.05)
(Xiao's error = 0.04)



(e) Pressure at ascending aorta



(f) Pressure at carotid artery



(g) Pressure at aortic arch

Fig. 4.4 (d)-(g) Flow and pressure results for subject 730

Referring to figures 4.4 (b) and (d), model error was low. The pressure magnitude predictions and overall form of the waves at the aorta (figures 4.4 (e) and (g)) were consistent with those derived using a transfer function. Overall, the model error, which had an average error of 3.19, was lower than Xiao's model, which had an average error of 5.71.

Subject: 281

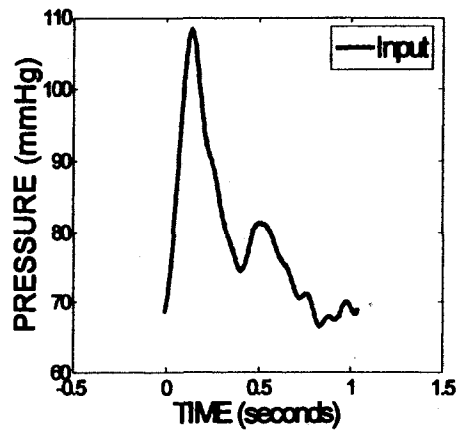
Age: 32 (years) [Predicted Age: 30]
 Height: 1800 (mm) [Predicted Height: 1791]
 Weight: 72.574 (kg) [Predicted Weight: 78.88]
 Gender: male [Predicted Gender: male]
 Heart Rate: 57.44 (beats/min)

Table 4.8 Cardiovascular parameters derived for subject 281

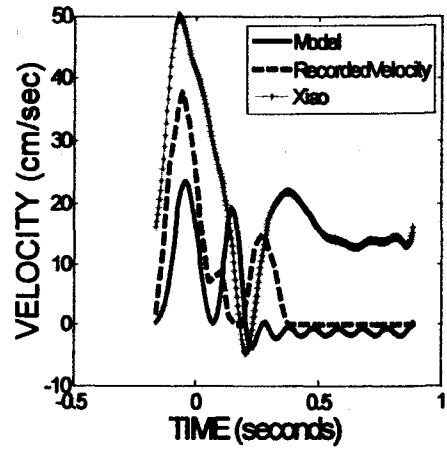
SVR	CO	Large Artery Compliance	Oscillatory Compliance
(dyne-sec/cm ⁵)	(L/min)	(ml/mmHg)	(ml/mmHg)
920.63	2.89	3.68	0.11

Table 4.9 Physiological data for arterial model of Subject 281

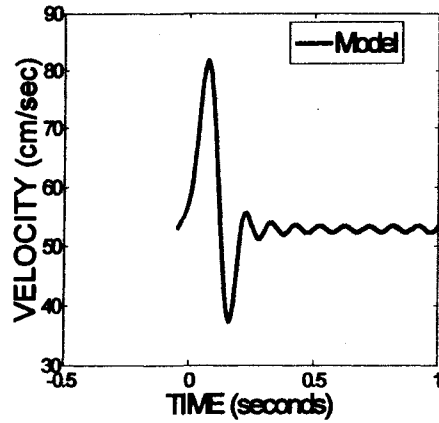
Vessel	length (mm)	radius (mm)		Elastic modulus (dyne/cm ²)x10 ⁶	Eh/r ratio (dyne/cm ²)x10 ⁶
		in	out		
1	240.58	2.43	1.08	13.00	1.32
2	120.29	3.11	3.11	13.66	1.36
3	120.29	1.63	0.84	12.47	1.32
4	120.29	0.42	0.42	12.47	1.32
5	419.39	2.53	1.04	17.79	1.42
6	29.38	2.66	2.66	7.90	0.61
7	108.72	3.45	2.70	5.36	0.26
8	34.81	9.10	6.87	3.83	0.18
9	49.65	12.94	12.18	3.00	0.13
10	2.48	12.18	11.41	5.95	0.18
11	127.76	3.45	2.70	5.36	0.26
12	4.96	11.41	10.65	8.07	0.41
13	186.19	10.65	9.88	11.22	0.72
14	15.04	9.88	9.12	9.83	0.46
15	9.02	9.12	8.36	9.25	0.42
16	9.02	8.36	7.59	8.78	0.38
17	42.11	7.59	6.83	7.28	0.22
18	39.10	6.83	6.06	3.83	0.06
19	64.76	3.03	2.82	4.47	0.19
20	64.76	3.03	2.82	4.47	0.19
21	163.33	2.81	2.33	14.66	0.57
22	163.33	2.81	2.33	14.66	0.57
23	435.02	3.76	2.07	17.22	0.45
24	435.02	3.76	2.07	17.22	0.45
25	361.04	1.03	1.03	18.56	0.63
26	361.04	1.03	1.03	18.56	0.63
27	337.32	1.03	0.43	18.56	0.63
28	337.32	1.03	0.43	18.56	0.63
29	240.58	2.28	1.01	11.75	1.31
30	120.29	0.79	0.79	11.58	1.16
31	120.29	0.81	0.42	11.58	1.31
32	120.29	0.36	0.36	11.88	1.31
33	419.39	2.53	1.04	10.56	1.01
34	36.73	2.66	2.66	8.88	0.49
35	146.42	1.18	0.93	10.43	0.81
36	146.42	1.18	0.93	21.17	1.27
37	122.89	1.99	1.99	17.22	0.45
38	122.89	1.99	1.99	17.22	0.45
39	56.32	1.62	1.62	9.70	0.32
40	56.32	1.62	1.62	9.70	0.32
41	41.98	1.50	1.50	5.57	0.20
42	27.28	1.98	1.98	8.50	0.38
43	27.28	1.98	1.98	8.99	0.41
44	50.37	9.12	9.12	9.45	0.45
45	8.40	2.83	2.83	10.14	0.51



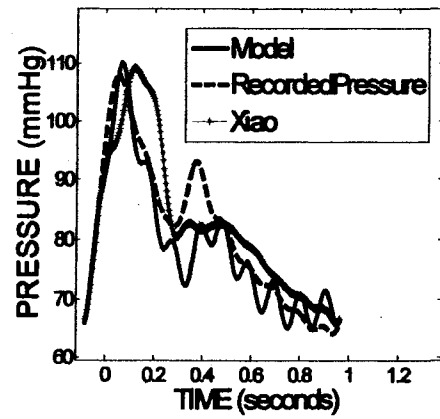
(a) Input pressure at radial artery



(b) Flow velocity at brachial artery (model error = 1.55) (Xiao's error = 8.43)

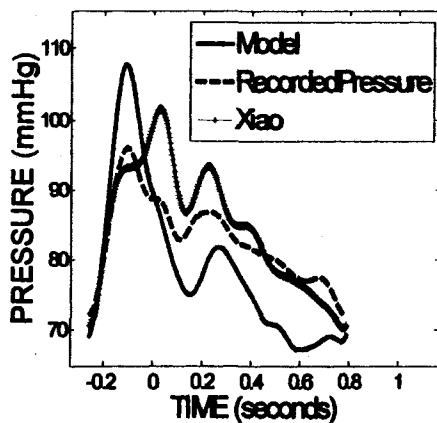


(c) Flow velocity at radial artery

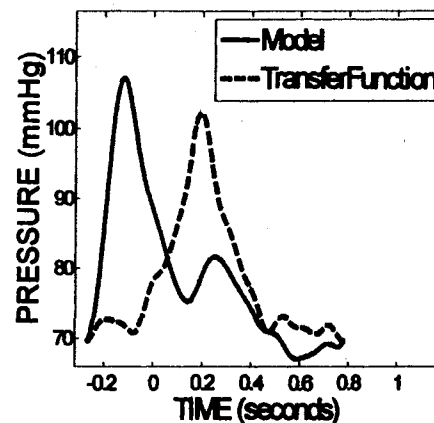


(d) Pressure at brachial artery (model error = 0.04) (Xiao's error = 0.05)

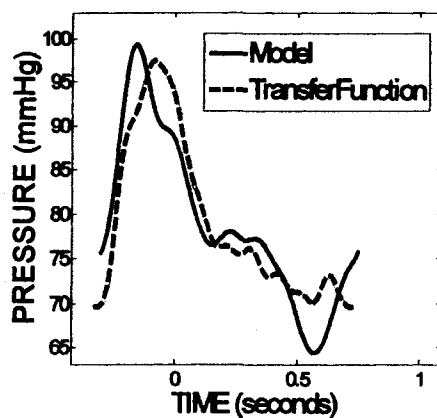
Fig. 4.5 (a)-(d) Flow and pressure results for subject 281



(e) Pressure at carotid artery
(model error = 0.08)
(Xiao's error = 0.04)



(f) Pressure at aortic arch



(g) Pressure at ascending aorta

Fig. 4.5 (e)-(g) Flow and pressure results for subject 281

Referring to figures 4.5 (b), (d) and (e), model error was low. The pressure magnitude predictions and overall form of the waves at the aorta (figures 4.5 (f) and (g)) were consistent with those derived using a transfer function. Overall, the model error, which had an average error of 0.56, was lower than Xiao's model, which had an average error of 2.84.

Subject: 472

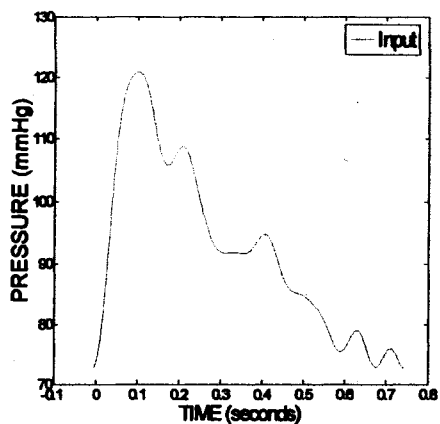
Age: 33 (years) [Predicted Age: 37]
 Height: 1780 (mm) [Predicted Height: 1690]
 Weight: 62.6 (kg) [Predicted Weight: 78.93]
 Gender: male [Predicted Gender: male]
 Heart Rate: 80 (beats/min)

Table 4.10 Cardiovascular parameters derived for subject 472

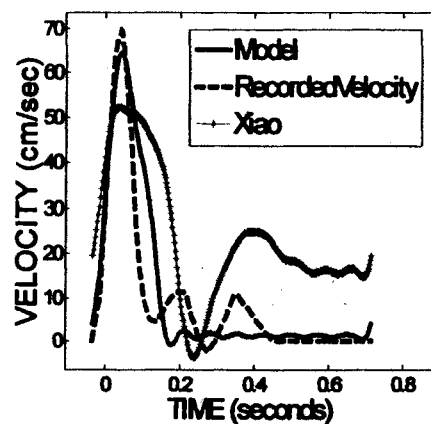
SVR	CO	Large Artery Compliance	Oscillatory Compliance
(dyne-sec/cm ⁵)	(L/min)	(ml/mmHg)	(ml/mmHg)
1484.89	2.04	0.92	0.04

Table 4.11 Physiological data for arterial model of Subject 472

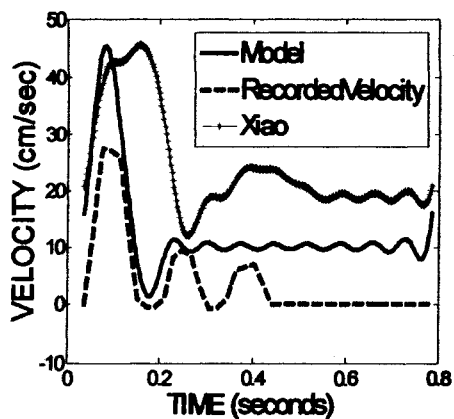
Vessel	length (mm)	radius (mm)		Elastic modulus (dyne/cm ²)x10 ⁶	Eh/r ratio (dyne/cm ²)x10 ⁶
		in	out		
1	237.90	2.43	1.09	19.24	2.03
2	118.95	3.10	3.10	20.89	2.15
3	118.95	1.63	0.85	17.69	2.02
4	118.95	0.42	0.42	17.69	2.02
5	414.73	2.52	1.04	32.04	2.32
6	29.06	2.64	2.64	13.20	1.05
7	107.51	3.47	2.73	5.05	0.22
8	34.42	8.80	6.59	5.48	0.27
9	49.35	12.42	11.66	5.75	0.31
10	2.47	11.66	10.90	7.81	0.31
11	126.34	3.46	2.73	5.05	0.22
12	4.93	10.90	10.14	9.68	0.48
13	185.06	10.14	9.38	12.92	0.78
14	14.95	9.38	8.62	11.07	0.52
15	8.97	8.62	7.86	10.51	0.48
16	8.97	7.86	7.10	10.06	0.44
17	41.86	7.10	6.34	8.60	0.26
18	38.87	6.34	5.58	5.06	0.09
19	64.04	2.79	2.58	5.72	0.24
20	64.04	2.79	2.58	5.72	0.24
21	161.51	2.58	2.10	16.56	0.65
22	161.51	2.58	2.10	16.56	0.65
23	430.19	3.78	2.08	21.29	0.84
24	430.19	3.78	2.08	21.29	0.84
25	357.03	1.04	1.04	25.81	1.21
26	357.03	1.04	1.04	25.81	1.21
27	333.58	1.04	0.44	25.81	1.21
28	333.58	1.04	0.44	25.81	1.21
29	237.90	2.27	1.02	15.84	2.01
30	118.95	0.79	0.79	15.53	1.75
31	118.95	0.81	0.42	16.10	2.01
32	118.95	0.36	0.36	16.10	2.01
33	414.73	2.52	1.04	13.65	1.49
34	36.32	2.64	2.64	10.70	0.59
35	144.79	1.17	0.92	13.41	1.14
36	144.79	1.17	0.92	31.82	2.02
37	121.52	1.79	1.79	21.29	0.84
38	121.52	1.79	1.79	21.29	0.84
39	55.69	1.49	1.49	11.29	0.38
40	55.69	1.49	1.49	11.29	0.38
41	41.51	1.39	1.39	6.89	0.25
42	26.98	1.85	1.85	9.80	0.43
43	26.98	1.83	1.83	10.27	0.47
44	49.81	8.62	8.62	10.70	0.51
45	8.30	2.67	2.67	11.35	0.58



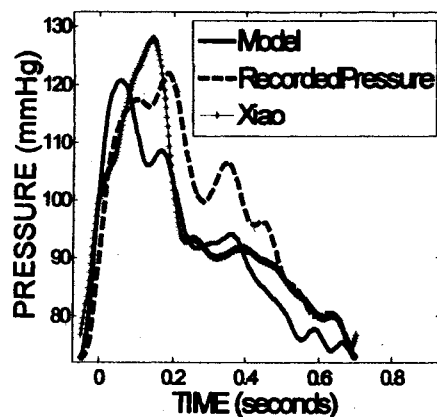
(a) Input pressure at radial artery



(b) Flow velocity at brachial artery (model error = 1.57) (Xiao's error = 8.83)

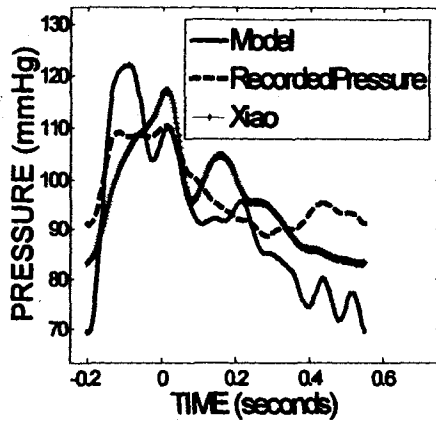


(c) Flow velocity at radial artery (model error = 6.80) (Xiao's error = 16.71)

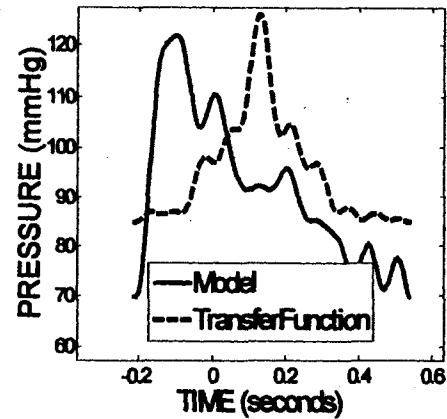


(d) Pressure at brachial artery (model error = 0.08) (Xiao's error = 0.06)

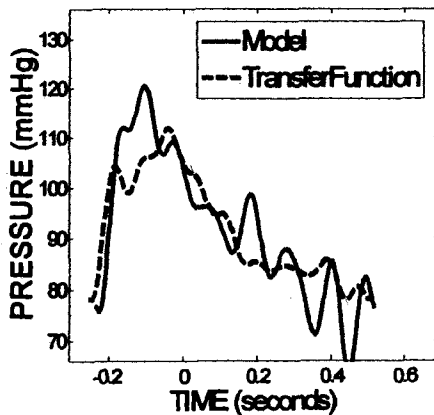
Fig. 4.6 (a)-(d) Flow and pressure results for subject 472



(e) Pressure at carotid artery
(model error = 0.09)
(Xiao's error = 0.06)



(f) Pressure at aortic arch



(g) Pressure at ascending aorta

Fig. 4.6 (e)-(g) Flow and pressure results for subject 472

Referring to figures 4.6 (b), (c), (d) and (e), model error was low. The pressure magnitude predictions and overall form of the waves at the aorta (figures 4.6 (f) and (g)) were consistent with those derived using a transfer function. Overall, the model error, which had an average error of 2.14, was lower than Xiao's model, which had an average error of 6.42.

Subject: 671 (heart failure patient)

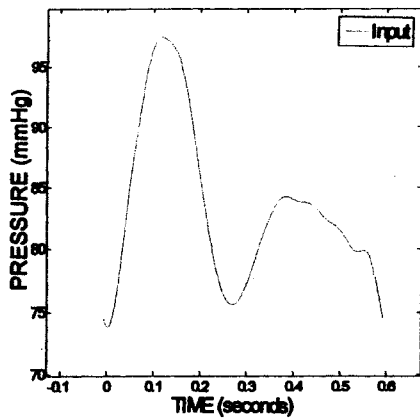
Age: 30 (years) [Predicted Age: -61]
 Height: 1905 (mm) [Predicted Height: 1546]
 Weight: 49.9 (kg) [Predicted Weight: 78.76]
 Gender: male [Predicted Gender: male]
 Heart Rate: 100 (beats/min)

Table 4.12 Cardiovascular parameters derived for subject 671

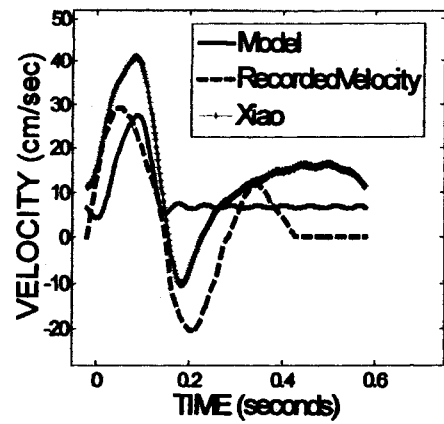
SVR	CO	Large Artery Compliance	Oscillatory Compliance
(dyne-sec/cm ⁵)	(L/min)	(ml/mmHg)	(ml/mmHg)
32308.88	0.21	0.16	0.003

Table 4.13 Physiological data for arterial model of Subject 671

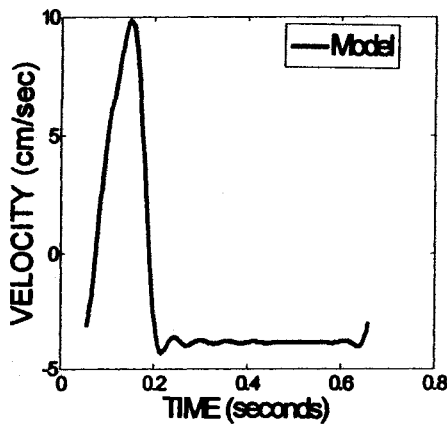
Vessel	length (mm)	radius (mm)		Elastic modulus (dyne/cm ²)x10 ⁶	Eh/r ratio (dyne/cm ²)x10 ⁶
		in	out		
1	254.61	2.62	1.11	32.11	1.98
2	127.30	3.35	3.35	34.04	2.12
3	127.30	1.74	0.87	30.11	1.97
4	127.30	0.43	0.43	30.11	1.97
5	443.86	4.25	2.67	44.78	2.31
6	31.10	4.46	4.46	12.31	0.97
7	115.06	3.95	3.16	1.80	0.06
8	36.84	7.92	5.55	2.61	0.122
9	48.42	10.47	9.72	3.09	0.17
10	2.42	9.72	8.97	3.57	0.15
11	135.21	3.95	3.16	1.80	0.06
12	4.84	8.97	8.23	4.17	0.21
13	181.58	8.23	7.48	4.50	0.34
14	14.67	7.48	6.74	3.44	0.23
15	8.80	6.74	5.99	3.42	0.22
16	8.80	5.99	5.25	3.41	0.20
17	41.07	5.25	4.50	3.37	0.15
18	38.13	4.50	3.76	3.25	0.10
19	68.54	1.88	1.65	4.66	0.19
20	68.54	1.88	1.65	4.66	0.19
21	172.86	1.65	1.13	9.38	0.41
22	172.86	1.65	1.13	9.38	0.41
23	460.40	4.74	2.61	21.07	0.96
24	460.40	4.74	2.61	21.07	0.96
25	382.10	1.30	1.30	36.50	1.39
26	382.10	1.30	1.30	36.50	1.39
27	357.00	1.30	0.66	36.50	1.39
28	357.00	1.30	0.66	36.50	1.39
29	254.61	2.46	1.04	24.14	1.95
30	127.30	0.81	0.81	22.43	1.65
31	127.30	0.83	0.41	25.54	1.95
32	127.30	0.37	0.37	25.54	1.95
33	443.86	4.25	2.67	14.45	1.36
34	38.87	4.46	4.46	5.14	0.32
35	154.96	1.98	1.54	13.25	0.95
36	154.96	1.98	1.54	38.55	1.97
37	130.06	0.97	0.97	21.07	0.96
38	130.06	0.97	0.97	21.07	0.96
39	59.61	0.95	0.95	7.13	0.26
40	59.61	0.95	0.95	7.13	0.26
41	44.43	0.99	0.99	3.31	0.15
42	28.88	1.22	1.22	3.40	0.20
43	28.88	1.15	1.15	3.42	0.21
44	53.31	6.74	6.74	3.43	0.23
45	8.89	2.09	2.09	3.45	0.25



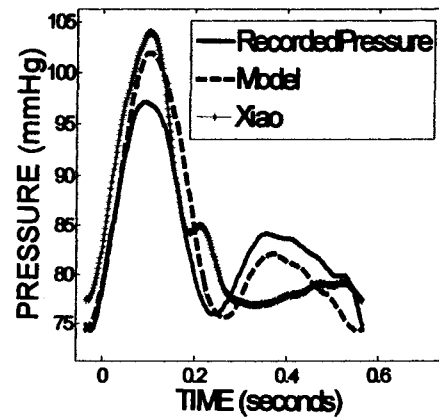
(a) Input pressure at radial artery



(b) Flow velocity at brachial artery (model error = 3.11) (Xiao's error = 5.48)

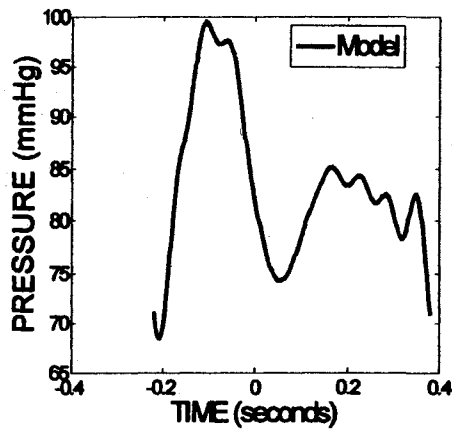


(c) Flow velocity at radial artery

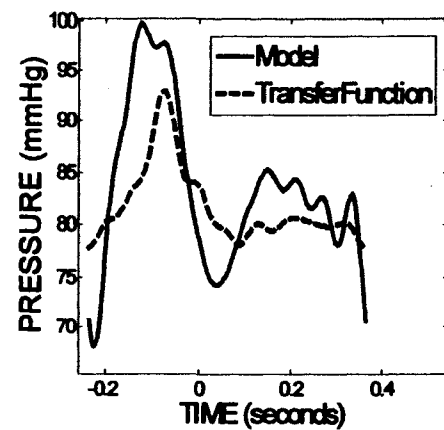


(d) Pressure at brachial artery (model error = 0.03) (Xiao's error = 0.04)

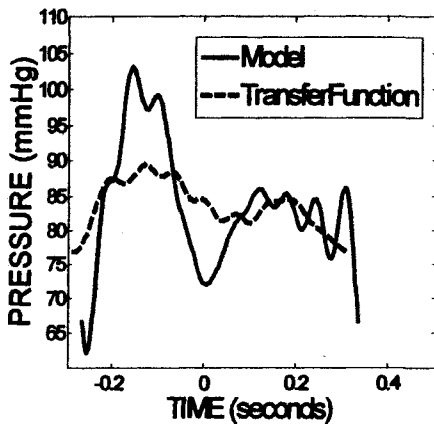
Fig. 4.7 (a)-(d) Flow and pressure results for subject 671



(e) Pressure at carotid artery



(f) Pressure at aortic arch



(g) Pressure at ascending aorta

Fig. 4.7 (e)-(g) Flow and pressure results for subject 671

Referring to figures 4.7 (b) and (d), model error was fair. The model was able to approximate pressure at the brachial artery (figure 4.7 (d)); however, it fell short of predicting the negative velocity flow (figure 4.7 (b)). This may be attributed to improper timing of the pressures that create the pressure gradient at the brachial artery. The pressure magnitude predictions and overall form of the waves at the aorta (figures 4.7 (f) and (g)) were inconsistent with those derived using a transfer function. Given the model's accurate pressure prediction at the brachial artery, the transfer functions may not

be applicable to this subject. Overall, the model error, which had an average error of 1.57, was lower than Xiao's model, which had an average error of 2.76.

Subject: Cr (heart failure patient)

Predicted Age: 45 (years)

Predicted Height: 1604.85 (mm)

Predicted Weight: 79.64 (kg)

Predicted Gender: male

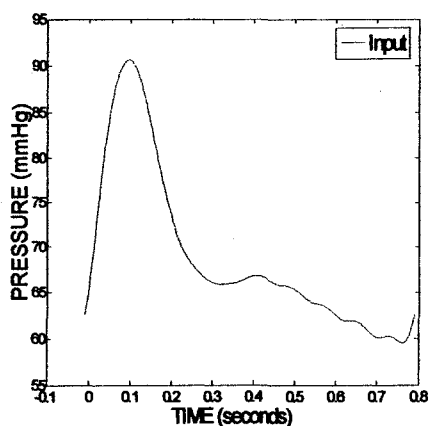
Heart Rate: 75 (beats/min)

Table 4.14 Cardiovascular parameters derived for subject Cr

SVR	CO	Large Artery Compliance	Oscillatory Compliance
(dyne-sec/cm ⁵)	(L/min)	(ml/mmHg)	(ml/mmHg)
1218.42	2.99	3.04	0.06

Table 4.15 Physiological data for arterial model of Subject Cr

Vessel	length (mm)	radius (mm)		Elastic modulus (dyne/cm ²)x10 ⁶	Eh/r ratio (dyne/cm ²)x10 ⁶
		in	out		
1	214.49	2.48	1.20	17.98	1.00
2	107.25	3.17	3.17	17.68	1.06
3	107.25	1.69	0.94	18.35	1.00
4	107.25	0.47	0.47	18.35	1.00
5	373.92	3.33	2.00	16.61	1.13
6	26.20	3.49	3.49	5.74	0.62
7	96.93	3.58	2.91	3.64	0.37
8	31.03	9.03	7.04	3.27	0.31
9	56.15	13.26	12.40	3.03	0.25
10	2.8	12.40	11.54	4.42	0.30
11	113.91	3.58	2.91	3.64	0.37
12	5.61	11.54	10.67	5.48	0.46
13	210.55	10.67	9.81	6.86	0.73
14	17.00	9.81	8.94	6.02	0.52
15	10.20	8.94	8.08	5.80	0.48
16	10.20	8.94	7.21	5.60	0.44
17	47.62	7.21	6.35	4.95	0.26
18	44.22	6.35	5.49	3.11	0.08
19	57.74	2.74	2.55	3.08	0.19
20	57.74	2.74	2.55	3.08	0.19
21	145.62	2.55	2.12	7.22	0.54
22	145.62	2.55	2.12	7.22	0.54
23	387.86	4.25	2.33	7.13	0.28
24	387.86	4.25	2.33	7.13	0.28
25	321.90	1.17	1.17	5.05	0.37
26	321.90	1.17	1.17	5.05	0.37
27	300.75	1.17	0.63	5.05	0.37
28	300.75	1.17	0.63	5.05	0.37
29	214.49	2.32	1.12	15.24	0.99
30	107.25	0.88	0.88	13.70	0.91
31	107.25	0.88	0.50	16.86	0.99
32	107.25	0.40	0.40	16.86	0.99
33	373.93	3.33	2.00	8.94	0.82
34	32.74	3.49	3.49	5.97	0.52
35	130.54	1.55	1.25	12.17	0.70
36	130.54	1.55	1.25	12.17	0.70
37	109.56	1.81	1.81	7.13	0.28
38	109.56	1.81	1.81	7.13	0.28
39	50.21	1.47	1.47	5.43	0.31
40	50.21	1.47	1.47	5.43	0.31
41	37.43	1.40	1.40	4.13	0.24
42	24.33	1.05	1.05	5.49	0.44
43	24.33	1.83	1.83	5.70	0.48
44	44.91	8.94	8.94	5.88	0.52
45	7.49	2.22	2.22	6.14	0.59



(a) Input pressure at radial artery

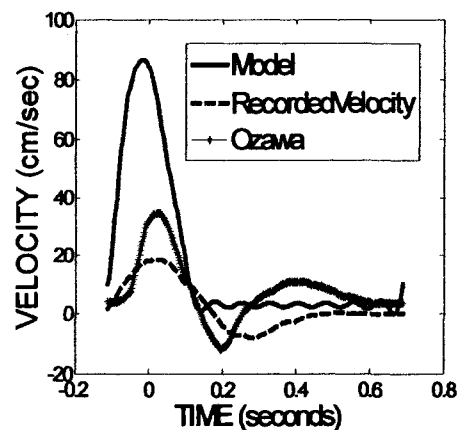
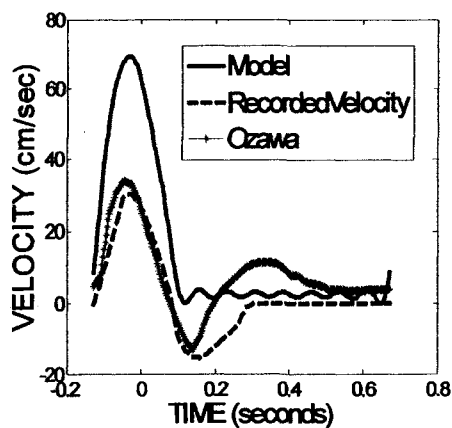
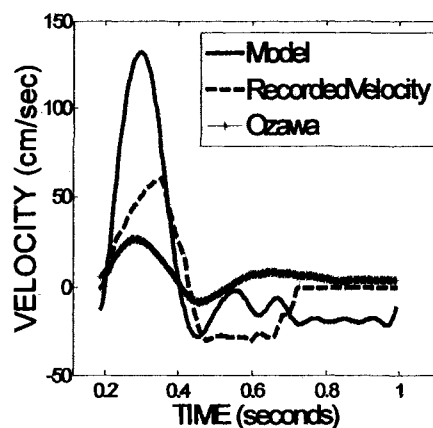
(b) Flow velocity at left brachial artery (model error = 3.72)
(Ozawa's error = 6.19)(c) Flow velocity at right brachial artery (model error = 2.82)
(Ozawa's error = 4.94)(d) Flow velocity at right femoral artery (model error = 7.26)
(Ozawa's error = 2.20)

Fig. 4.8 (a)-(d) Flow and pressure results for subject Cr

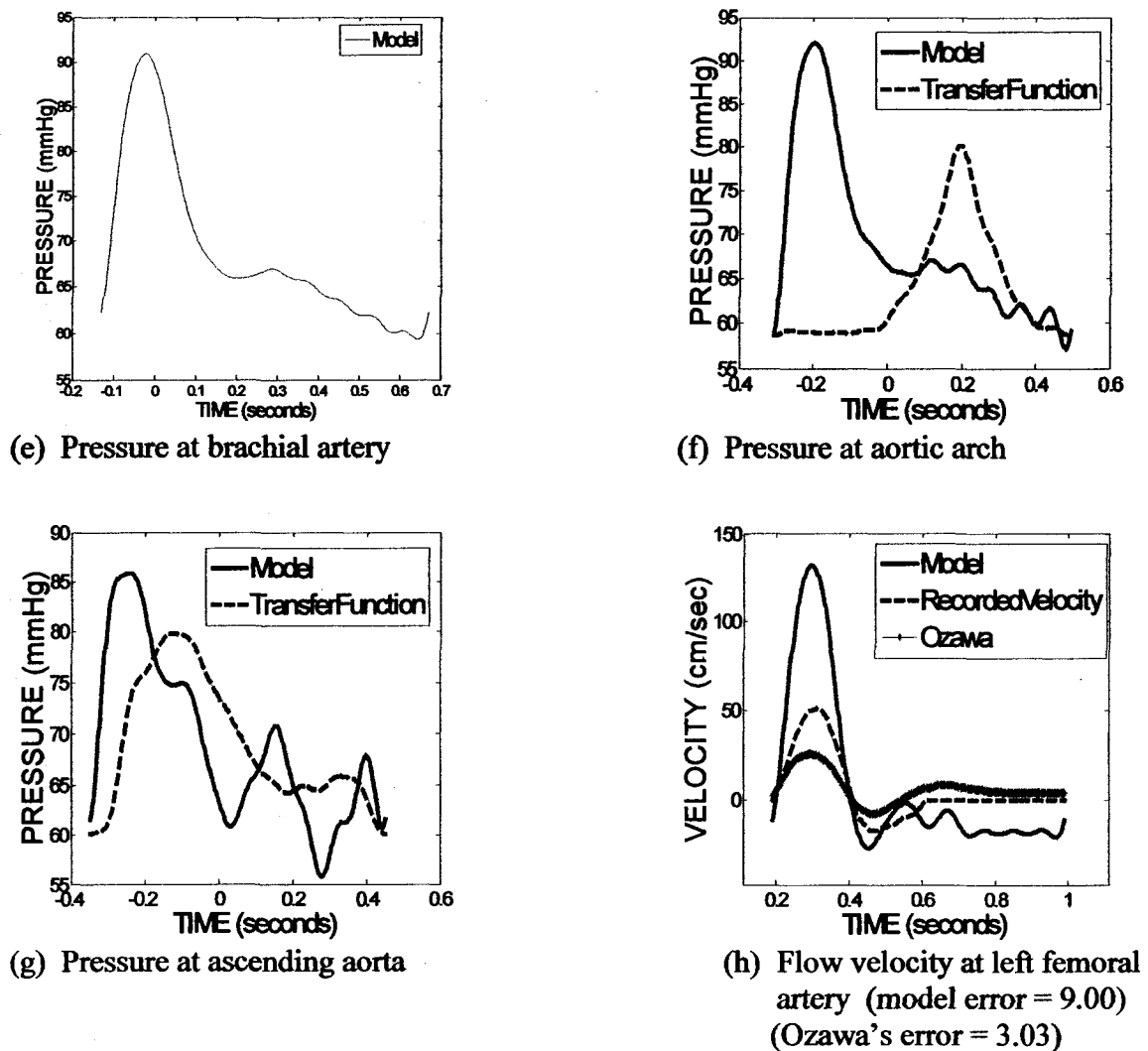


Fig. 4.8 (e)-(h) Flow and pressure results for subject Cr

Referring to figures 4.8 (b), (c), (d) and (h), model error was higher than those for previous subjects. This is attributed, in part, to the lack of age, weight, height and gender input data, which compounded the error during pressure and flow calculations.

Additionally, this subject was a heart failure patient and possessed arterial disorders that were not compensated for in this model. Methods of compensating for preexisting arterial disorders will be pursued for future versions of this model. Overall, the model

error, which had an average error of 4.09, was higher than Ozawa's model, which had an average error of 5.70.

Subject: Lf (heart failure patient)

Predicted Age: 38 (years)

Predicted Height: 1603.15 (mm)

Predicted Weight: 79.23 (kg)

Predicted Gender: male

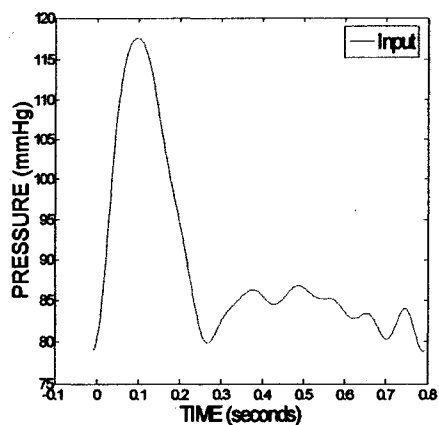
Heart Rate: 75 (beats/min)

Table 4.16 Cardiovascular parameters derived for subject Lf

SVR	CO	Large Artery Compliance	Oscillatory Compliance
(dyne-sec/cm⁵)	(L/min)	(ml/mmHg)	(ml/mmHg)
1170.98	2.72	12.80	0.06

Table 4.17 Physiological data for arterial model of Subject Lf

Vessel	length (mm)	radius (mm)		Elastic modulus (dyne/cm ²)x10 ⁶	Eh/r ratio (dyne/cm ²)x10 ⁶
		in	out		
1	214.27	2.24	1.08	15.07	1.67
2	107.13	2.86	2.86	16.34	1.77
3	107.13	1.53	0.85	13.87	1.66
4	107.13	0.42	0.42	13.87	1.66
5	373.53	2.38	1.05	24.91	1.90
6	26.17	2.50	2.50	10.23	0.85
7	96.83	3.42	2.75	5.16	0.27
8	31.00	9.26	7.27	3.93	0.21
9	52.92	13.70	12.88	3.19	0.16
10	2.65	12.88	12.07	6.72	0.22
11	113.79	3.42	2.75	5.16	0.27
12	5.29	12.07	11.25	9.36	0.45
13	198.47	11.25	10.44	14.56	0.86
14	16.03	10.44	9.62	13.42	0.56
15	9.62	9.62	8.81	12.55	0.51
16	9.62	8.81	7.99	11.86	0.47
17	44.89	7.99	7.18	9.70	0.28
18	41.68	7.18	6.37	4.90	0.08
19	57.68	3.18	2.99	5.14	0.25
20	57.68	3.18	2.99	5.14	0.25
21	145.47	2.99	2.56	16.52	0.72
22	145.47	2.99	2.56	16.52	0.72
23	387.45	3.79	2.09	18.00	0.63
24	387.45	3.79	2.09	18.00	0.63
25	321.56	1.04	1.04	16.98	0.90
26	321.56	1.04	1.04	16.98	0.90
27	300.44	1.04	0.50	16.98	0.90
28	300.44	1.04	0.50	16.98	0.90
29	214.27	2.10	1.02	12.60	1.65
30	107.13	0.79	0.79	12.48	1.45
31	107.13	0.81	0.45	12.71	1.65
32	107.13	0.36	0.36	12.71	1.65
33	373.53	2.38	1.05	11.69	1.25
34	32.71	2.50	2.50	10.47	0.56
35	130.40	1.11	0.90	11.59	0.98
36	130.40	1.11	0.90	24.76	1.66
37	109.45	2.18	2.18	18.01	0.63
38	109.45	2.18	2.18	18.01	0.63
39	50.16	1.72	1.72	11.01	0.41
40	50.16	1.72	1.72	11.01	0.41
41	37.39	1.58	1.58	7.28	0.25
42	24.30	2.09	2.09	11.46	0.46
43	24.30	2.07	2.07	12.18	0.51
44	44.86	9.62	9.62	12.85	0.55
45	7.48	2.98	2.98	13.88	0.63



(a) Input pressure at radial artery

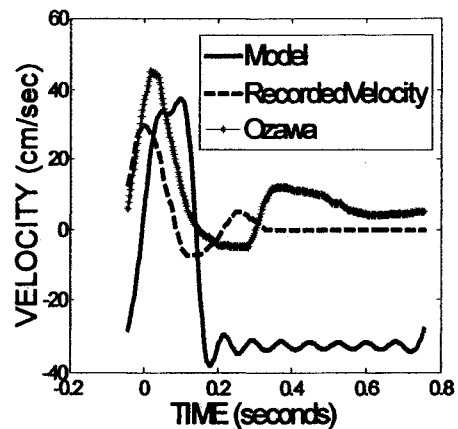
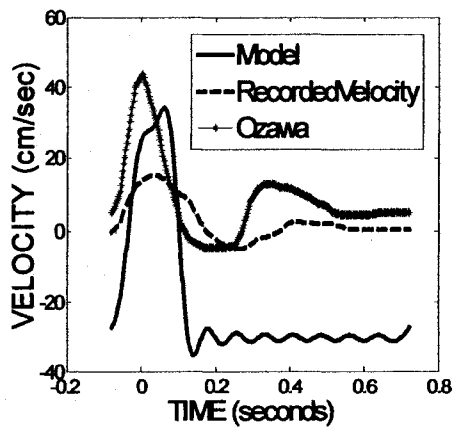
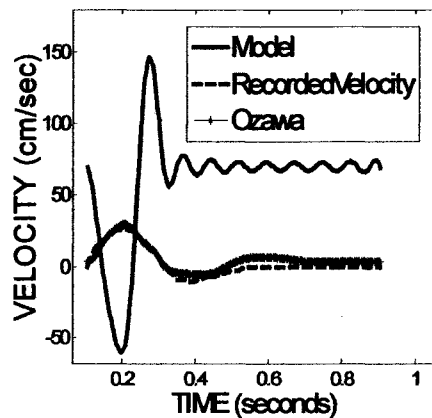
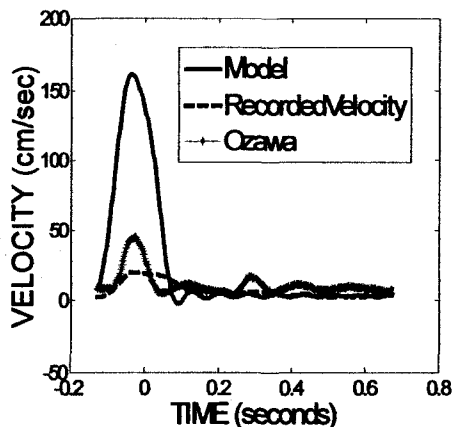
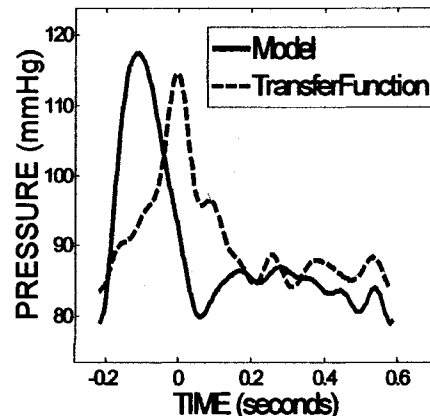
(b) Flow velocity at left brachial artery (model error = 22.04)
(Ozawa's error = 5.08)(c) Flow velocity at right brachial artery (model error = 21.82)
(Ozawa's error = 7.42)(d) Flow velocity at femoral artery (model error = 49.44)
(Ozawa's error = 3.38)

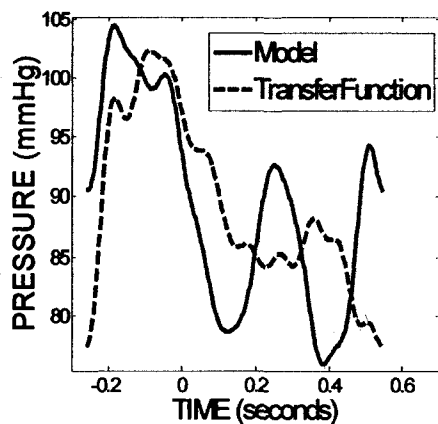
Fig. 4.9 (a)-(d) Flow and pressure results for subject Lf



(e) Flow velocity at carotid artery
(model error = 1.60)
(Ozawa's error = 0.87)



(f) Pressure at aortic arch



(g) Pressure at ascending aorta

Fig. 4.9 (e)-(g) Flow and pressure results for subject Lf

Referring to figures 4.9 (b), (c), (d) and (e), model error was the highest of the 8 subjects studied. Again, this is attributed to the lack of age, weight, height and gender input data, as well as, not compensating for preexisting arterial disorders. Overall, the model error, which had an average error of 23.73, was higher than Ozawa's model, which had an average error of 4.19.

4.3.1 Increasing segment increments from 10 to 30

This section provides the results of increasing the discretization of the vessels from 10 segments to 30 segments, using subject 471.

Subject: 471

Age: 36 (years)

Height: 1830 (mm)

Weight: 113.398 (kg)

Gender: male

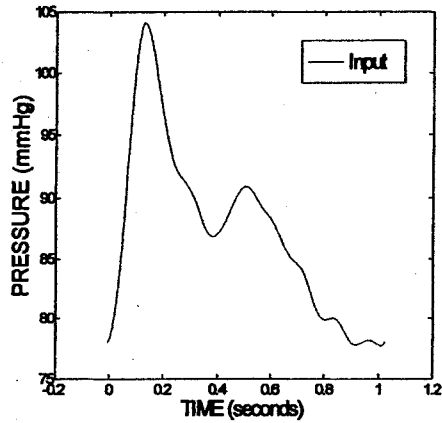
Heart Rate: 62 (beats/min)

Table 4.18 Cardiovascular parameters derived for subject 471 (30 segments)

SVR	CO	Large Artery Compliance	Oscillatory Compliance
(dyne-sec/cm ⁵)	(L/min)	(ml/mmHg)	(ml/mmHg)
1225	5.68	3.97	0.10

Table 4.19 Physiological data for arterial model of Subject 471 (30 segments)

Vessel	length (mm)	radius (mm)		Elastic modulus (dyne/cm ²)x10 ⁶	Eh/r ratio (dyne/cm ²)x10 ⁶
		in	out		
1	244.58	2.70	1.11	27.29	0.71
2	122.29	3.45	3.45	27.70	0.67
3	122.29	1.78	0.87	26.90	0.71
4	122.29	0.43	0.43	26.90	0.71
5	426.38	4.32	2.69	29.89	0.64
6	29.87	4.54	4.54	11.36	0.27
7	110.53	4.07	3.25	7.08	0.16
8	35.39	18.28	15.83	4.96	0.10
9	51.89	29.84	27.26	3.72	0.05
10	2.59	27.26	24.69	5.33	0.08
11	129.89	4.07	3.25	7.08	0.16
12	5.19	24.69	22.12	6.21	0.10
13	194.60	22.12	19.54	8.70	0.10
14	15.72	19.54	16.97	10.58	0.09
15	9.43	16.96	14.	9.41	0.08
16	9.43	14.39	11.82	8.56	0.08
17	44.01	11.82	9.24	6.30	0.05
18	40.87	9.24	6.67	2.90	0.02
19	65.84	3.34	3.10	4.45	0.09
20	65.84	3.34	3.10	4.45	0.09
21	166.05	3.10	2.57	14.08	0.26
22	166.05	3.10	2.57	14.08	0.26
23	442.27	4.85	2.51	20.64	0.30
24	442.27	4.85	2.51	20.64	0.30
25	367.06	1.25	1.25	31.96	0.73
26	367.06	1.25	1.25	31.96	0.73
27	342.95	1.25	0.59	31.96	0.73
28	342.96	1.25	0.59	31.96	0.73
29	244.59	2.53	1.04	23.05	0.71
30	122.29	0.81	0.81	21.77	0.61
31	122.29	0.83	0.40	24.25	0.71
32	122.29	0.37	0.37	24.25	0.71
33	426.38	4.32	2.69	14.82	0.50
34	37.34	4.54	4.54	7.05	0.14
35	148.86	2.02	1.55	14.11	0.36
36	148.86	2.02	1.55	31.22	0.55
37	124.94	2.19	2.19	20.64	0.30
38	124.94	2.19	2.19	20.64	0.30
39	57.26	1.79	1.79	9.74	0.15
40	57.26	1.79	1.79	9.74	0.15
41	42.68	2.03	2.03	4.43	0.04
42	27.74	2.74	2.74	8.11	0.08
43	27.74	2.37	2.37	8.96	0.08
44	51.21	16.97	16.97	9.82	0.09
45	8.54	5.26	5.26	11.30	0.10



(a) Input pressure at radial artery

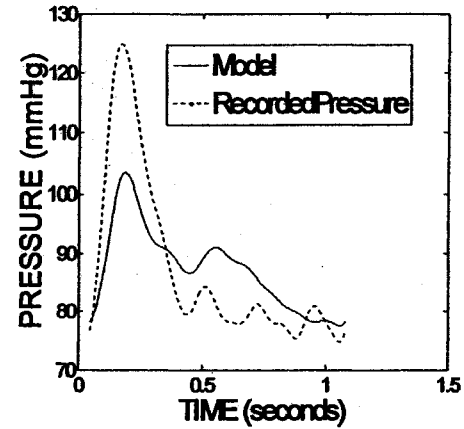
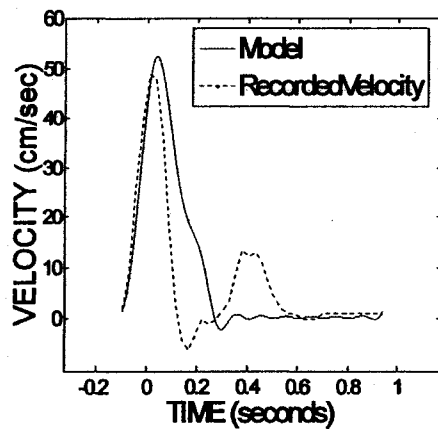
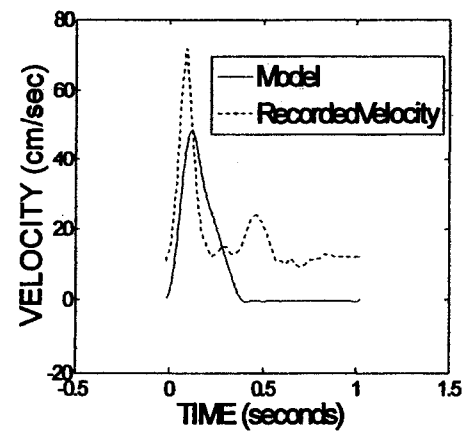
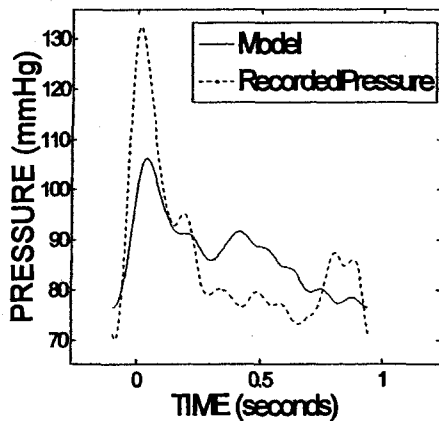
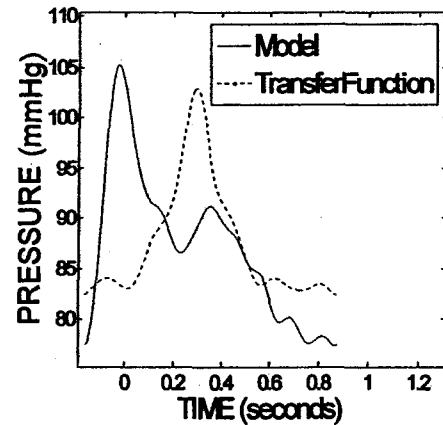
(b) Pressure at left brachial artery
(model error = 0.08)(c) Flow velocity at right brachial
artery (model error = 3.62)(d) Flow velocity at radial artery
(model error = 0.79)

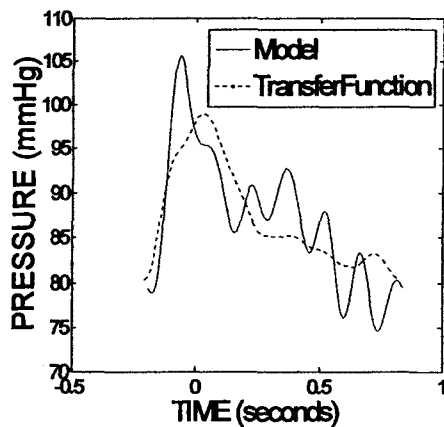
Fig. 4.10 (a)-(d) Flow and pressure results for subject 471 (with 30 segments)



(e) Pressure at left carotid artery
(model error = 0.09)



(f) Pressure at aortic arch



(i) Pressure at ascending aorta

Fig. 4.10 (e)-(g) Flow and pressure results for subject 471 (with 30 segments)

A vessel discretization of 30 segments, instead of 10, was used for subject 471. As a result, the best case (of the 3 sets of output) shifted from the one selected in the previous run. This shift resulted in the selection of different physiological parameters (see tables 4.19 and 4.3). Referring to figures 4.10 (a) and 4.2 (a), a fractional improvement of 0.01 in the brachial pressure prediction reduced error in brachial flow velocity from 5.53 (see figure 4.2 (c)) to 3.62 (see figure 4.10 (c)). The prediction of velocity at the radial artery showed a reduction in error of 0.02 (refer to figures 4.10 (d) and 4.2 (d)). Additionally,

the pressure and flow pulse spectrums, in plots for all 3 cases, changed in the diastolic region. Although this change resulted in slightly reduced error, further investigation revealed a need for more data regarding the tibial blood vessels. The physiological parameters for this area are extrapolated from the femoral arteries. A high number of increments at those 4 vessels result in $\frac{Eh}{r}$ values that in turn produce excessive reflections (most notably along the aorta). Both the quantity and magnitude of the oscillations grow progressively with increments above 50. Presently, discretization should be limited to 50 segments.

4.3.2 Sensitivity to parameter change

This section shows the model's sensitivity to a wide variation of input parameters. Age, height, gender, weight and heart rate are independently given extreme values for Subject 730. Subject y11 is also included to look at changing a subject's gender from a woman to a man. A representative plot of pressure and velocity of the results of each variation are provided along with a summary.

4.3.2.1 Increasing / decreasing age

This section addresses changing the age of subject 730 from 42 years to 76 and 11 years of age.

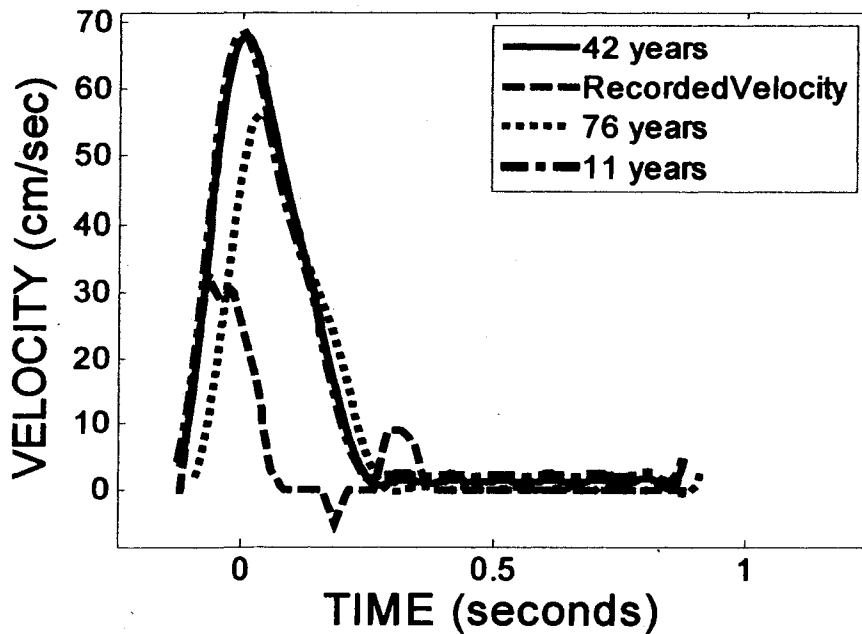


Fig. 4.11 (a) Sensitivity to age variation

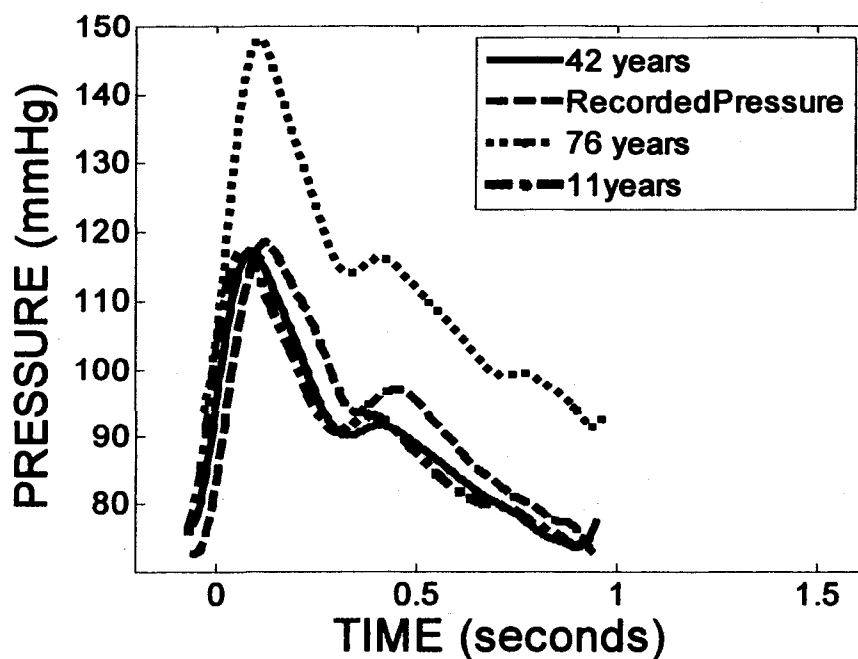


Fig. 4.11 (b) Sensitivity to age variation

The radial pulse input required an amplification of 25% (to maximum systolic pressure of 147.9 mmHg) to fully run the program using 76 years as the input age. This is consistent with expectations of the model performance. Blood pressure is expected to rise with age (see figure 4.11 (b)). Since the program parameterized the model elements with values applicable to a person 76 years old, the higher pressure was required to get adequate results. Reducing the age to 11 did not require this special treatment. Referring to figures 4.11 (a) and 4.11 (b), the model did not produce wide fluctuations when age was varied; however, model results are sensitive to advancing age.

4.3.2.2 Increasing / decreasing height

This section addresses changing the height of subject 730 from 1560 mm (5.12 ft.) to 2133.6 mm (7 ft.) and 914.4 mm (3 ft.).

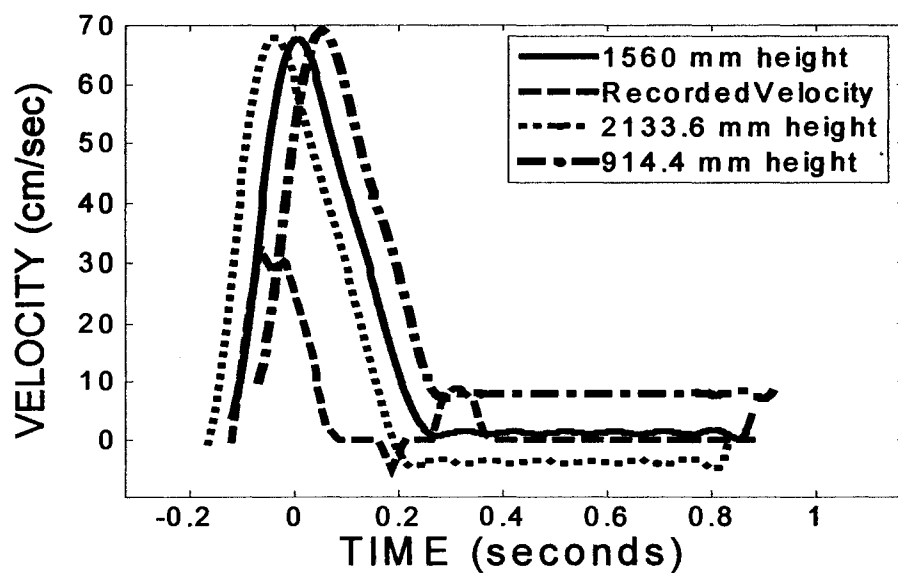


Fig. 4.12 (a) Sensitivity to height variation

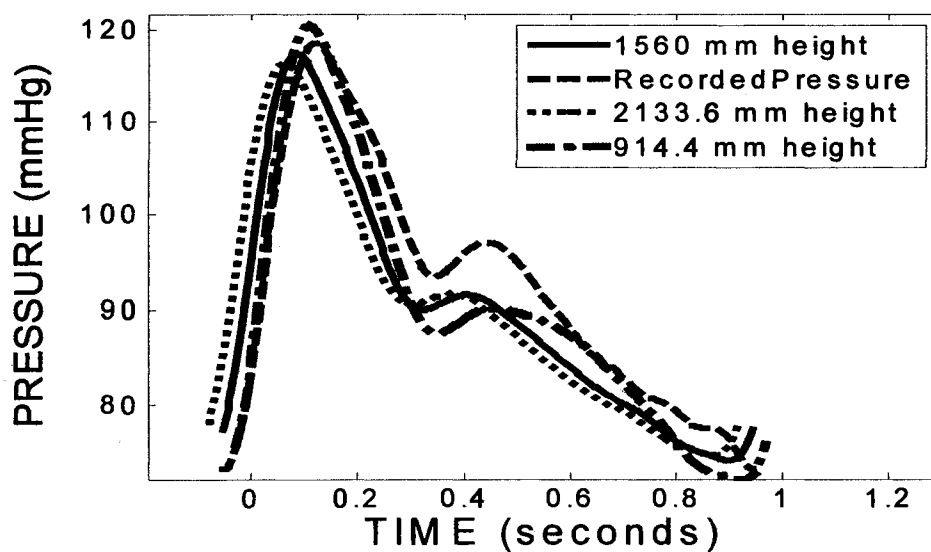


Fig. 4.12 (b) Sensitivity to height variation

Varying the height from 3 ft to 7 ft. (914.4 mm to 2133.6 mm) did not produce instabilities or significant differences in the results. However, referring to figures 4.12 (b) and (d), it was noted that the shorter subject (with the height of 914.4 mm) exhibited higher velocity during the diastolic period. This may be due in part to the greater fluid resistance developed in the taller subject. This was expected, since the inputted radial wave was the same for the 3 cases of a size variation of the arterial model.

4.3.2.3 Increasing / decreasing weight

This section addresses changing the weight of subject 730 from 81.65 kg. (180.01 lbs.) to 136.08 kg. (300 lbs.) and 36.29 kg. (80 lbs.).

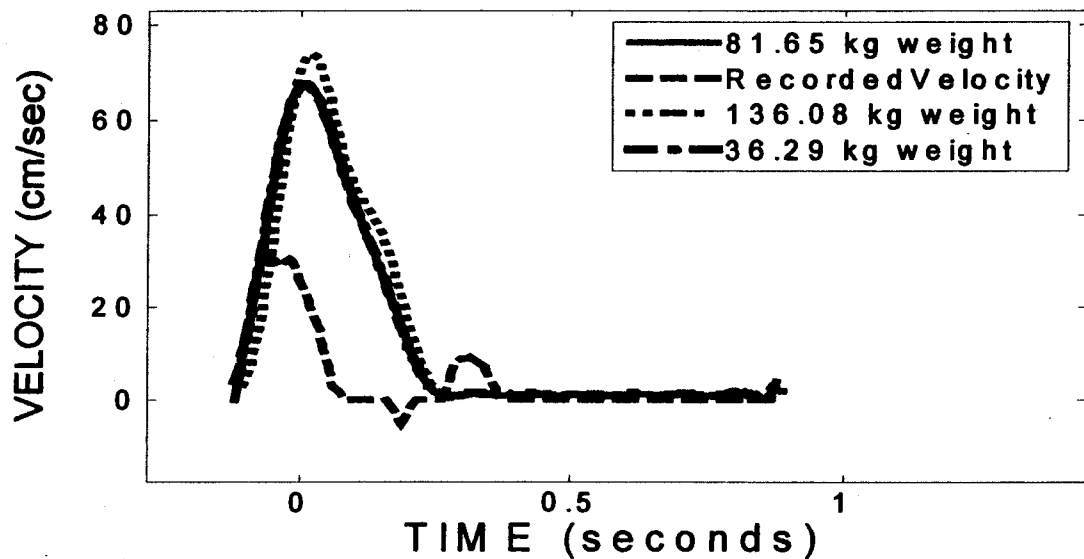


Fig. 4.13 (a) Sensitivity to weight variation

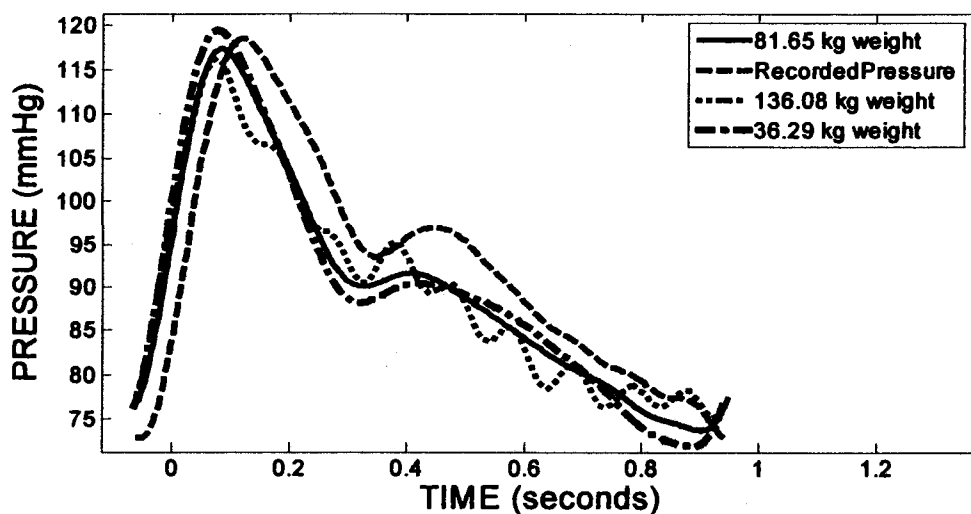


Fig. 4.13 (b) Sensitivity to weight variation

Reducing the subject's weight to 80 lbs (36.29 kg) did not introduce any significant variations when comparing velocity and pressure waves in figures 4.13 (a) and (b).

However, some added oscillations were noted in the pressure waves when weight was increased to 300 lbs. (136.08 kg) (in figure 4.13 (b)). The increased oscillations did not significantly disrupt the form of the pressure waves and are attributed to the resulting increase in diameters of the aorta, carotid and femoral arteries, as well as an increase in cardiac output. These increases are a requisite of the increased weight, and the resulting oscillations may be a future method for optimizing subsequent versions of this model.

4.3.2.4 Increasing / decreasing heart rate

This section addresses changing the heart rate of subject 730 from 60 beats/min (bpm) to 100 bpm and 45 bpm.

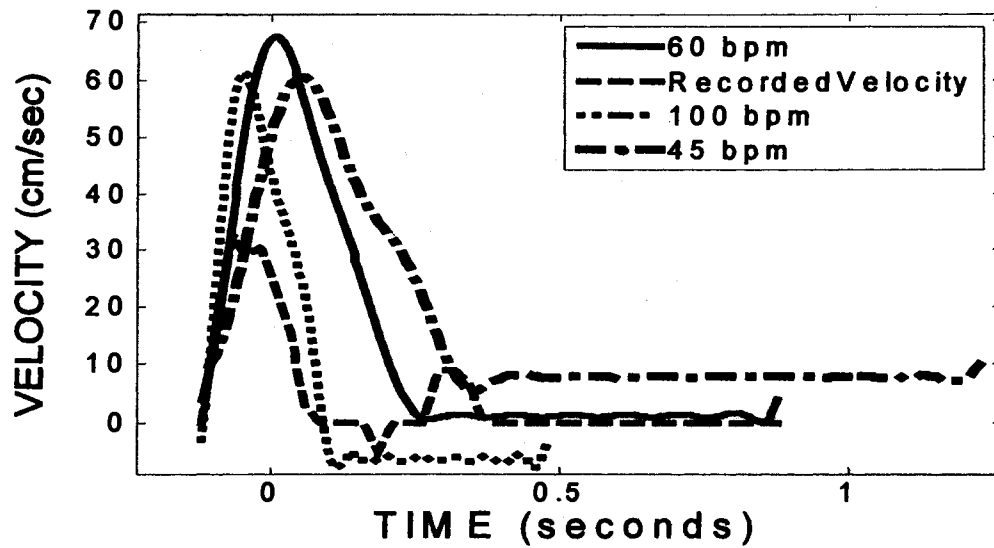


Fig. 4.14 (a) Sensitivity to heart rate variation

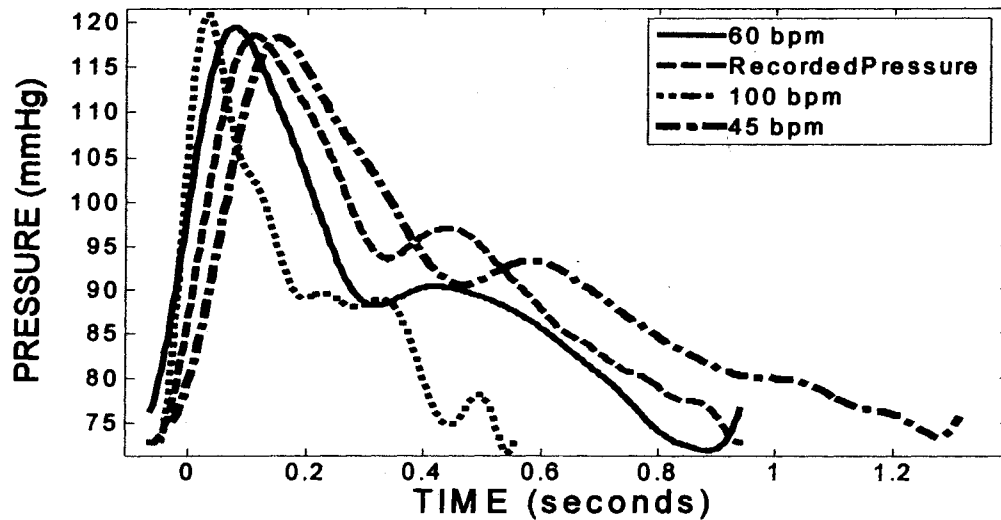


Fig. 4.14 (b) Sensitivity to heart rate variation

Referring to figures 4.14 (a) (brachial blood flow velocity) and 4.14 (b) (brachial blood pressure), drastic changes in heart rate did not produce instabilities in the results.

Additionally, as expected, the overall duration of the waves became longer as the pulse rate decreased. This characteristic is directly related to the lengthening of the duration of each heartbeat as the pulse rate decreased.

4.3.2.5 Changing Gender

This section addresses changing the gender of subject 730 from male to female and the gender of subject y11 from female to male. Blood velocity and pressure at the brachial artery are provided in figures 4.15 (a)-(d).

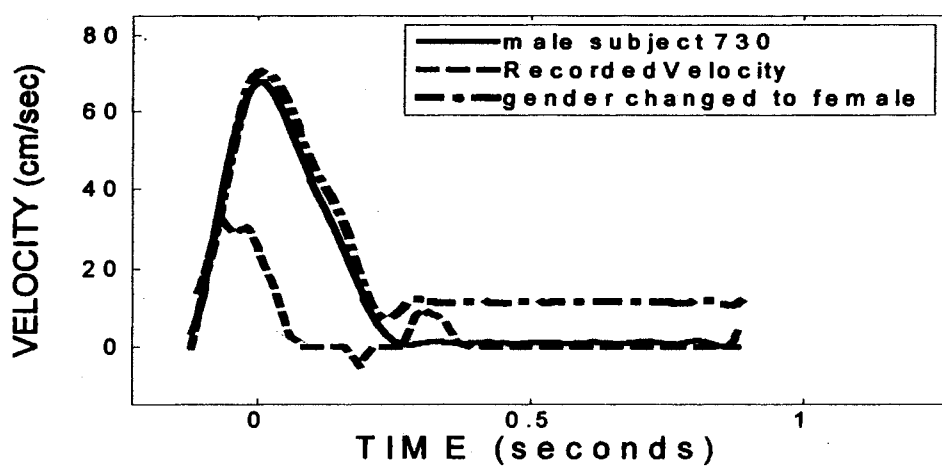


Fig. 4.15 (a) Sensitivity to gender variation

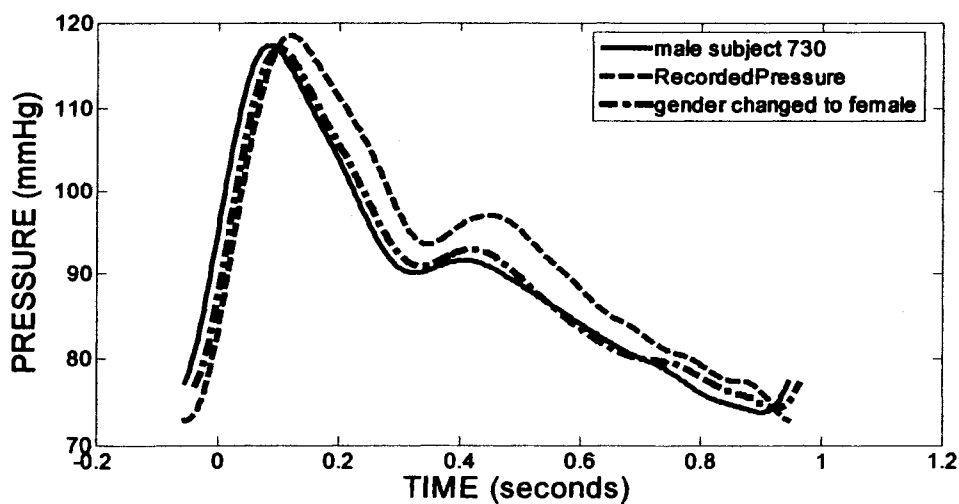


Fig. 4.15 (b) Sensitivity to gender variation

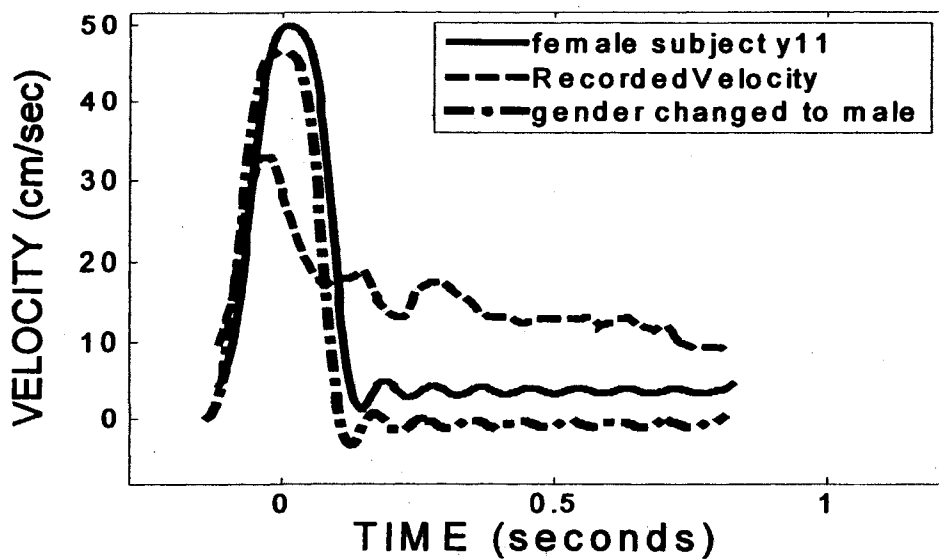


Fig. 4.15 (c) Sensitivity to gender variation

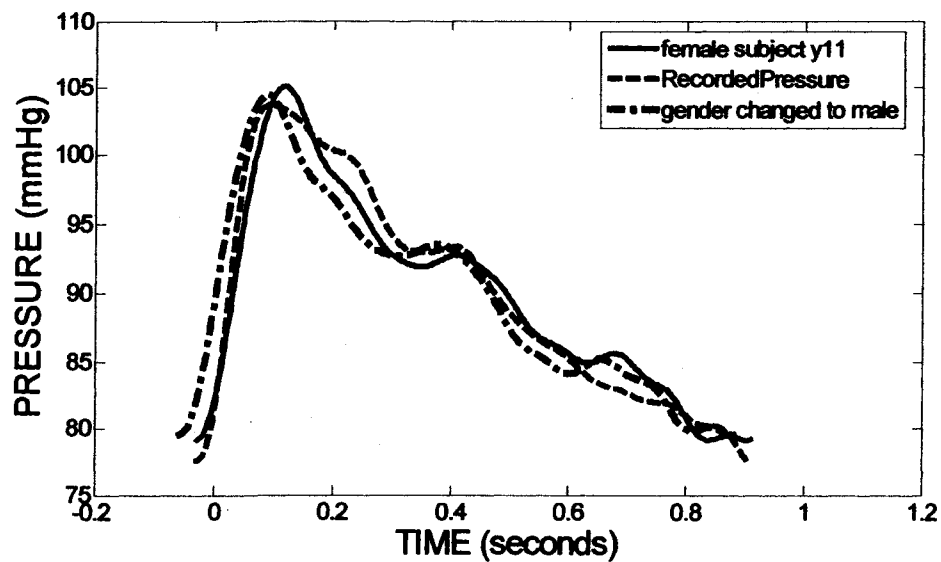


Fig. 4.15 (d) Sensitivity to gender variation

Referring to figures 4.15 (a)-(d), no instabilities or trends attributed to gender change were noted during this evaluation.

4.4 Discussion

The data needed to accurately assess the suitability is more scarce than that used to create it. It required simultaneously recorded pressure and/or flow curves from various points of a subject's arterial tree, along with other vital parameters. Finding the requisite input data represented a challenge. The works of Ozawa (1996) and Xiao (2000) contained some of the information but neglected points along the aorta. Because of this drawback, the transfer function from Karamanoglu et al., (1993) was used to convert radial pulse input to an ascending aortic pulse. This ascending aortic pulse was, in turn, converted to pulses at three other locations along the aorta with transfer functions from Hope (2003b). It should be noted though that these are generalized functions to describe statistically possible pressure curves and were therefore confined for use in general trending of calculated values. The physiological output consisted of the predicted length of each vessel, its blood flow inlet and outlet radii, the average elastic modulus of the vessel and the average $\frac{Eh}{r}$ ratio. For cardiovascular parameters, the program outputted the subject's SVR, CO, large artery compliance and oscillatory compliance.

One of the objectives of this project was to limit internal modification of the program algorithms between subjects, with the exception of subject data input and output selection. With the exception of fitting the Goldwyn-Watt windkessel to the input radial wave, this condition was met. The initial guess used by the Davidon-Fletcher-Powell method for fitting a model pressure curve to the diastolic portion of the radial pulse

required some modification between subjects. Furthermore, the resulting fits, although adequate for subsequent calculations, could have been closer to the contour of target diastolic curve. This identified an area for improvement.

The model obtained better results from the subjects for which age, height, gender and weight were provided on input. This included the subjects from Xiao (2000). Of those results, the model more accurately predicted pressure. On the other hand, the model tended to predict excessive flow velocities. This points to possible problems with timing and, subsequently, wave speed, c_0 . With either more statistical data to populate the ratio $\frac{Eh}{r}$ or some rationale to iteratively synchronize the pressure gradient across segments, this issue may be overcome.

With regard to the results from the subjects in Ozawa's study, the only available input to the model came in the form of a radial pressure wave, so some additional error was expected since the major determinants for the physiological parameters of the arterial tree also required estimation. This error however, was compounded because the subjects were heart failure patients. Some improvement, which is not reported here, was gained through the manual manipulation of parameters such as age and vessel diameter. This identified another important area of improvement - tracking alterations to the arterial system due to disease (Patel et al., 1980; Nichols et al., 1998; O'Rourke et al., 1999 and McVeigh et al., 2002). The modification of parameters in one area, like aortic diameters, produced significant changes in the pressure wave contours throughout the model. It became clear that a disease specific to one region of the vasculature can have a

reverberating effect throughout the arterial system. With further modification, this model may be adapted to predict certain alterations that have occurred due to disease.

To check the algorithm's ability to predict the input data of age, height, weight and gender, one of these parameters was systematically left out on entry of subject from each Xiao's six subjects. Error was then calculated between the missing input and the predicted parameter. Overall, this portion of the program was successful; however, there were some program limitations with determining inputs for the heart failure subject (subject 671). The erratic behavior of the subject's blood pressure is, in part, attributed to this problem.

Additionally, the algorithm was run using a vessel discretization of 30 segments, instead of 10, for subject 471 (see section 4.3.1 for results). As a result, the best case (of the 3 sets of output) shifted from the one selected in the previous run. Although this change resulted in slightly reduced error, further investigation revealed a need for more data regarding the tibial blood vessels. The physiological parameters for this area are extrapolated from the femoral arteries. A high number of increments at those 4 vessels result in $\frac{Eh}{r}$ values that produce excessive reflections (most notably along the aorta).

Presently, discretization should be limited to 50 segments.

Having the ability to predict parameters across a subject's arterial network can enormously impact the medical community. Ignoring the potential for service as a teaching aid or as a tool for research into vascular diseases, the arterial model can be used

in conjunction with medical devices. Ozawa et al. (2001) used a model of the arterial system to optimize the timing of an enhanced external counterpulsation (EECP) device. This instrument uses inflatable cuffs to sequentially apply pressure to the extremities to enhance circulation in heart failure patients. Then there are Vandenberghe et al. (2003), Timms et al. (2005) and Shi et al. (2006), who have used cardiovascular models to evaluate the operation of ventricular assist pumps and devices.

In the end, methodology for a more complete marriage of global clinical parameters to local characteristics was demonstrated. With the accomplishments noted below, arterial models, of the type reported on, can have greater practicality.

- Realistic boundary conditions with the inclusion of actual subject SVR, SI, Compliance and CO data.
- Tracking of vessel compliance through the use of gradual (*natural*) changes in physiological parameters - some of which are correlated with actual clinical measures.
- Greater flexibility with a minimum amount of required data.
- Larger coverage of the arterial tree, tailored to an individual subject.

CHAPTER 5

5. Conclusion

This chapter lists the benefits of the project model, future work for the project and gives concluding remarks.

5.1 The benefits of the model

Although the contributions of this project to the field of hemodynamic modeling are discussed in section 4.4 of this report, the overall benefits are listed in table 5.1.

Table 5.1 Benefits of the project model

Model attributes	Benefits
Noninvasively determined relationships developed between subject and model	Realistic model calculations
Automatic calculation of physiologic parameters for model components	Increased usability
Minimum required inputs	Reduced implementation time
Uses reduced / closed end equations	Reduced implementation time
	Rapid calculation time

5.2 Concluding Remarks

The robustness of this model represents a contribution to the field of cardiovascular modeling. It provides realistic and individualized cardiovascular parameters without requiring major adjustment to the internal algorithms. This has been of interest to researchers, yet most of the development in this area has been centered around predicting

parameters in isolated locations of the arterial system (Fetics et al., 1999; Segers et al., 2000 and Hope et al., 2002). There have been models that looked at calculating actual parameters of a subject's arterial tree (Ozawa, 1996; Xiao, 2000 and Steele, 2007); however, they posed the challenge to obtain both clinical accuracy and subject individualization. This model is an incremental step in that direction that captures a larger picture of the cardiovascular operation with implications for clinical use, as well as research. Although this phase of the study is concluded, this model will remain a work-in-progress, where further optimization is expected.

5.3 Future work

Future work will include increasing the model's accuracy, usability and applicability.

The implementation of leakage factors to account for blood flows that are not represented by the present model will be considered, to enhance accuracy. Additionally, the specification of physiologic parameters will be revisited to find areas for optimization. A graphical user interface will be developed to increase the usability of this program.

Finally, relations that account for various disorders will be pursued.

LITERATURE CITED

Ahlgren, A., Sundkvist, G., Sandgren, T., and Lanne, T., 2002. Female gender increases stiffness of elastic but not of muscular arteries in type I diabetic patients. *Clinical Physiology and Functional Imaging* 22, 409-415.

Avolio, A., 1980. Multi-branched model of the human arterial system. *Medical and Biological Engineering and Computing* 18, 709 - 718.

Benetos, A., Laurent, S., Hoeks, A., Boutouyrie, P. and Safar, M., 1993. Arterial alterations with aging and high blood pressure - a noninvasive study of carotid and femoral arteries. *Arteriosclerosis, Thrombosis and Vascular Biology* 13, 90-97.

Bergel, D., 1961a. The static elastic properties of the arterial wall. *Journal Physiology* 156, 445-457.

Bergel, D., 1961b. The dynamic elastic properties of the arterial wall. *Journal Physiology* 156, 458-469.

Boutouyrie, P., Bussy, C., Lacolley, P., Girerd, X., Laloux, B. and Laurent, S., 1999. Association between local pulse pressure, mean blood pressure, and large artery remodeling. *Circulation* 100, 1387-1393.

Bowman, F., 1958. *Introduction to Bessel Functions*. Dover Publications, New York, pp. 1-19.

Burantini, R. and Gnudi, G., 1982. Computer identification of models for arterial tree input impedance: comparison between two new simple models and first experimental results. *Medical and Biological Engineering and Computing* 20, 134-144.

Chandran, K. B., 1992. *Cardiovascular Biomechanics*. New York University Press, New York, pp. 195-198.

Chen, C., Nevo, E., Fetis, B. Pak, P., Yin, F., Maughan, L. and Kass, D., 1997. Estimation of central aortic pressure waveform by mathematical transformation of radial tonometry pressure: validation of generalized transfer function. *Circulation* 95, 1827-1836.

Dotter, C. T., Roberts, D. J., and Steinberg, I., 1950. Aortic length: angiocardiographic measurements. *Circulation* 2, 915-920.

- Elzinga, G. and Westerhof, N., 1973. Pressure and flow generated by the left ventricle against different impedances. *Circulation Research* 32, 178-186.
- Fetics, B., Nevo, E., Chen, CH. Kass, D., 1999. Parametric model derivation of transfer function for noninvasive estimation of aortic pressure by radial tonometry. *IEEE Transactions on Biomedical Engineering* 46(6), 698-706.
- Formaggia, L., Lamponi, D., Quarteroni, A., 2003. One-dimensional models for blood flow in arteries. *Journal of Engineering Mathematics* 47, 251-76.
- Frasher, W. G., 1981. What is known about the physiology of larger blood vessels. In: Fung, Y. C. (Ed.), *Biomechanics: Mechanical Properties of Living Tissues*. Springer-Verlag, New York, pp. 2.
- Goldwyn, R. and Watt, T., 1967. Arterial pressure pulse contour analysis via a mathematical model for clinical quantification of human vascular properties. *IEEE Transactions on Bio-Medical Engineering* 14, 11-17.
- Guerin, A., London, G., Marchais, S. and Metivier, F., 2000. Arterial stiffening and vascular calcifications in end-stage renal disease. *Nephrology Dialysis Transplantation*. 15, 1014-1021.
- Henry Dreyfuss Associates, 1993. *The Measure of Man and Woman: Human Factors in Design*, Whitney Library of Design, New York, pp. 22-25.
- Hlavac, M., undated. Windkessel model analysis in Matlab. Paper, Brno University of Technology, Czech Republic.
- Hope, S., Tay, D., Meredith, I. and Cameron, J., 2002. Comparison of generalized and gender-specific transfer functions for the derivation of aortic waveforms. *American Journal of Physiology* 283, H1150-H1156.
- Hope, S., Tay, D., Meredith, I. and Cameron, D., 2003a. Reply. *Journal of Hypertension* 21, 2197-2199.
- Hope, S., Tat, D., Meredith, I. and Cameron, D., 2003. Use of arterial transfer function for the derivation of aortic waveform characteristics. *Journal of Hypertension* 21, 1299-1305.
- Imura, T., Yamamoto, K., Satoh, T., Kanamori, K., Mikami, T. and Yasuda, H., 1990. In vivo viscoelastic behavior in the human aorta. *Circulation Research* 66, 1413-1419.
- Jager, G. N., Westerhof, N., Noordergraaf, A., 1965. Oscillatory flow impedance in an electrical analog of the arterial system: representation of sleeve effect and non-newtonian properties of blood. *Circulation Research* 26, 121-133.

- Karamanoglu, M., O'Rourke, M., Avolio, A. and Kelly, R., 1993. An analysis of the relationship between central aortic and peripheral upper limb pressure waves in man. *Eur. Heart J.* 14, 160-167.
- Karamanoglu, M., Gallagher, D. E., Avolio, A. P., and O'Rourke, M. F., 1995. Pressure wave propagation in a multibranched model of the human upper limb. *American Journal Physiology* 269, H1363-H1369.
- Karamanoglu, M. and Feneley, M., 1996. Derivation of the ascending aortic-carotid pressure transfer function with an arterial model. *American Journal of Physiology* 271, H2399-H2404.
- Karamanoglu, M., 1997. A System for Analysis of Arterial Blood Pressure Waveforms in Humans. *Computers and Biomedical Research* 30, 244-255.
- Kelly, R., Hayward, C., Avolio, A. and O'Rourke, M., A., 1989. Noninvasive determination of age-related changes in the human arterial pulse. *Circulation* 80, 1652-1659.
- Kiechl, S. and Willeit, J., 1999. The natural course of atherosclerosis - Part II: vascular remodeling. *Arteriosclerosis, Thrombosis and Vascular Biology* 19, 1491-1498.
- Ku, D. N., 1997. Blood flow in arteries. *Annual Review of Fluid Mechanics* 29, 399 - 434.
- Lambermont, B., Kolh, P., Ghuysen, A., Moonen, M., Morimont, P., Gerard, P., Tchana-Sato, V., Rorive, G. and D'Orio, V., 2003. Effect of hemodiafiltration on pulmonary hemodynamics in endotoxic shock. *Artificial Organs* 27, 1128-1133.
- Laurent, S., Girerd, X., Mourad, J., Lacolley, P. Beck, L., Boutouyrie, P., Mignot, J. and Safar, M., 1994. Elastic modulus of the radial artery wall material is not increased in patients with essential hypertension. *Arteriosclerosis, Thrombosis and Vascular Biology* 14, 1223-1231.
- Learoyd, B. and Taylor, M., 1966. Alterations with age in the viscoelastic properties of human arterial walls. *Circulation Research* 18, 278-292.
- Li, A., Kamel, I., Rando, F., Anderson, M., Kumbasar, B., Lima, J. and Bluemke, D., 2004. Using MRI to assess aortic wall thickness in the multiethnic study of atherosclerosis: distribution by race, sex and age. *American Journal of Roentgenology* 182, 593-597.
- Li, J. K., 1987. *Arterial System Dynamics*. New York University Press, New York, pp. 6-19.

- Livingston, E. and Lee, S., 2001. Body surface area prediction in normal-weight and obese patients. *American Journal of Physiology-Endocrinology and Metabolism* 281, 586-591.
- Marieb, E., 1995. *Human Anatomy and Physiology*. The Benjamin / Cummings Publishing Company, Inc., California, pp. 643-690.
- Mates, R. E., 1995. Arterial Macrocirculatory Hemodynamics. In: Bronzino, J. D., (Chief Ed.), *The Biomedical Engineering Handbook*. Hartford, Connecticut, pp. 454-462.
- McLachlan, N., 1961. *Bessel Function for Engineers*. Clarendon Press, Oxford, pp. 239.
- McVeigh, G., Bratteli, C., Morgan, D., Alinder, C., Glasser, S., Finkelstein, S. and Cohn, J., 1999. Age-related abnormalities in arterial compliance identified by pressure pulse contour analysis - aging and arterial compliance. *Hypertension* 33, 1392-1398.
- McVeigh, G., Hamilton, P. and Morgan, D., 2002. Evaluation of mechanical arterial properties: clinical, experimental and therapeutic aspects. *Clinical Science* 102, 51-67.
- Nichols, W., O'Rourke, M., Avolio, A., Yaginuma, T., Murgu, J., Pepine, C. and Conti, C., 1985. Effects of age on ventricular-vascular coupling. *American Journal of Cardiology* 55, 1179-1184.
- Nichols, W. and O'Rourke, M., 1998. *McDonald's Blood Flow in Arteries, Theoretical, experimental and clinical principles*, 4th edition. Oxford University Press, New York, pp. 11-417.
- Olufsen, M. S., 1998. Modeling the arterial system with reference to an anesthesia simulator. Ph.D. thesis, Department of Mathematics, Roskilde University.
- Olufsen, M., 2001. A one-dimensional fluid dynamic model of the systemic arteries. In: *Computational Modeling in Biological Fluid Mechanics*, L. Fauci and S. Gueron (Eds.), The IMA Volumes in Mathematics and its Applications. Springer-Verlag, New York, pp. 167-187.
- O'Rourke, M. and Mancia, G., 1999. Arterial stiffness. *Journal of Hypertension* 17, 1-4.
- O'Rourke, M. and Nichols, W., 2003. Use of arterial transfer function for the derivation of aortic waveform characteristics. *Journal of Hypertension* 21, 2195-2197.
- O'Rourke, M., Kim, M., Adji, A., Nichols, W. and Avolio, A., 2004. Use of arterial transfer function for the derivation of aortic waveform characteristics. *Journal of Hypertension* 22, 431-434.

- O'Rourke, M. and Hashimoto, J., 2007 (Reprint). Mechanical factors in arterial aging - a clinical perspective. *Journal of the American College of Cardiology* 50, 1-13.
- Otto, F., 1899. Die Grundform des arteriellen Pulses. *Zeitung fur Biologie* 37, 483-586.
- Ozawa, E. T., 1996. A Numerical Model of The Cardiovascular System for Clinical Assessment of the Hemodynamic State. Ph.D. thesis, Department of Health Sciences and Technology, Massachusetts Institute of Technology.
- Ozawa, E., Bottom, K., Xiao, X. and Kamm, R., 2001. Numerical simulation of enhanced external counterpulsation. *Annals of Biomedical Engineering* 29, 284-297.
- Patel, D. J. and Vaishnav, R. N., 1980. Basic hemodynamics and its role in disease processes, University Park Press, Baltimore, pp. 2-25.
- Pennington, N. and Soames, R., 2005. The anterior visceral branches of the abdominal aorta and their relationship to the renal arteries. *Surgical and Radiologic Anatomy* 27, 395-403.
- Peterson, L. H., Jensen, R. E., and Parnell, J., 1960. Mechanical properties of arteries in vivo. *Circulation Research* 8, 622-639.
- Putz, R. and Pabst, R., 1994. Atlas of human anatomy. Urban and Schwarzenberg, Munich, pp. 71.
- Raines, J. K., Jaffrin, M. Y., Shapiro, A. H., 1974. A Computer Simulation Of Arterial Dynamics In The Human Leg. *Journal of Biomechanics* 7, 77-91.
- Riekkinen, H., Karkola, K. and Kankainen, A., 2003. The radial artery is larger than the ulnar, *Annals of Thoracic Surgery* 75, 882-884.
- Romanes, G., 1981. Cunningham's Textbook of Anatomy, 12th edition. Oxford University Press, New York, pp. 893-959.
- Sass, C., Herbeth, B., Chapet, O., Siest, G., Visvikis, S. and Zannad, F., 1998. Intima-media thickness and diameter of carotid and femoral arteries in children, adolescents and adult from the Stanislas cohort: effect of age, sex, anthropometry and blood pressure. *Journal of Hypertension* 16, 1593-6102.
- Schaaf, B. W., and Abbrecht, P. H., 1972. Digital computer simulation of human systemic arterial pulse wave transmission: a nonlinear model. *Journal of Biomechanics* 5, 345-364.
- Segers, P. and Verdonck, P., undated. Arterial Mechanics. Paper, Institute of Biomedical Technology, Ghent University, Belgium.

- Segers, P., Stergiopoulos, N., Westerhof, N., Wouters, P., Kolh, P. and Verdonck, P., 2003. Systemic and pulmonary hemodynamics assessed with a lumped-parameter heart-arterial interaction model. *Journal of Engineering Mathematics* 47, 185-199.
- Segers, P., Carlier, S., Pasquet, A., Rabben, S., Hellevik, L., DeBacker, T., DeSutter, T., Thomas, J. and Verdonck, P., 2000. Individualizing the aorto-radial pressure transfer function: feasibility of a model-based approach. *American Journal of Physiology* 279 (2), H542-H549.
- Sherwin, S. J., Formaggia, L., Piero, J., Franke, V., 2003. Computational modeling of 1D blood flow with variable mechanical properties and its application to simulation of wave propagation in the human arterial system. *International Journal for Numerical Methods in Fluids* 43, 673-700.
- Shi, Y. and Korakianitis, T., 2006. Numerical simulation of cardiovascular dynamics with left heart failure and in-series pulsatile ventricular assist device. *Artificial Organs* 30, 929-948.
- Snyder, M. F., Rideout, V. C. and Hillestad, R. J., 1968. Computer Modeling Of The Human Arterial Tree. *Journal of Biomechanics* 1, 341-353.
- Sonesson, B., Hansen, F., Stale, H., and Lanne, T., 1993. Compliance and diameter in the human abdominal aorta – the influence of age and sex. *European Journal of Vascular Surgery* 7, 690-697.
- Sonesson, B., Lanne, T., Hansen, F. and Sandgren, T., 1994. Infrarenal aortic diameter in the healthy person. *European Journal of Vascular Surgery* 8, 89-95.
- Steele, B., Olufsen, M. and Taylor, C., 2007. Fractal network model for simulating abdominal and lower extremity blood flow during resting and exercise conditions. *Computer Methods in Biomechanics and Biomedical Engineering* 10, 39-51.
- Steinberg, C., Weinstock, D. J., Gold, J. P., and Notterman, D. A., 1992. Measurements of central blood vessels in infants and children: normal values. *Catheterization and Cardiovascular Diagnosis* 27, 197-201.
- Stergiopoulos, N., Young, D. and Rogge, T., 1992. Computer simulation of arterial flow with applications to arterial and aortic stenosis. *Journal of Biomechanics* 25, 1477-1488.
- Stergiopoulos, N., Westerhof, B. and Westerhof, N., 1998. Physical basis of pressure transfer from periphery to aorta: a model-based study. *American Journal of Physiology* 274, H1386-H1392.

Stergiopoulos, N., Westerhof, B. and Westerhof, N., 1999. Total arterial inertance as the fourth element of the fourth element of the windkessel. *American Journal of Physiology* 276, H81-H88.

Takazawa, K., Tanaka, N., Takeda, K., Kurosu, F. and Ibukiyama, C., 1995. Underestimation of vasodilator effects of Nitroglycerin by upper limb blood pressure. *Hypertension* 26(3), 520-523.

Takazawa, K., Tanaka, N., Fujita, M., Matsuoka, O., Saiki, T., Aikawa, M., Tamura, S. and Ibukiyama, C., 1998. Assessment of vasoactive agents and vascular aging by the second derivative of photoplethysmogram waveform. *Hypertension* 32, 365-370.

Taylor, M. G., 1966. The input impedance of an assembly of randomly branching elastic tubes. *Biophysical Journal* 6, 29-51.

Timms, D., Hayne, M., McNeil, K. and Galbraith, A., 2005. A complete mock circulation loop for the evaluation of left, right and biventricular assist devices. *Artificial Organs* 29, 564-572.

Uflacker, R., 1997. *Atlas of Vascular Anatomy: An Angiographic Approach*. Williams & Wilkins, Baltimore, pp. 160-342.

United States Department of Health, Education, and Welfare 1977. Arteriosclerosis. DHEW Publication No. 78-1526.

Vandenberghe, S., Segers, P., Meyns, B. and Verdonck, P., 2003. Unloading effect of a rotary blood pump assessed by mathematical modeling. *Artificial Organs* 27, 1094-1101.

Van den Wijngaard, J., Ross, M. and Van Gemet, M., 2007. Twin-Twin Transfusion Syndrome Modeling. *Annals of New York Academy of Sciences* 1101, 215-234.

Van der Heijden-Spek, J., Staessen, J., Fagard, R., Hoeks, A., Struijker Boudier, H. and Van Bortel, L., 2000. Effect of age on brachial artery wall properties differs from the aorta and is gender dependent. *Hypertension* 35, 637-642.

Watt, T. and Burrus, C., 1976. Arterial pressure contour analysis for estimating human vascular properties. *Journal of Applied Physiology* 40(2), 176-176.

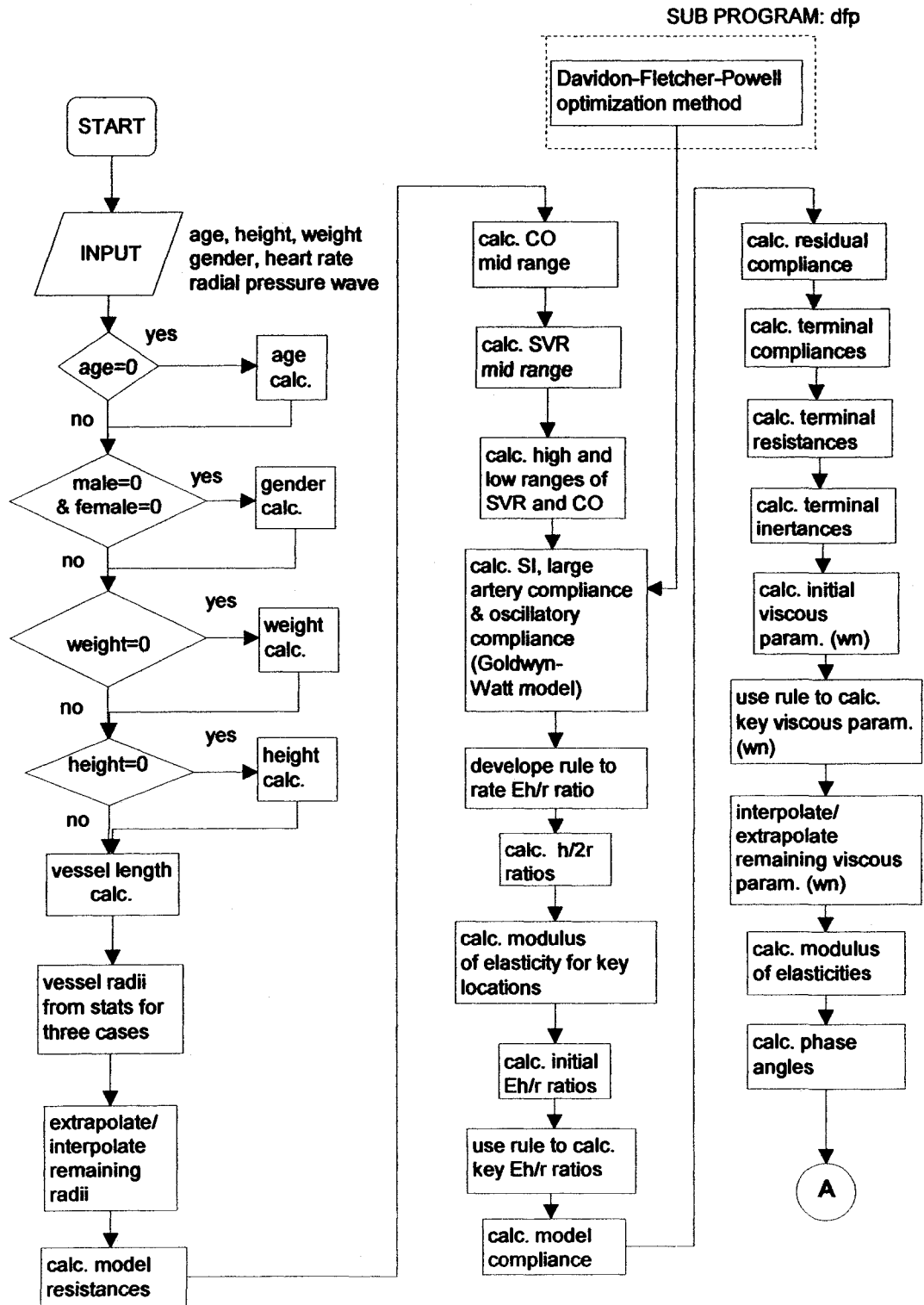
Weissler, A., Harris, L. and White, G., 1963. Left ventricular ejection time index in man. *Journal of Applied Physiology* 18(5), 919-923.

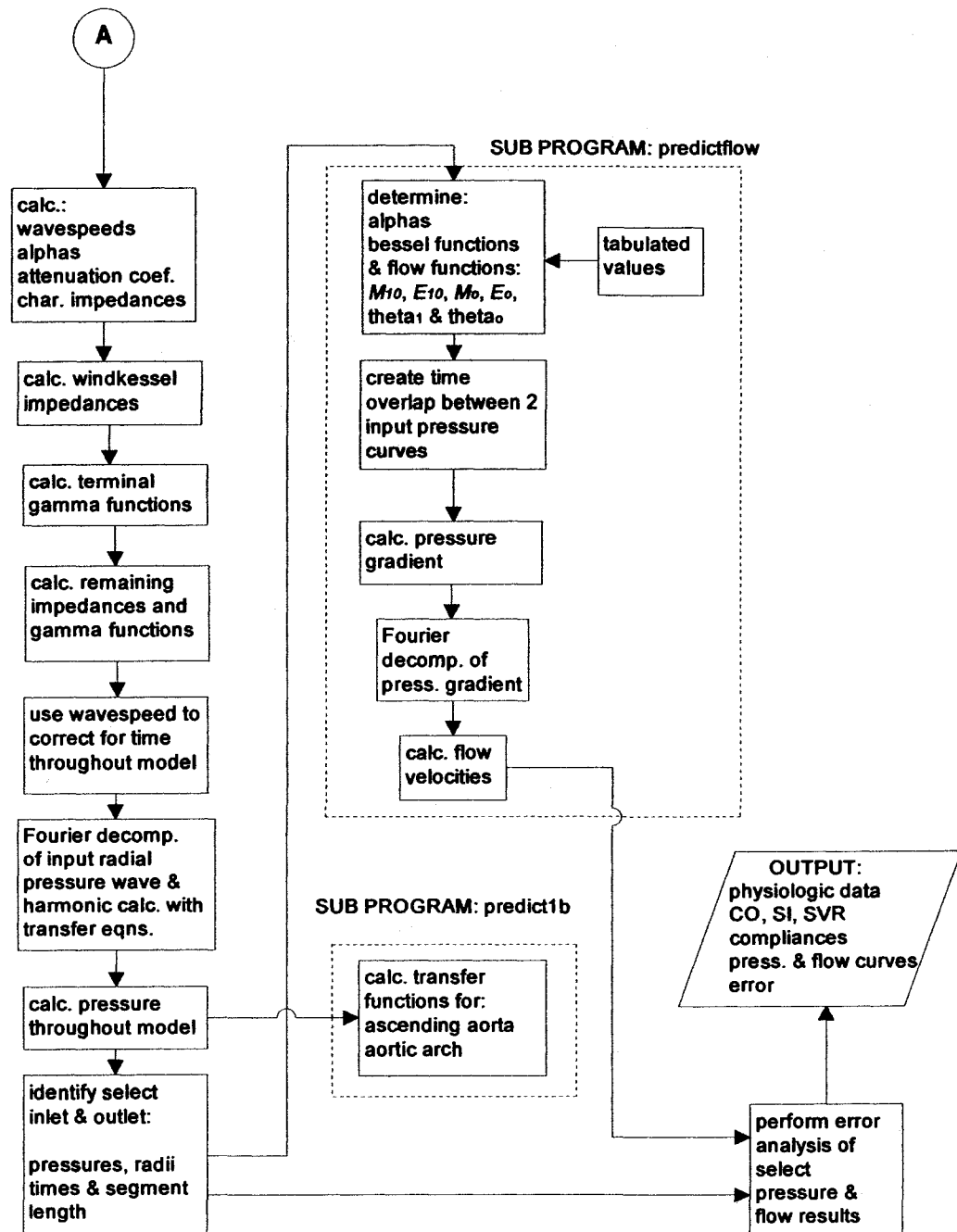
Westerhof, N., Bosman, F., De Vries, C. J., Noordergraaf, A., 1969. Analog Studies Of The Human Systemic Arterial Tree. *Journal of Biomechanics* 2, 121-143.

- Westerhof, N., Noordergraf, A., 1970. Arterial viscoelasticity: a generalised model. *Journal of Biomechanics* 3, 357-379.
- Womersley, J. R., 1957. The mathematical analysis of the arterial circulation in a state of oscillatory motion. Wright Air Development Centre, Technical Report, WADC-TR56 – 614.
- Woodman, R. J., and Watts, G. F., 2003. Measurement and application of arterial stiffness in clinical research: focus on new methodologies and diabetes mellitus. *Medical Science Monitor* 9(5), RA101-RA109.
- Xiao, X., 2000. Noninvasive assessment of cardiovascular health. M.S. thesis, Department of Mechanical Engineering, Massachusetts Institute of Technology.
- Xiao, X., Ozawa, E. T., Huang, Y., Kamm, R. D., 2002. Model-Based Assessment of Cardiovascular Health from Noninvasive Measurements. *Annals of Biomedical Engineering* 30, 612-623.
- Yahel, J. and Arensburg, B., 1998. The topographic relationships of unpaired visceral branches of the aorta. *Clinical Anatomy* 11, 304-309.
- Zamir, M., 2005. *The Physics of Coronary Blood Flow; Biological and Medical Physics - Biomedical Engineering*. Springer, New York, pp. 101.

APPENDIX A

COMPUTER PROGRAM FLOW CHART





**The functions M_{10} , E_{10} , M_0 , E_0 , θ_{10} are θ_{10} are M_{10} , E_{10} , M_0 and E_0 , respectively

VITA

The author was born in 1967 to James and Lucy Carter. He graduated from Aviation Trades High School, in New York City, in 1985. That same year he enlisted in the United States Navy for a term of six years and graduated from the Naval Nuclear Power Training program. Since 1991 he has worked on various equipment on Naval vessels, while employed with first American Systems Engineering Corporation, then Northrop Grumman Newport News Shipbuilding. During this time, he received his Associate in Science degree from Tidewater Community College (1994) and his Bachelor of Science in Mechanical Engineering degree (1996) and Master of Engineering degree (1999) from Old Dominion University.